

An integrated sediment budget for the Root River watershed, southeastern Minnesota

Patrick Belmont, Toby Dogwiler, Karthik Kumarasamy,

With contributions from: Justin Stout, Michael Souffront, Angus Vaughan, Blake Lea, Mitchell Donovan,
Bastiaan Notebaert, Shannon Belmont, Sara Kelly, Jay Hemmis, Adam Fisher, Tim Beach



Contents

1. Summary of Findings.....	4
2. Introduction	6
3. Description of the Study Area	7
4. Hydrologic analysis.....	13
Precipitation.....	13
Flows	16
5. Discharge-TSS relationships	18
Motivation for analyzing discharge-TSS relationships.....	18
Methods for analyzing discharge-TSS relationships	19
Q-TSS relation results.....	19
6. Monitoring of sediment gages and springs	21
Sediment Yield of Springs	24
7. Grain size and bulk density	26
Methods.....	26
Results.....	27
8. Terrain analysis	29
9. Mapping of existing water detention basins	34
10. Mapping and quantifying sedimentation in cutoff meander bends.....	35
11. Sediment fingerprinting.....	37
12. Meander migration and channel width analysis.....	45
Introduction	45
Methods.....	46
Results.....	51
13. SWAT model of the Root River Basin.....	59
Motivation for development of a SWAT model.....	59
Model Description.....	60
Model Assumptions	61
Input Data	61
Topography data.....	61
Land Cover and Land Use and soils data.....	61
Weather data	62
Management data.....	62

Karst data	62
River network and streamflow gages	63
Methods for implementing water impoundment structures	64
Calibration and Validation	64
SWAT model hydrologic simulation results	68
SWAT model USLE estimates	79
14. Integrated sediment budget	80
References cited	83
Appendix A	89
Appendix B	97

Acknowledgements

Many state and SWCD staff members have contributed data, insights and feedback to support this research, including Kevin Kuehner, Heidi Peterson, Joe Magee, Shaina Keseley, Jennifer Ronnenberg, Donna Rasmussen. We are also grateful to Frank Wright and Peggy Hanson for their hospitality and providing pleasant location for us to camp during field campaigns over the past few years. Funding for this project came from the Minnesota Department of Agriculture and the Minnesota Clean Water, Land and Legacy Amendment.

1. Summary of Findings

The goal of this project was to determine the primary factors influencing erosion and sediment dynamics in the 4300 km² (1660 mi²) Root River watershed, in southeastern Minnesota. Developing a comprehensive and robust understanding of sediment dynamics at such a large spatial scale is challenging due to the wide range of non-linear processes that control erosion and deposition of sediment and the immense variability of those processes in space and time. In an effort to overcome those challenges, we have conducted a wide variety of analyses that elucidate the key factors governing sediment dynamics in the Root River watershed over the range of relevant time and space scales. A coherent story has emerged from these analyses, indicating that recent (i.e., over the past few decades) agricultural soil erosion and streambank erosion are both prominent sediment sources in the Root River watershed. Additional soil conservation and soil management practices (e.g., conservation tillage, grassed waterways and buffer strips, etc.) will need to play an important role in developing a sediment reduction strategy. Furthermore, we have demonstrated that such practices can effectively reduce erosion at the farm field scale and that such practices are most important on steeper terrain.

Our analysis also confirms and greatly expands our understanding of the role of streambank erosion. The Root River and major tributaries are very active river channels with access to many large and easily erodible banks. Our analysis demonstrates, in fact, that sediment concentrations increase with river flow at a greater rate in the Root River than almost any other river in Minnesota. It is possible that streambank erosion could be reduced by bank stabilization practices or reductions in streamflow via water storage in upstream detention basins. However, large-scale bank stabilization is likely prohibitively expensive and may have unanticipated negative impacts, such as destabilizing banks upstream or downstream. For those reasons, we suggest that bank stabilization should only be implemented on smaller tributaries, where infrastructure is at risk or where aquatic habitat can be substantially improved. We have demonstrated that streamflow in the mainstem Root River can be reduced via water detention basins. However, a considerable amount of water storage would be required and historical suspended sediment data suggests that the mainstem Root River can attain very high sediment concentrations even at relatively low flows. Therefore, well placed detention basins may improve water quality in tributary streams, but the benefits will be less apparent in the main stem Root River.

Precipitation and flows have both increased in the past few decades in the Root River watershed. While numerous other studies have demonstrated that changes in precipitation regime and changes in artificial drainage both contribute to increased flows throughout the upper Midwest, it is not possible to deconvolve the effects of these two factors with the data available in the Root River Basin. Increased flows are especially problematic in the Root River Basin because of the extraordinarily high sensitivity of suspended sediment to increases in flow. The exceptionally high sensitivity of suspended sediment concentrations to discharge in the Root River is caused by the prevalence of readily erodible sediment sources (large alluvial terraces, which can be natural or anthropogenic) lining the mid to lower reaches of the channel network. While we observed a considerable hysteresis of suspended sediment concentrations in the Root River, especially at upstream gages, we did not observe systematic hysteresis in the grain size distributions in transport at any gages. This indicates that while some portions of the Root River network may be limited by sediment supply at very high flows, the grain sizes transported by the river are constant.

Data generated and synthesized by the Minnesota Department of Agriculture and Fillmore SWCD demonstrate immense spatial and temporal variability in erosion rates at edge-of-field to small watershed scales. Further, these data demonstrate substantial differences in the relationship between flow and erosion between frozen and thawed soils and a significant decrease in sediment yield (sediment load divided by drainage area) from local (edge of field, 0.2 mi^2) to small watershed (6 mi^2) scales. These observations underscore the importance of constructing a sediment budget that utilizes multiple sources of information to understand sediment sources, sinks and dynamics. The flow and sediment data collected across a wide range of scales by the Field to Stream Partnership are invaluable for groundtruthing analyses and models and will be essential for documenting the effects of future changes in land and water management.

Analysis of the Stream Power Index and an extensive field campaign mapping presence/absence of Best Management Practices (BMPs) and occurrence of erosion shows that BMPs are highly effective at reducing soil erosion in vulnerable locations throughout the watershed. Specifically, the probability of erosion increases by 3.9% for each percentile in the Stream Power Index and probability of erosion is 2.4 times higher at sites lacking BMPs compared to sites with BMPs. Local-scale soil loss predictions using the Universal Soil Loss Equation within a 15-year watershed scale SWAT simulation corroborate high erosion rates in the lower, steeper portions of the watershed. Thus, multiple analyses point to the fact that BMPs targeted at reducing agricultural field erosion (e.g., contour and reduced tillage practices, cover crops) as well as BMPs that reduce delivery of sediment to the streams (e.g., grassed waterways, water and sediment control structures, buffer strips and sub-surface saturated buffers) are both essential for reducing sediment loading throughout the Root River watershed. The effects of such practices will be most readily observed at small spatial scales.

Sediment fingerprinting represents a line of information that is entirely independent of other estimates of sediment sources (e.g., lidar, air photo, or field measurements). Yet, the general conclusions of our extensive fingerprinting analysis are highly consistent with findings from other sources of information. Specifically, fingerprinting results indicate that nearly half (44%) of sediment that reaches the mouth of the Root River watershed has been derived from agricultural fields within the past two to four decades. The percentage of sediment derived from agricultural fields during the past few decades varies throughout the watershed, from 60-70% at small watershed scales to 25-30% for large sub-watersheds. Also, nearly half (43%) of the sediment that reaches the mouth of the Root River is derived from channel sources, specifically, bank erosion. Based on their Beryllium-10 concentration, much of the sediment identified as coming from bank sources appears to have been initially derived from agricultural fields, presumably within the past 150 years, but has been temporarily stored in, and reworked from, floodplains and alluvial terraces.

River channels typically comprise less than 1% of a watershed in terms of areal extent, but are often among the most dynamic portions of the landscape where the confluence of all flow and sediment transport are densely concentrated. This is found to be especially true in the Root River, where channel widening and lateral migration of channels into tall banks (terraces) represents a primary sediment source. We have conducted an extensive analysis of historical changes in channel width and lateral channel migration rates over the past 8 decades in the mainstem Root River and major tributaries. Results demonstrate considerable variability in both width and migration rate, with a slight trend of widening, especially in the past decade. Channel migration rates are consistently higher in the transition

reaches of the Root River, where the steep bedrock reaches meet the relatively low gradient, wide alluvial valley of the main Root River.

One overarching implication of this sediment budget is that sediment from agricultural fields is not negligible. Field-derived sediments constitute nearly half of the contemporary sediment load. Therefore, additional agricultural field management and best management practices are essential for reducing sediment loading throughout the watershed. We have identified many locations that are most in need of BMPs (using SPI, USLE). However, small watershed monitoring has shown that BMPs must be adequately maintained to remain effective. Effects of improved field management practices would be most easily measured at small spatial scales and will be increasingly difficult to discern at the Houston or Mound Prairie gaging sites. This is due to the low proportion of sediment delivered to those lower sites and the fact that sediment cycles, perhaps multiple times, between channel transport and channel-floodplain storage during its slow journey from its point of origin to the mouth of the watershed. Another overarching implication of this work is that channel widening and meander migration are also important sediment sources and comprise nearly half of the sediment load at Mound Prairie. To some extent, bank erosion is a natural process and has been a net source of sediment in the Root River basin for thousands of years. At the same time, bank erosion has likely been exacerbated in recent years due to the presence of legacy sediment that comprises the tall and pervasive alluvial terraces that we have mapped throughout the upper mainstem Root River and tributaries. In addition, the potential for bank erosion has been amplified in recent decades as human-exacerbated climate change and increased efficiency of agricultural drainage have resulted in significantly higher flows.

Given the (i) considerable amount of legacy sediment stored throughout the Root River channel-floodplain network, (ii) naturally high rates of channel migration and bank erosion, (iii) repeated cycling of sediment in and out of storage within the channel-floodplain network, and (iv) expectation that climate change will continue to increase the amount and intensity of rainfall, significant reductions in sediment loading may not be observable at the mouth of the watershed for many decades. Yet, conservation practices and reductions in erosion will improve, and should be measurable within several years to a decade at smaller scales (<100 km²), and are ultimately essential for improving water quality and aquatic habitat in the mainstem river over the long term.

2. Introduction

Rivers throughout Minnesota have been degraded by a combination of stressors such as altered hydrology, habitat loss, excess nutrients, and elevated Total Suspended Solids (TSS). Each of these stressors, and others, appear to have negatively impacted biological communities in the Root River Basin (RRB) in southeastern Minnesota (MPCA, 2015). Many segments of the Root River are considered impaired for aquatic life, recreation and drinking water due to elevated TSS, in addition to mercury, nutrients and bacteria (MDA, 2012). Higher turbidity and sediment loads in streams have direct negative impacts on fish (e.g., Brown trout, Common carp, Golden red horse, and Small mouth bass (MPCA, 2012; Chapman, 1996)) and macroinvertebrates as well as indirect negative effects via habitat loss, competition with invasive species, and trophic level interactions (Wang, et al. 2001; MSUM and MPCA, 2009; Jamieson, 2004; Sutherland and Meyer, 2007; USGS, 2014).

The Clean Water, Land, and Legacy Amendment has provided Minnesotans an extraordinary opportunity to make a significant and lasting improvement in environmental quality. Excessive sedimentation is

among the top water quality concerns. However, decades of watershed-scale sediment research have demonstrated formidable challenges in determining sources of sediment at the watershed scale (Dietrich, et al. 1982; Beach, 1994; Trimble, 1999; Trimble and Crosson, 2000; Collins and Walling, 2004; Wilcock, 2009; Belmont et al., 2011; Smith et al., 2011; Stout et al., 2014). First and foremost, the sources themselves are difficult to measure because they are typically comprised of small rates of erosion and deposition that are highly variable in both time and space. In addition, the routing of sediment through the landscape and channel-floodplain network can significantly influence sediment fluxes and lag times experienced by sediment within the system. In addition, sediment is a natural constituent of aquatic ecosystems and natural 'background' rates of sediment vary considerably, so determining the amount of sediment that exceeds natural conditions is challenging (Gran et al., 2011).

Excessive sedimentation in the Root River watershed could be attributed to a variety of different sources, each of which may imply a different sediment reduction strategy moving forward. A primary distinction to be made is the proportion of sediment derived from terrestrial soil erosion versus streambank erosion. To the extent that terrestrial soil erosion is a significant sediment source, it is important to identify erosion hotspots and determine which Best Management Practices (BMPs) might most effectively mitigate erosion. To the extent that streambank erosion is a significant sediment source, it is important to understand where easily erodible sediment is stored near the stream network, the extent to which that sediment is natural or derived from historic human activities in the landscape and what practices might effectively address those sediment sources. This project has generated and compiled a wide variety of datasets that span multiple temporal and spatial scales to provide basic insights into the sources and transport pathways of sediment within the Root River watershed for the purposes of guiding future management, conservation and restoration decisions.

The objectives of this project were to:

- 1) Develop an integrated sediment budget, which compiles multiple, redundant sources of information
- 2) Conduct a hydrologic analysis to understand if and how discharge and related metrics (e.g., runoff ratio) have changed over time throughout the watershed.
- 3) Develop a conceptual model illustrating how sediment is routed downstream.
- 4) Develop and distribute computational tools that can be used for source identification and feature extraction from high resolution (lidar) topography data.

Throughout the process of conducting this research we have been in active, two-way communication with Minnesota Department of Agriculture and other state and local agency staff. As a result, a variety of additional questions have emerged which have helped guide our approach and compelled us to include numerous additional analyses in working towards the ultimate goal of understanding sediment dynamics in the Root River watershed.

3. Description of the Study Area

The Root River Basin (HUC 07040008) covers about 4,300 km² (1,663 square miles) within the Upper Mississippi River Basin, ranging from 438 to 191 meters (1437 to 625 feet) above sea level. Six Minnesota counties (Dodge, Mower, Olmsted, Winona, Fillmore, and Houston) contain varying parts of the RRB in addition to a small portion of the basin in Winneshiek County, Iowa (Figure 3.1). The western

third of the basin is characterized as part of the 'Western Corn Belt Plains' ecoregion and is underlain by fine-grained glacial till, similar to much of the rest of south central Minnesota (MPCA, 2012). This portion of the basin is relatively flat and is dominated by row crop agriculture (Figure 3.2). Stream channels in this zone are characterized by relatively low gradients. The remainder of the Root River Basin lies within the 'Driftless Area' ecoregion that has not been glaciated within the past 500,000 years (Knox, 1987; Troelstrup and Perry, 1989; Trimble, 2013). The geology of this zone is dominated by Paleozoic limestone and dolostone with occasional outcrops of St. Peter sandstone (Figure 3.3). The topography of this zone is characterized by relatively steep, forested hillslopes with row crop agriculture and pasture on lower sloped terrain. Many of the stream channels in this zone initiate as relatively low gradient streams but transition to steep channels and confined within narrow valleys and ultimately debouch into lower gradient, unconfined valleys extending from the unconfined mainstem Root River. The presence of Karst topography forms underground streams, springs, and sink holes, which presents limited capacity for development of lakes (Figure 3.4). Flow is rapidly routed through the complex and poorly mapped Karst network to surface water (MPCA, 2011) and interaction between the surface and groundwater is exceptionally difficult to quantify (MDA, 2012).

The longitudinal profiles (river elevation with distance downstream) of the Root River and major tributaries exhibit several significant anomalies (Figure 3.5), which are understood to influence sediment transport and the relationship between the channel and floodplain (Mackin, 1948; Wobus et al., 2007; Belmont, 2011). Specifically, plots of channel slope versus upstream contributing drainage area indicate areas where slope increases in the downstream direction, which increases sediment transport capacity, and other areas where slope decreases rapidly, which decreases sediment transport capacity, potentially causing deposition (Figure 3.6). Similar trends are observed in each of the Root River tributaries and implications for these sediment transport discontinuities are discussed in multiple sections below.

Modern and future sediment dynamics in the Root River watershed are influenced by the legacy of historical land cover and land use. Prior to Euro-American settlement the watershed was dominated by upland prairie and oak plant communities (Dogwiler, 2010). However, since early settlement in the 1850's the land has been cleared for agricultural production, initially wheat (Troelstrup and Perry, 1989). The impacts of agriculture in the early 1900s are qualitatively described in the first reconnaissance of the Root River by Thadeus Surber (1924). Surber described incision in the tributaries of the river and an increase in the magnitude of floods. More recently, Knox (2006) described how the development of Euro-American agriculture caused detrimental impacts on runoff, soil erosion, and river morphology throughout the region. Significant changes in agricultural management did not begin until the 1940s, driven by recommendations from the Soil Conservation Service. Improved conservation and field management practices appear to have reduced erosion from agricultural fields throughout the region (Trimble, 1999; Knox, 2006).

Stout and Belmont (2014) observed that many fluvial terraces (old floodplains) exist within the river valleys of the Root River and major tributaries. These terraces represent large deposits of sediment, by definition taller than average streambanks, that are highly vulnerable to erosion by the stream. Stout and Belmont (2014) developed the TerEx Tool to systematically map and measure the height of these terraces relative to the local river (Figure 3.7). Results indicated that indeed, tall terraces abound throughout the stream network, with especially high prevalence of terraces found in the South Fork, Rushford Creek and Money Creek. Some portion of these terraces have likely formed naturally as old

floodplains have been abandoned and incised through by the river or natural impoundments temporarily blocked flow and sediment transport of the channel. However, many of them likely represent the human influences of elevated sediment delivery from the uplands in the late 1800s and early to mid-1900s combined with human-constructed impoundments and flow constrictions. In any case, results from terrace mapping clearly demonstrate the prevalence of readily erodible fluvial terraces throughout the watershed.

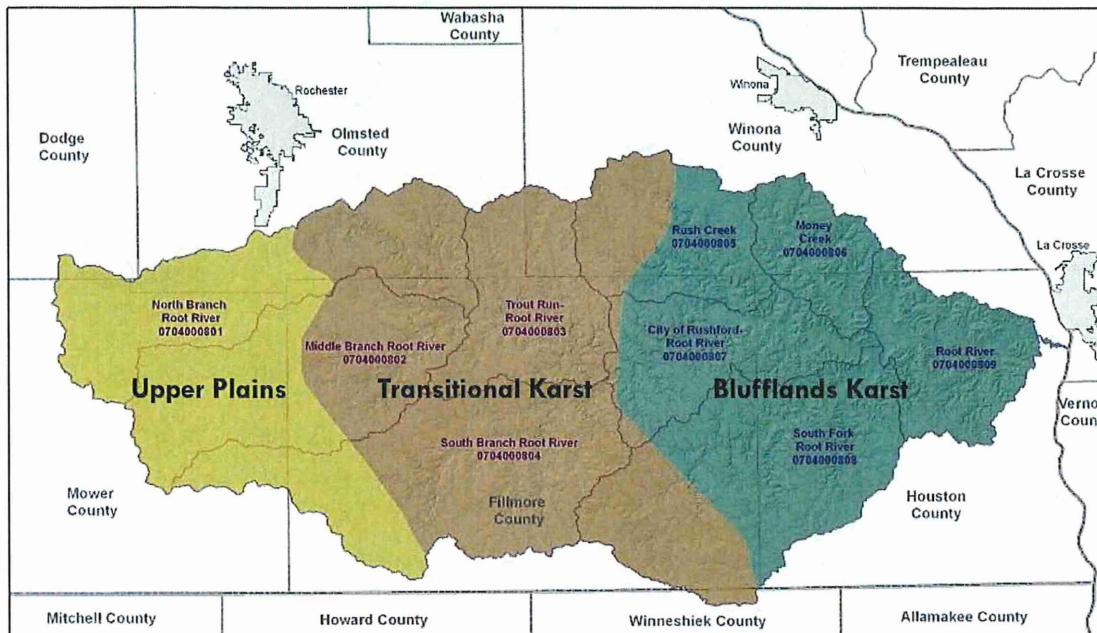


Figure 3.1. Location of the Root River Basin in Southeastern Minnesota and Northeastern Iowa, illustrating approximate boundaries between distinct geomorphic regions. Adapted from Rasmussen, 2011.

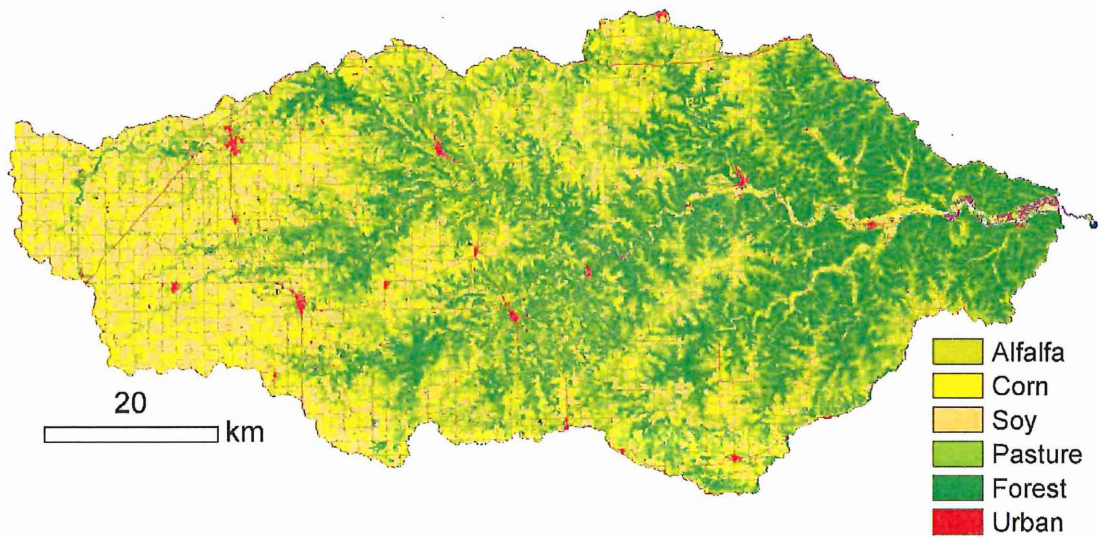


Figure 3.2. Major Landuse/landcover in the Root River Basin.

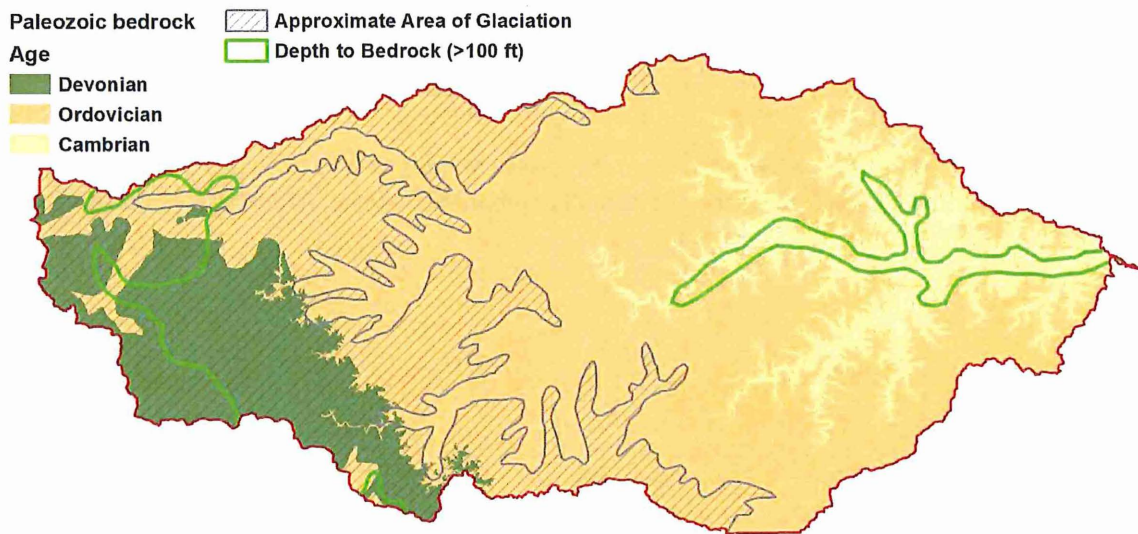


Figure 3.3. Glacial and bedrock geology of the Root River basin. Data for map compiled and adapted by Toby Dogwiler.

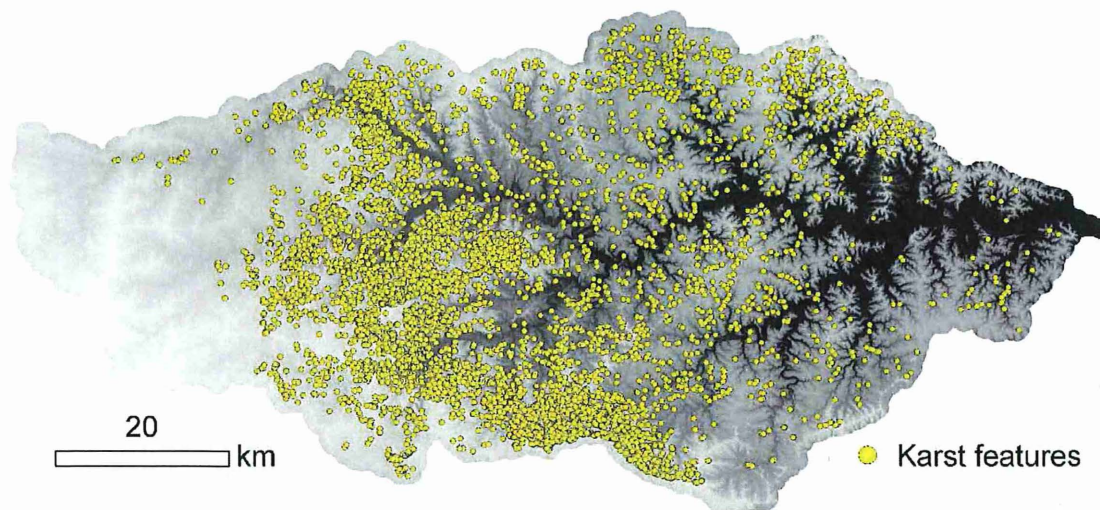


Figure 3.4. Location of karst features overlaid on topography (data from MN DNR).

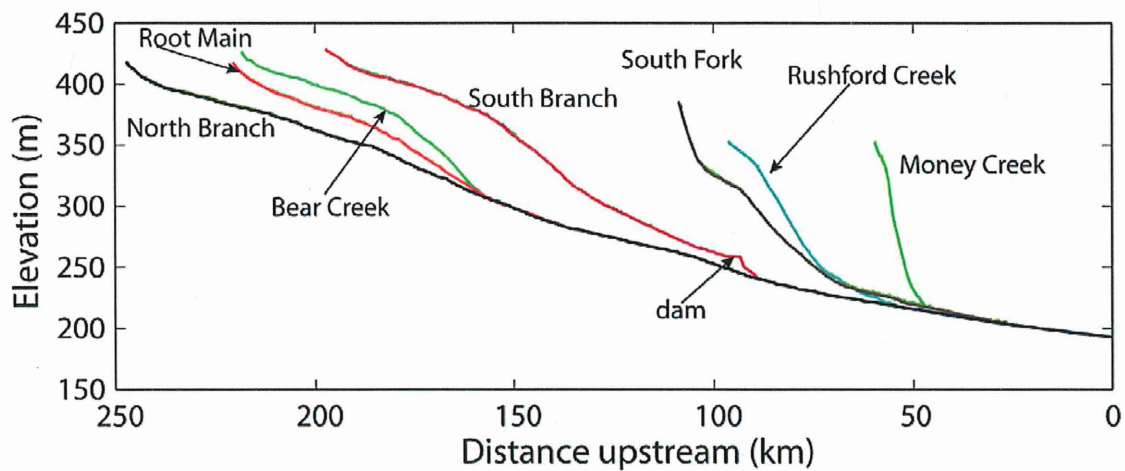


Figure 3.5. Longitudinal profiles of the Root River watershed and each of the major tributaries.

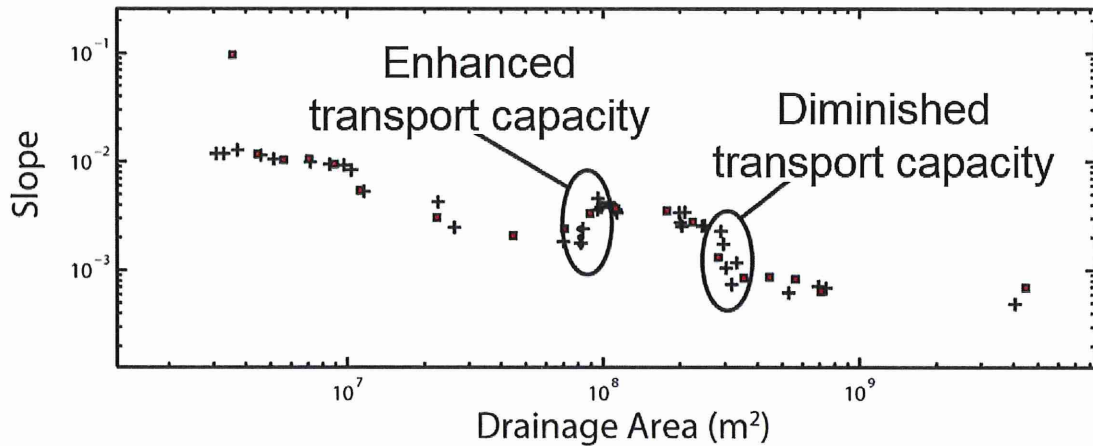


Figure 3.6. Slope-area analysis of the South Fork Root River longitudinal profile indicating two distinct sediment transport discontinuities, one at approximately 10^8 m^2 (100 km^2) where slope increases significantly, thereby increasing sediment transport capacity through the steep bedrock reaches, and another around $3 \times 10^8 \text{ m}^2$ (300 km^2) where slope decreases anomalously, thereby reducing sediment transport capacity as the river enters the wide alluvial valley.

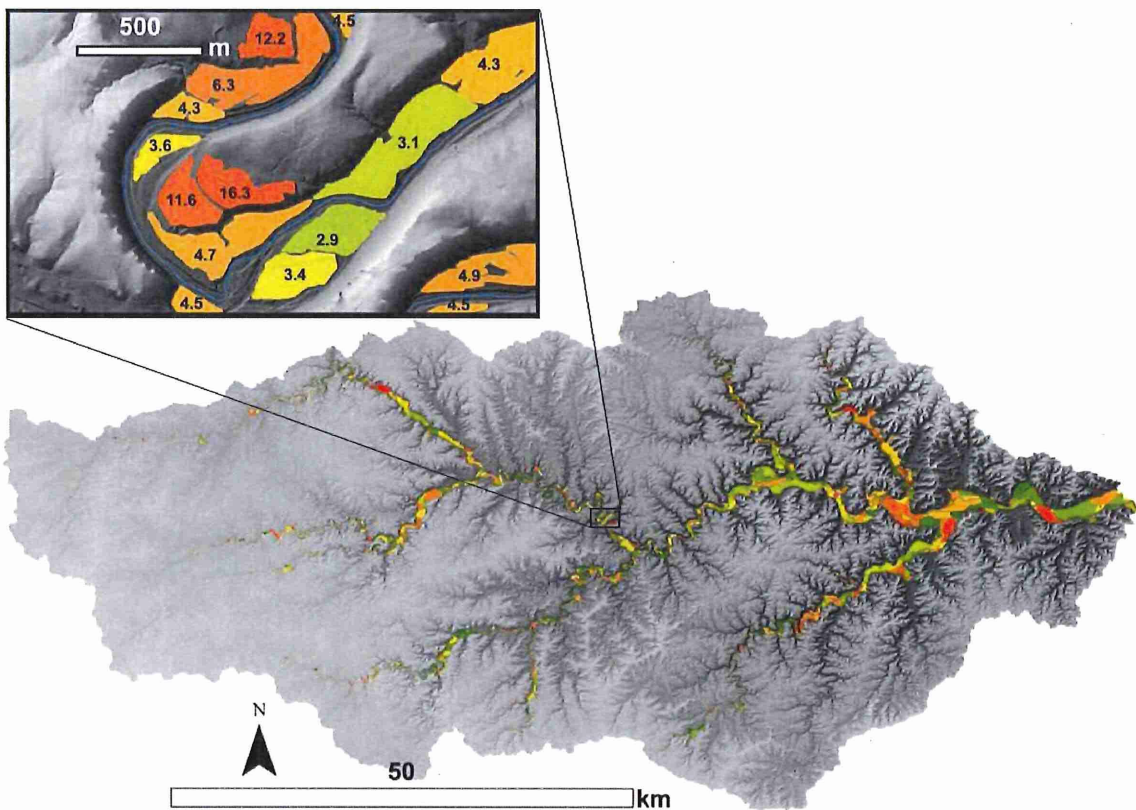


Figure 3.7. Map of fluvial terraces distributed throughout the Root River watershed, with colors illustrating the height above the local river elevation and heights shown in meters in the inset pane.

4. Hydrologic analysis

Hydrology is changing in watersheds throughout the upper midwest (Schilling et al., 2008; Schottler et al., 2014; Foufoula-Georgiou et al., 2015). Significant increases in river discharge have been observed in many systems in the past few decades. Precise quantification of the extent to which the observed increases in flows can be allocated to changes in precipitation versus agricultural drainage practices versus changes in crop type or soil organic matter content have proven challenging, but a large and growing literature has established that each of these factors have played a role.

Precipitation

Many climate change forecasts for the Upper Midwest predict increases in annual precipitation but with a shift in seasonal patterns that will leave the summer months drier with less frequent, higher magnitude storm events (WICCI, 2011). Changes in precipitation patterns have the potential to alter the sediment budget, the timing of erosion events, and discharge patterns in watersheds. To better understand how changes in precipitation patterns may have influenced the Root River sediment budget and hydrology an analysis of the frequency, magnitude, duration, and intensity of precipitation in the Upper Midwest was performed. Hourly precipitation data from 21 sites in MN, WI, ND, SD, NE, and IA from 1948 to 2013 was obtained from the National Climatic Data Center archives (Figure 4.1). An additional 19 stations (Figure 4.1) within, or near, the Root River basin also provide hourly precipitation data over the same time period; however, these stations switched the resolution of their data recording from 0.01 in (0.254 mm) to 0.1 in (2.54 mm) at some point in the period of record. The changes in resolution prevented a meaningful comparison of the data and, as such, were excluded from the analysis. The hourly precipitation data provide a high-resolution archive that is ideal for analyzing changing patterns in rainfall at multiple scales, including decadal, yearly, monthly, and per storm. Based on our analyses, the Upper Midwest, in general, and eastern and southern Minnesota, in particular, is experiencing decreasing storm durations, increasing average rainfall intensities, increasing maximum rainfall intensities, increasing rainfall per storm, decreasing frequencies of storms, and increasing average annual precipitation. The closest observing station to the Root River watershed was the Rochester Airport station. The preceding results could have been mostly discerned from analysis of just that station, but by looking at those data in the context of the other 20 stations there is more confidence that the observed trends in Rochester are representative of the broader region of southern and eastern Minnesota that surrounds it. The data demonstrate that significant changes in precipitation patterns have occurred over the past 60 years. Observed changes are consistent with predictions derived from various climate models and, as such, may lend support to forecasts of additional shifts in precipitation patterns in the coming decades. Understanding and quantifying these changes, particularly the trend of shorter more intense storms, has large implications on the sediment budget and discharge patterns of watersheds.

Changes in the characteristics of precipitation were highly variable across the region (Figure 4.1). The overall trend for the Upper Midwest is increasing amounts of total rainfall (Figure 4.2 and Table 4.1) with the greatest increase in total rainfall occurring in the fall. The general trend is also upward for both summer and spring although there is greater spatial variation and more nuance in the pattern of change. Precipitation during the winter months is decreasing. These results are similar to those of Groisman et al. (2001) who found precipitation totals during the 20th century have increased significantly (7-15%) in the contiguous United States in all seasons, except winter. They also found that the number of extreme rainfall events was growing with largest increases for the Southwest, Midwest, and Great Lakes regions.

In the Upper Midwest the increases in total annual precipitation are the result of increasing storm intensities and increasing numbers of storm events in the summer and fall. Rainfall intensities are increasing most in the spring and winter months. The characteristic of precipitation that is most prominently responsible for the increasing amounts of total annual rainfall is an increase in the average maximum hourly intensity of a storm. Increases in total annual rainfall are occurring even though storm events are decreasing in duration across much of the region. The observed pattern of increasing rainfall totals and intensities combined with decreasing storm durations is consistent with observations of an acceleration in the warming of the Earth's atmosphere and accompanying changes in the overall hydrologic cycle (Held and Soden, 2006; Villarini et al., 2001; Voss et al., 2002).

Seasonal shifts in rainfall totals are highly variable across the region. Winter and fall show the most consistent changes. The amount of total winter precipitation in the Upper Midwest is decreasing. Eighteen of the 23 sites have experienced decreases in winter precipitation totals, with statistically significant decreases at 5 of the 18 stations. The sites where winter precipitation is increasing are mostly located in the southern and southeastern parts of the Upper Midwest. Two factors likely contribute to the increases at these sites: changes in the jet stream and decreasing ice cover on Lake Michigan leading to increased lake effect precipitation events. Recent studies have documented a poleward shift in the jet stream (Archer and Caldeira, 2008; Woolings and Blackburn, 2012). When the jet stream shifts northward during the winter, it allows warm, moist air masses from the Gulf of Mexico to move into the southeastern region of the study area.

Spring and summer precipitation totals are generally increasing, but not in a statistically significant manner. Seventeen of the 23 sites are increasing in the spring and 15 of the 23 sites are increasing in the summer. Fall precipitation totals show the clearest pattern of increase, with 8 of the 23 stations experiencing statistically significant upward changes and 12 additional sites showing increases that fall below the level of statistical significance. The pattern for the amount of rainfall per event follows the same general trends as rainfall totals (winter decreasing and all others increasing or stable). However, spring shows the most significant increase while fall shows only a slight increase. The increase in the total amount of fall

precipitation is due to a combination of longer storm durations and more storm events. Conversely, in the spring the changes are due to more rain per event.

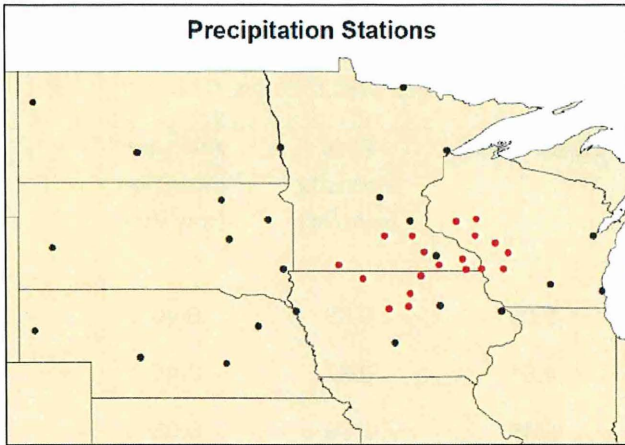


Figure 4.1. Map of the weather stations in the Upper Midwest with hourly precipitation data used in this analysis. Black dots show locations that record at 0.01 in (0.254 mm) for the entire time period. Red dots show stations that switch from 0.01 in to 0.1 in (2.54 mm) resolution sometime between 1963 and 1990. Stations that switched to the lower resolution (i.e., 0.1 in) were excluded from the study because the resolution prevented comparison of precipitation duration, magnitude, and intensity across the full period of record.

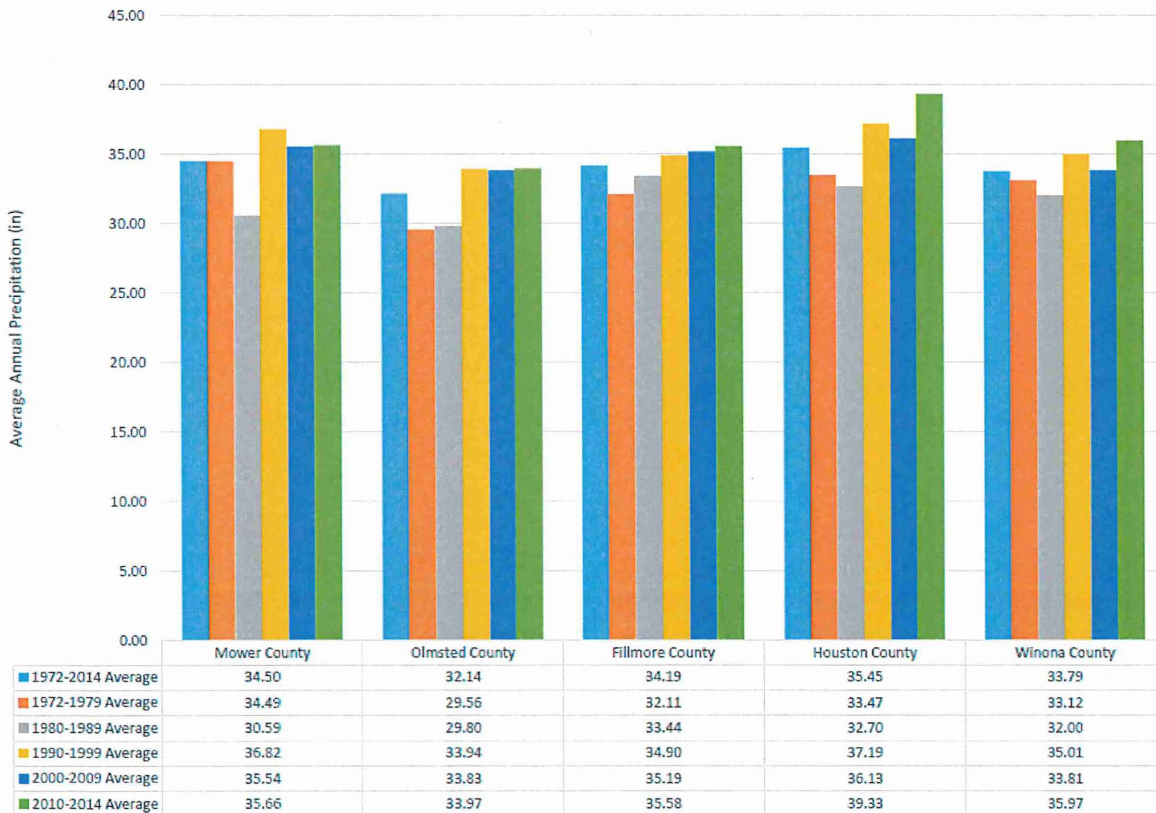


Figure 4.2. Decadal precipitation averages for the five southeastern Minnesota counties that comprise most of the Root River watershed. In all cases, the lowest decadal average since 1990 is always higher than the highest decadal average for the preceding decades. In other words, the wettest decade preceding 1990 is always drier than the driest decade after 1990.

Table 4.1. Precipitation summary for the precipitation data from Rochester, MN. Rochester's trends are generally representative of southeastern Minnesota. The data exhibit a strong seasonal component with June, July, and August experiencing the most intense and highest total precipitation.

	Average Total Rainfall per Storm (mm)	Total Monthly Rainfall (mm)	Duration (hr)	Max Intensity (mm/hr)	Average Intensity (mm/hr)
January	2.30	22.10	5.09	0.69	0.40
February	2.37	21.08	4.61	0.82	0.45
March	4.06	48.01	5.45	1.39	0.65
April	6.21	82.04	5.33	2.18	1.05
May	6.37	91.95	4.04	3.02	1.45
June	7.99	119.13	3.48	4.46	2.06
July	9.10	116.08	2.98	5.63	2.82
August	9.45	115.06	3.58	5.09	2.25
September	7.20	87.88	3.92	3.40	1.58
October	5.28	56.90	4.83	1.87	0.84
November	4.79	49.02	6.07	1.34	0.61
December	3.02	30.99	5.38	0.86	0.44

Flows

Significant increases in high and low flows have been observed in the Root River Basin. Specifically, Stout et al., (2014) demonstrated a significant increase in flows in the Root River over the past two decades. High flows (defined here as the flows that were exceeded only 10% of the time in any given decade) had increased by 60% and low flows (defined here as the flows that were exceeded 90% of the time) had increased by approximately 80% (Figure 4.3).

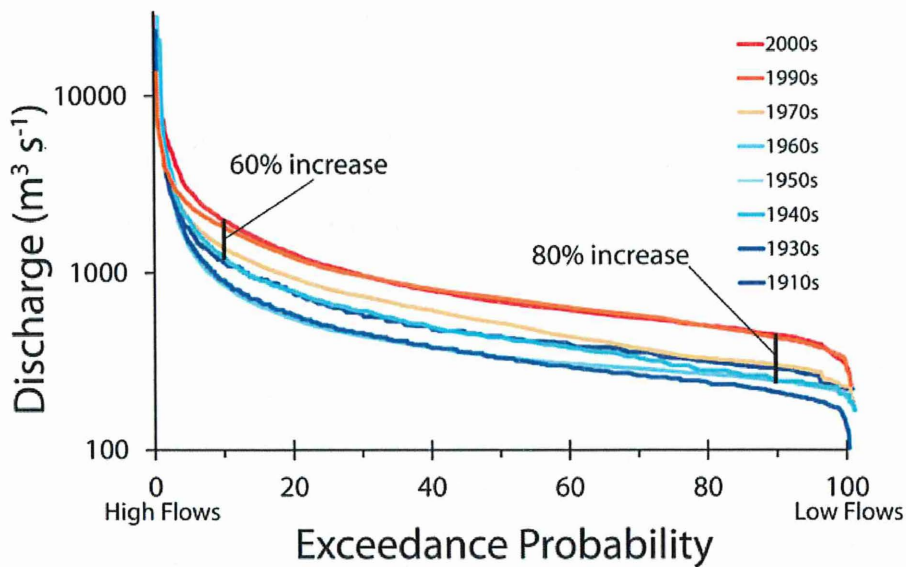


Figure 4.3. Flow duration curves for the Root River gage near Houston, from 1910s through 2013.

To better understand how, when and why these flows have increased, we analyzed how the timing of flows has changed. Figure 4.4 shows hydrographs for daily averaged flows that have been averaged on a decadal basis. Results indicate that much of the increase in high flows has occurred in the April to June time period (days ~ 200 – 250 on x axis). Figure 4.5 further shows that the cumulative flow volume has increased considerably in the past few decades. The exact date of the center-of-timing of flow for each decade is presented in Table 4.2. This is contrary to what is observed in many other temperate systems throughout North America as the center-of-timing of flow is typically observed to be occurring earlier due to earlier snow melt. Some evidence for earlier snow melt exists, as indicated by the earlier inflection point in Figure 4.6, but this effect is offset by the dramatic increase in late spring to mid-summer rainfall events.

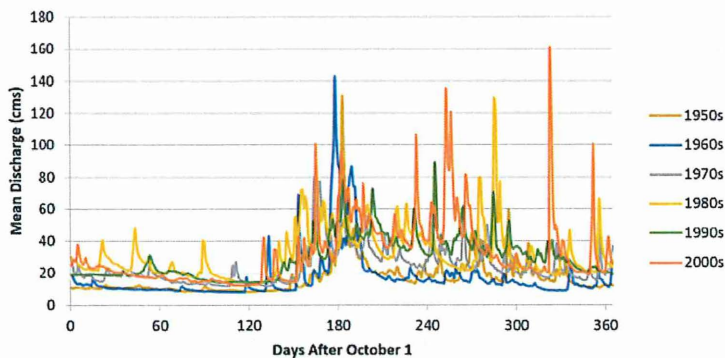


Figure 4.4. Mean daily flows averaged on a decadal basis for the USGS gage near Houston. The y-axis depicts the water year, 0 being October 1, 180 being March 29, and 365 being September 30. Thus, the significant increase in mid to high flows observed in the flow duration curves is due to increases in flow during the April to June time period.

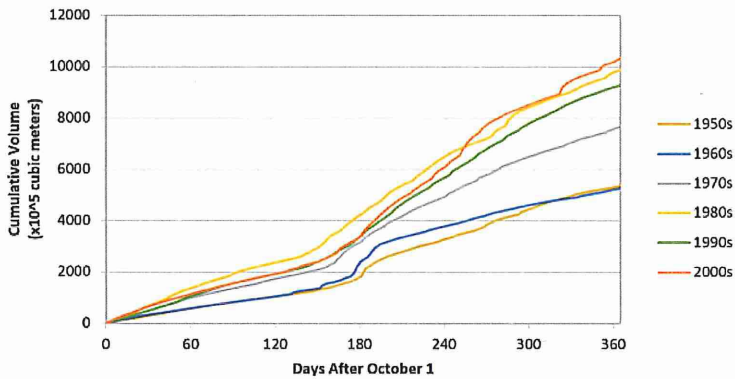


Figure 4.5. Decade-averaged cumulative flow volume for each decade throughout the water year for the USGS gage at Houston. The y-axis depicts the water year, 0 being October 1, 180 being March 29, and 365 being September 30. Total flows have increased considerably since the 1970s.

Figure 4.6 shows a consistent increase in the number of days in each decade that the 5% exceedance flow (7320 cfs or 207 cms, computed for the entire time period of interest, 1950-2013) was exceeded. Considering the observations provided above, it is expected that most of this increase in flow is accounted for by increases in late spring to mid-summer rainfall events. However, sub-surface tile drainage, which has been shown in other basins to increase the precipitation-runoff relationship (Schottler et al., 2014; Foufoula-Georgiou et al., 2015; Foufoula-Georgiou et al., in press; Belmont et al., in press), may also contribute to the observed increase in flows.

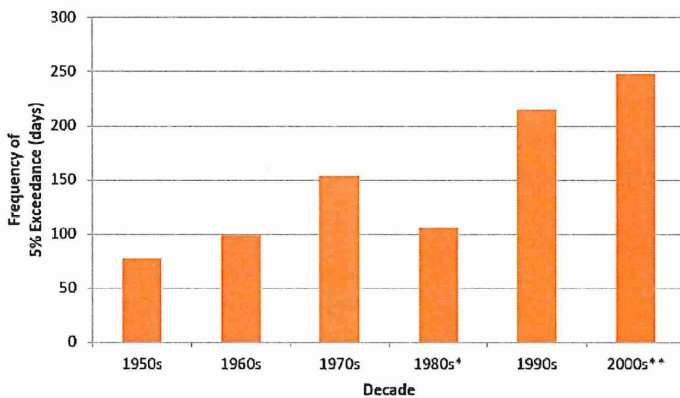


Figure 4.6. Positive trend in the frequency at which the 5% exceedance flow (7320 cfs or 207 cms) occurred in the past 6 decades for the USGS gage near Houston.

* Incomplete record for 1983-1990
 ** Incomplete records for 2001-2004, 2009-2011

5. Discharge-TSS relationships

Motivation for analyzing discharge-TSS relationships

Concentrations of suspended sediment transport depend not only on the transport capacity of the river, but also on the supply of fine sediment from the watershed (Asselman, 2000; Fan et al., 2012). The relationship between river discharge (Q) and concentration of suspended sediment (TSS), known as the empirical sediment rating curve, is one key metric for evaluating the suspended sediment transport regime. The Q-TSS curves typically take the form of a power function:

$$TSS = aQ^b$$

Where a and b are the sediment rating coefficient and exponent (Asselman, 2000; Fan et al., 2012; Hu et al., 2011; Mimikou, 1982; Sadeghi et al., 2008; Syvitski et al., 2000; Warrick, 2014; Yang et al., 2007). Some studies have demonstrated improved regression fits to the data by subdividing Q/TSS data by rising limb and falling limb in an effort to account for sediment supply limitation within a storm event (Walling, 1974; Loughran, 1976; Walling and Webb, 1982; Klein, 1984; Asselman, 2000; Sadeghi et al., 2008; Soler et al., 2008; Fan et al., 2012). Here, we examine Q-TSS relationships at several gages throughout the Root River Basin to identify if and how the strength or shape of the relationships vary spatially. This work takes place within a much broader analysis by Angus Vaughan (USU graduate student), who is examining Q-TSS relationships throughout Minnesota in an effort to identify watershed or stream network characteristics that influence suspended sediment regimes.

Methods for analyzing discharge-TSS relationships

We obtained Q and TSS data from the Minnesota Department of Natural Resources (MDNR) and Pollution Control Agency (MPCA) Cooperative Stream Gaging website and Minnesota Department of Agriculture. We extracted daily mean discharge data that correspond to each of the available TSS measurements. We normalized discharge by the geometric mean of the discharge for each gage, as suggested by Warrick (2014). The normalization allows for comparison between basins of different size and also decreases the auto-correlation between the coefficient and exponent parameters.

We fit linear least-squares power function regressions to the normalized and log-transformed Q and TSS data, generating \hat{a} (intercept) and b (slope) values for each rating curve. However, in cases where the Q-TSS relations are not well represented by a single log-log linear regression we split the data at breakpoints located at the transitions in slope on applicable rating curves. To identify breakpoints, we used the Python programming language function “`scipy.interpolate.splprep`”, which implements the spline interpolation method outlined by Dierckx (1975).

We further split the dataset into rising versus falling limb based on the derivative of the discharge time series. For relations exhibiting breakpoints, we classified points to the left of the lowest breakpoint as “low flow”, and excluded them from further analysis. We classified the remaining points as rising limb or falling limb by whether the mean daily discharge for the data point was larger or smaller, respectively, than the previous day’s discharge. We fit separate regressions to the rising and falling limb data.

Q-TSS relation results

We observe hysteresis in all four of the Q-TSS relations show in figure 5.1, as indicated by the rising limb (red) regression plotting consistently above the falling limb (blue) regression. The hysteresis is most pronounced at the two sites that are relatively high up in the tributary systems (South Branch at Carimona and South Fork at Amherst). Presumably related, both of these sites exhibit a distinct relationship at relatively low flows (shown in green, excluded from regressions). The South Branch at Lanesboro and the mainstem Root River at Mound Prairie both exhibit simple power functions with the rising limb regression slightly steeper than the falling limb.

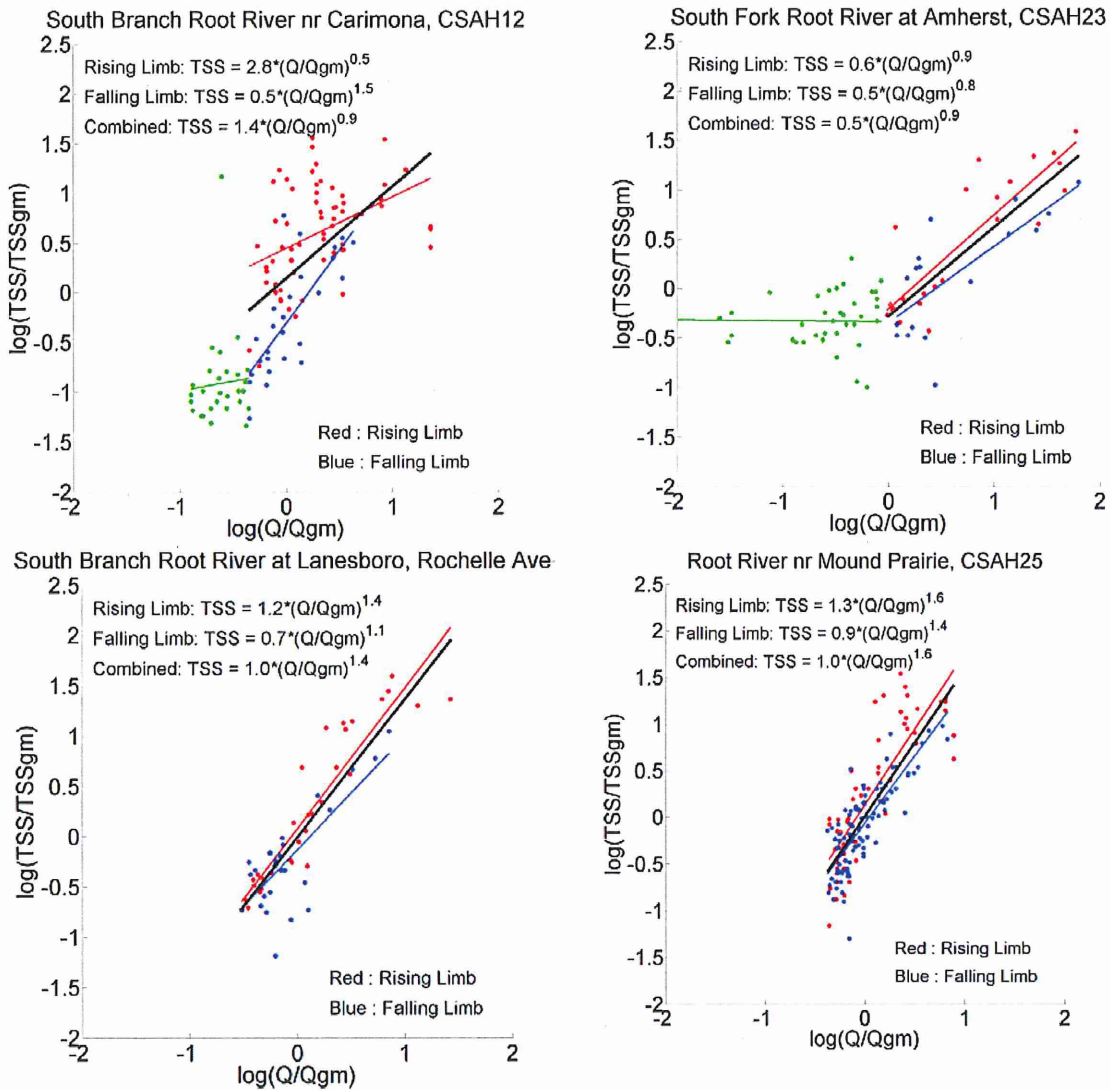
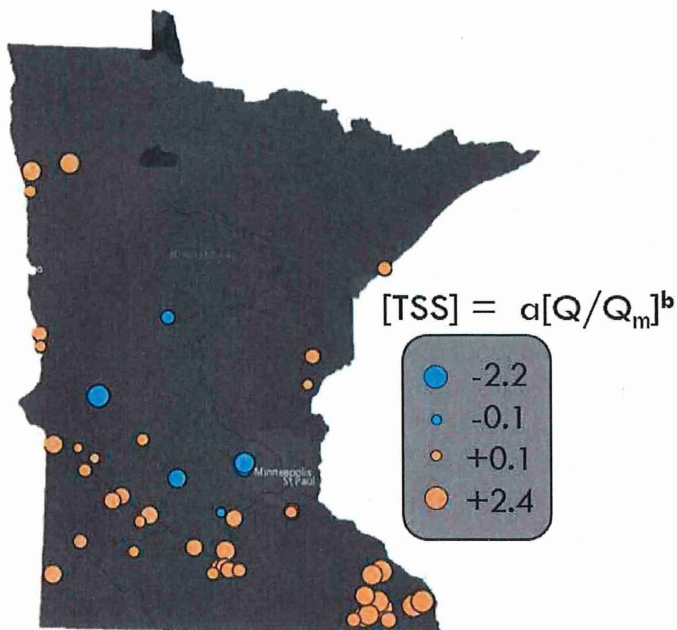


Figure 5.1. Q-TSS rating relations at four Root River gages. Data have been normalized by the geometric mean of the dataset and log transformed to standardize regressions for comparison. Thus, a value of 0 on either axis is the geometric mean of each sample dataset.

The Q-TSS relations in the Root River Basin are among the steepest observed in the State of Minnesota, as shown in Figure 5.2, in which the area of each dot is scaled to the magnitude of the exponent (b). Sites lower in the Root River watershed have considerably steeper Q-TSS relationships, suggesting that near-channel sediment sources are highly sensitive to flow in these mid to lower reaches.

Figure 5.2. Rising limb power function exponents from analysis of Q-TSS relationships through the State of Minnesota.



6. Monitoring of sediment gages and springs

The Root River Basin has been monitored for flow and sediment at multiple locations, though the period and frequency of monitoring varies considerably. While instantaneous suspended sediment measurements are valuable, as discussed above and further below, annual loads computed at gages over recent years are essential to provide a mass balance constraint on the sediment budget. At the time of writing, sediment loads for the watershed are available from 2009 to 2014 (Table 6.1). Fortunately, this time period represents two low flow years (2009 and 2012), three moderate flow years (2010, 2011 and 2014) and one high flow year (2013). The mean peak flow value for the Root River between 1940 and 2014 is 11,070 cfs.

Table 6.1. Sediment loads computed at Mound Prairie, data from Mike Walerak (MPCA)

Year	Total Annual (Mg)	Peak Flow (cfs)
2014	235,456	9,400
2013	657,046	22,800
2012	28,530	4,250
2011	268,671	12,000
2010	238,992	13,900
2009	94,165	4,070
Average	253,810	11,070

An extraordinary amount of sediment monitoring data at edge of field and small watershed scales are also available for recent years, thanks to the efforts of Minnesota Department of Agriculture and Fillmore County SWCD (Figures 6.1 and 6.2). Edge of field monitoring data, synthesized here as annual loads, illustrate the immense inter-annual variability observed at small scales and highlight the fact that

the vast majority of erosion takes place after soils have thawed, despite the fact that a significant proportion of flows may occur while soils are still frozen. Further, sediment loads computed across a wide range of scales show a significant decrease (~50% decrease) in sediment yield (load divided by upstream contributing drainage area) between the smallest scales (<0.2 square miles) and the next smallest monitored scales (6 square miles), sediment yields are relatively constant at progressively larger scales (300 square miles, 1250 square miles, 1600 square miles). While data at each of these scales are only available for 2013 and 2014, the same pattern was observed in both years and we expect that the general trend is robust. The trend indicates a considerable decrease in sediment delivery between very small (<0.2 mi²) and moderately small scales (< 6 mi²). Further, near-channel sediment sources (bank erosion) are significant sediment sources at moderate to large spatial scales, largely offsetting the decrease in sediment delivery from uplands that occurs due to increased sediment storage between small and large scales (Walling, 1983; De Vente et al., 2007). While this explanation for the general trend observed here can only be considered as a hypothesis based on these data alone, additional lines of evidence, discussed below, corroborate this explanation.

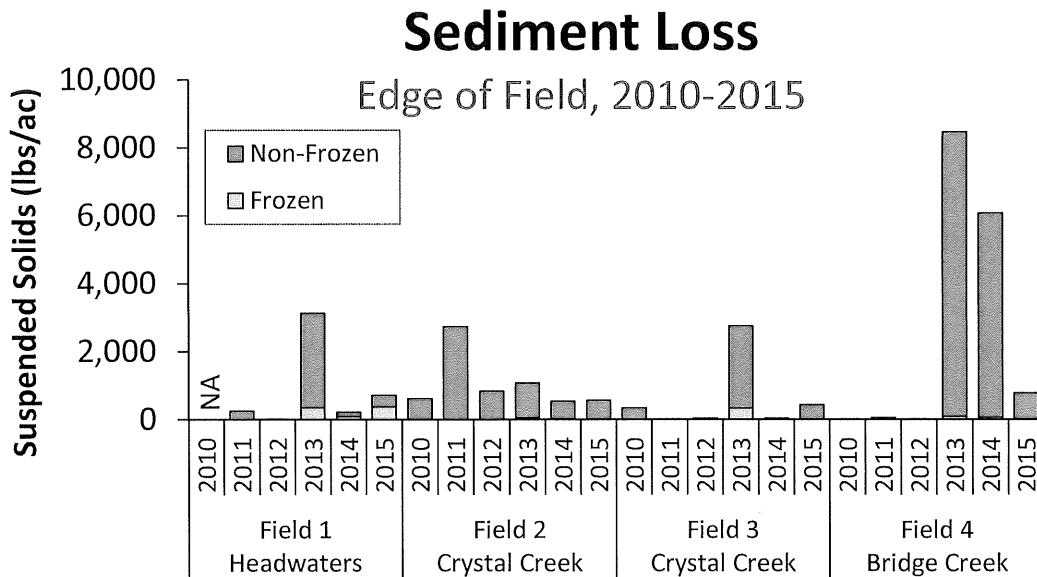


Figure 6.1. Annual suspended solids measurements from edge of field monitoring. Figure from Kevin Kuehner, MDA.

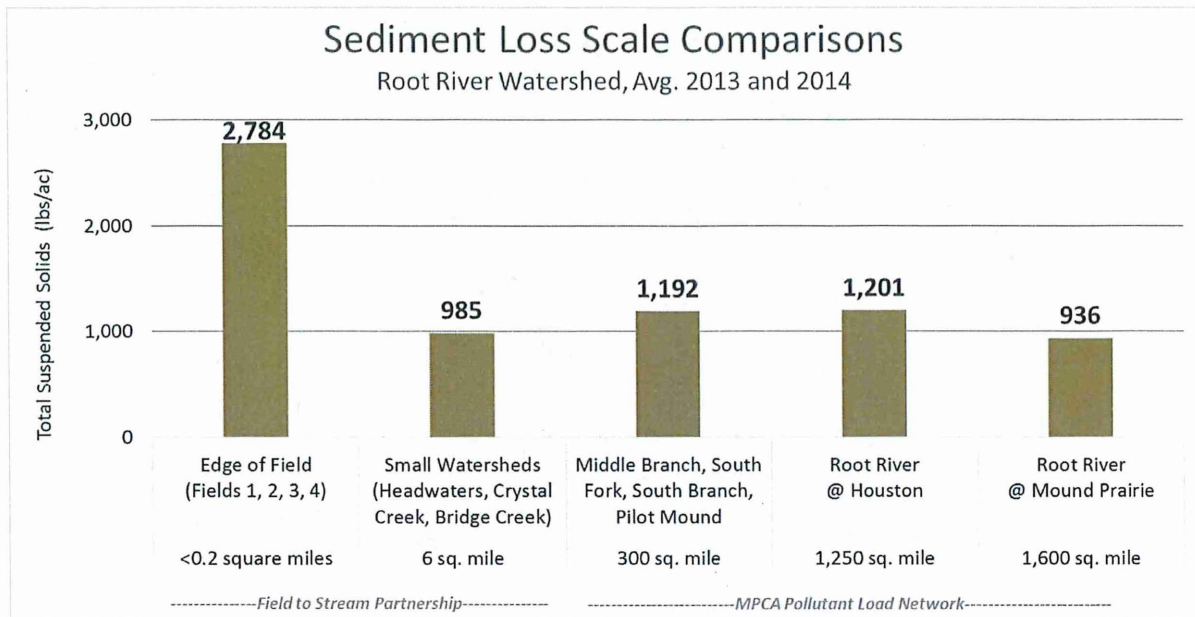


Figure 6.2. Figure from Kevin Kuehner with data from Fillmore SWCD, Minnesota Department of Agriculture and MPCA Pollutant Load Network.

Historical monitoring of discharge and suspended sediment provide additional insight into longer term and higher temporal resolution dynamics. The US Geological Survey conducted intensive monitoring of Suspended Sediment Concentrations (SSC) from 1968 to 1981. SSC and TSS are often used interchangeably in the literature (Gray et al., 2000), but there is an important methodological distinction between the two. Specifically, SSC data are obtained by measuring the dry weight of all the sediment from a known sample volume, whereas TSS data are obtained by measuring the dry weight of sediment from a known (subsample) volume of the original sample. Thus, for samples containing substantial proportions of sand, TSS values tend to be lower than the corresponding SSC values. For this reason, the SSC values presented in Figure 6.3 are not directly comparable to other TSS data presented throughout this report. But the results show two trends that are noteworthy. First, there is a considerable seasonality to the SSC data, such that virtually all of the high SSC values occur in the spring or summer. Second, relatively high SSC values occur even at relatively low flows (<2000 cfs, well below the mean annual flow of the Root River). These results suggest that it may not be feasible to reduce sediment loads in the lower reaches of the mainstem Root River by simply reducing flows via stormwater management practices, as has been suggested for other watersheds in south central Minnesota (Belmont et al., 2011; Cho et al., in prep). While far fewer data are available for recent years, Figure 5.1 shows that the highest TSS concentrations occur at relatively low discharges (just above the mean flow for the sample dataset, indicated as 0 on the x-axis).

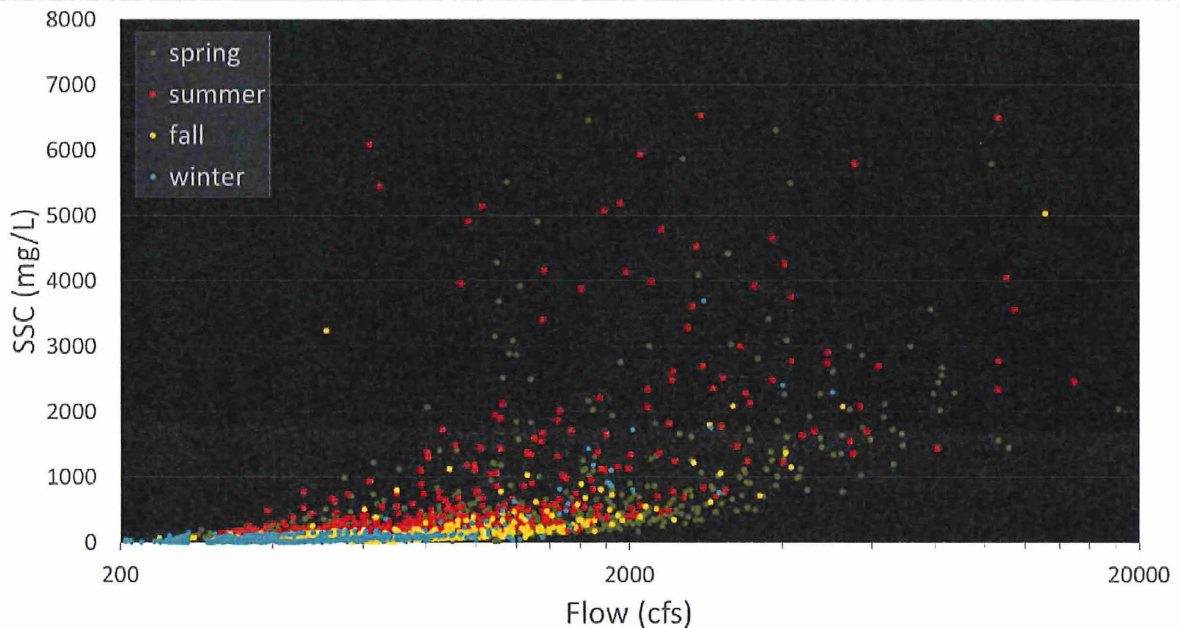


Figure 6.3. Relationship between river flow and Suspended Sediment Concentration from the Root River gage near Houston. Data from USGS, 1968 – 1981.

Sediment Yield of Springs

As described above, the Root River watershed has unique characteristics of geology, geomorphology, and especially karst hydrology relative to other major watersheds in Minnesota. The karst hydrology includes subsurface flow paths that potentially bypass surficial barriers to sediment transport and BMPs and could be important pathways along which sediment is transported from the upland areas to the floodplain. Luhmann et al. (2010) provide a framework for segregating springs in southeastern Minnesota based on their "thermal effectiveness". They characterize these springs in two groups, termed "thermally effective" and "thermally ineffective". The thermally ineffective springs are associated with localized recharge and with surface water directly entering subsurface conduits. As such, these flow paths presumably provide little opportunity for suspended sediment to be filtered out within the subsurface. The thermally ineffective springs include two types: "pattern 1" and "pattern 2", which are delineated based on the scale of their variability.

Pattern 1 springs have the most potential for discharging large amounts of sediment because they exhibit event-scale variability in flow and physicochemistry—including suspended sediment concentrations. Thus, we focused our sampling at Pattern 1 springs, which have the potential to be significant conveyors of suspended sediments from upland areas to the floodplain. As part of our source sampling campaign we collected TSS samples using autosamplers from both base flow and storm-induced flows at selected Pattern 1 springs within the watershed. We selected the springs based on consultations with Jeff Green (Karst Hydrogeologist, Minnesota Department of Natural Resources and Dr. Calvin Alexander (Professor, University of Minnesota, Department of Geology and Geophysics).

During spring, summer, and fall of 2014 and spring 2015 we deployed autosamplers at four Pattern 1 springs north of Rushford, Minnesota (Figure 6.4). Baseflow conditions at all the springs had TSS values of 0.0 mg/L. During 2014, no high flow events occurred during our period of monitoring. In the late spring and early summer of 2015 we were able to capture some moderately high flow events caused by storm events. None of the events yield significant amounts of TSS and many barely got above 0.0 mg/L Table 6.2. As a result, we have concluded that although springs may occasionally yield high amounts of sediment during extreme events (as has been qualitatively documented by various workers on a number of occasions), they are unlikely to be significant contributors of sediment to surface streams over time.

Table 6.2. Total Suspended Solids (TSS) concentrations for sampled Pattern 1 springs in the Root River Watershed. These results represent several moderately high flow events that occurred in response to storms. None of the springs yield significant concentrations of TSS.

Location	Date Sampled	TSS (mg/L)
Unnamed Spring	4/7/2015	1.8
Unnamed Spring	4/8/2015	0.2
Unnamed Spring	4/9/2015	0.0
Unnamed Spring	5/28/2015	0.0
Borson Spring	4/7/2015	3.5
Borson Spring	4/9/2015	0.1
Wolfram Spring	4/7/2015	1.0
Wolfram Spring	4/9/2015	0.2
Ehlenfeldt Spring	4/9/2015	0.5

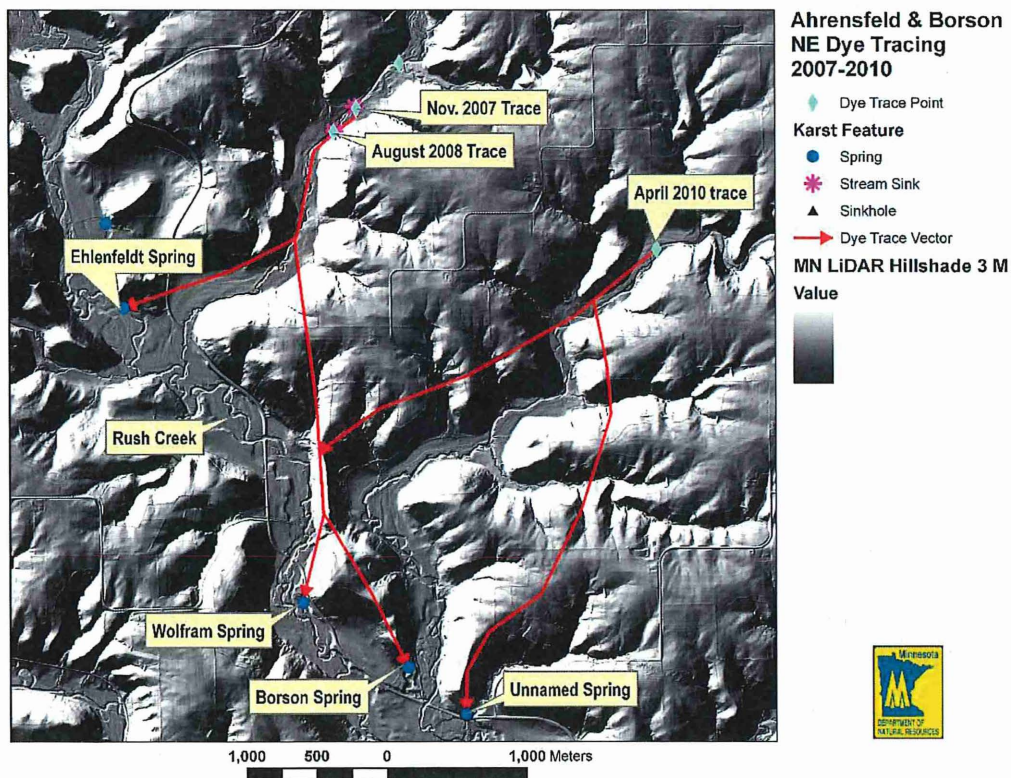


Figure 6.4. Springshed map showing karst hydrological pathways determined for the springs sampled in this study for TSS concentrations. The springs are located north of Rushford, Minnesota, along the floodplain of Rush Creek. Map provided by Jeff Green, MnDNR (modified from Green et al, 2014).

7. Grain size and bulk density

Grain size and bulk density are essential measurements for converting volumetric estimates of erosion to mass for use in the sediment budget and they have the potential to inform our understanding of how grain sizes are fractionated within the system through erosional and depositional processes. Previous work (Stout, 2012) showed that a relationship exists in the Root River Basin between grain size and terrace/floodplain height relative to the local river. However, this relationship included many high elevation (Pleistocene) terraces. We conducted a grain size sampling campaign, collecting sediment samples from banks and floodplains at 20 locations throughout the Root River watershed (green stars in Figure 7.1) to determine if this relationship was robust for the relatively low floodplains and terraces that comprise the majority of the banks throughout the drainage network. This was important to determine so that we can extrapolate our grain size and bulk density data in the most meaningful manner possible, considering the extraordinary diversity in bank types found throughout the watershed. Sample locations were selected based on floodplain height and local channel width change/migration rates. Samples were collected from vertical, actively eroding banks, with 3 replicate samples collected at the each location.

Methods

Grain size distributions were measured using a Sequoia Scientific LISST-Portable particle size laser diffractometer (Sequoia, 2011). The analysis procedure consisted of placing a small, well-mixed portion of the sample into the 175 mL chamber of the instrument filled with deionized water where a laser detects the light scattering pattern of the sample. The instrument offers two methods that assume different particle shapes (spherical or random) for processing of the data. The random shape assumption was applied in this study as previous work (Agrawal et al., 2008) has shown that the scattering signature of particles that have large angles (as expected here, given the glacial and carbonate bedrock parent materials) is recognizably different from sphere-like particles. Following Stout, 2012, we used a 20 second laser diffraction measurement interval and used a sufficient amount of sample material to ensure that the transmission rates were between 30 and 70%, as recommended by the manufacturer. The chamber of the instrument was rinsed after analyzing the three samples for the same location to make sure that no particles from a previous location remained when analyzing another location.

Bulk density samples were collected at the same sample locations as the grain size samples. A 114.5 cm³ metal cylinder was used to collect the samples. The cylinder was inserted into the vertical bank, which was previously cleared of vegetation, and then excavated and scraped into a bag using a small trowel. Bulk density samples were collected at 17 of the 20 sites selected. In the lab, samples were weighed before and after being dried at 120 °F for 48 hours. Mass was measured on a Mettler Toledo SB12001 balance, which has precision of 0.1 g. Samples were weighed twice to test the repeatability. Results were within 0.1g for all samples. Bulk density was calculated as:

$$\rho = M / V$$

where ρ is the bulk density, M is the dry weight, and V is the sample volume.

Results

Figure 7.2 shows that no systematic relationship exists between our two grain size metrics and bank height for these relatively low floodplain and terrace surfaces. This indicates that it is reasonable to use a simple average to convert volumetric erosion measurements to mass for the purpose of the sediment budget. The relationship observed by Stout, 2012, in which higher terraces contained significantly coarser sediments, suggests that the amount of silt and clay stored in the system has increased in the recent past as humans have exerted stronger control over erosion and sediment transport dynamics compared with the Pleistocene when high glacial discharges limited the amount of silt and clay stored. Floodplain bulk density measurements were also homogenous throughout the watershed, with an average bulk density of 1.3 g/cm^3 (Souffront, 2014). This is similar to bulk density of 1.39 g/cm^3 measured from 14 agricultural soil samples collected near the BCE edge-of-field monitoring station by Minnesota Department of Agriculture (data from Kevin Kuehner).

Stout, 2012 evaluated grain size distributions of suspended sediment to determine whether or not grain size distributions were significantly different on rising and falling limbs of the hydrograph. Evaluating data from multiple locations, Figure 7.3 shows that there is no significant trend in the downstream direction, nor is there a significant difference between the rising and falling limb grain size distributions.

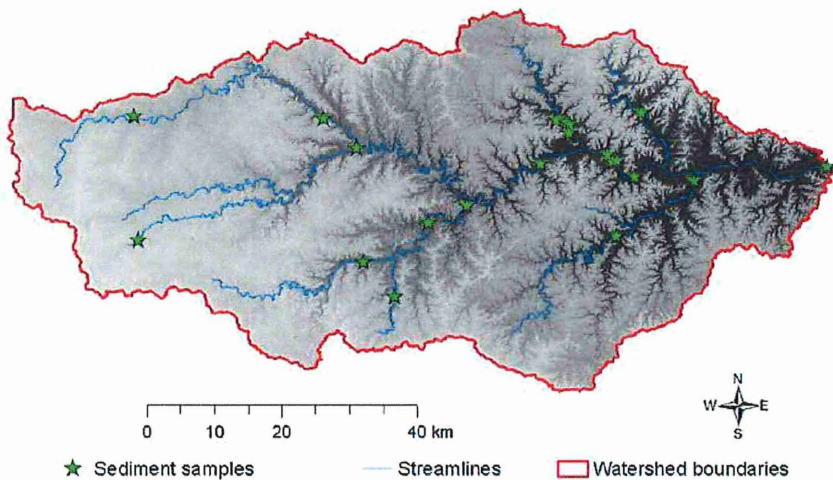


Figure 7.1. Locations for grain size samples from banks and terraces distributed throughout the Root River watershed.

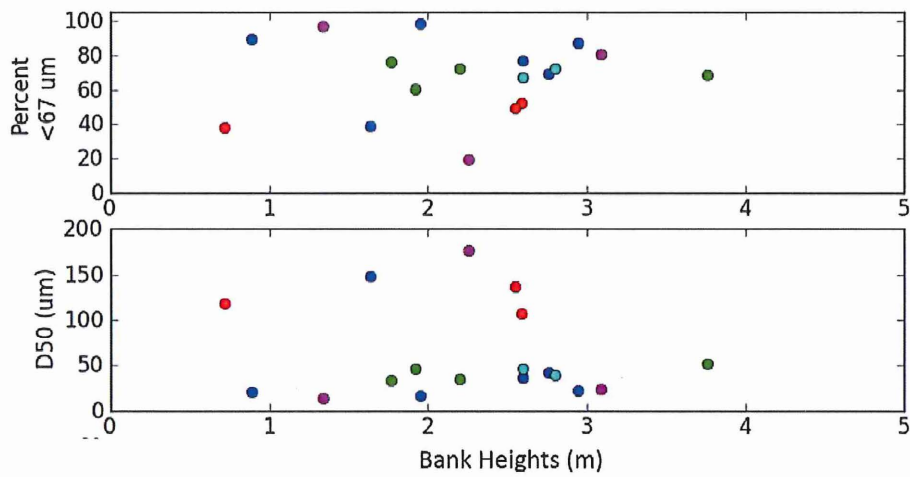


Figure 7.2. Bank and terrace sediment samples that were analyzed for two metrics of grain size distribution (percent of sediment mass smaller than 67 microns, which primarily contributes to turbidity, and D50 or median grain size).

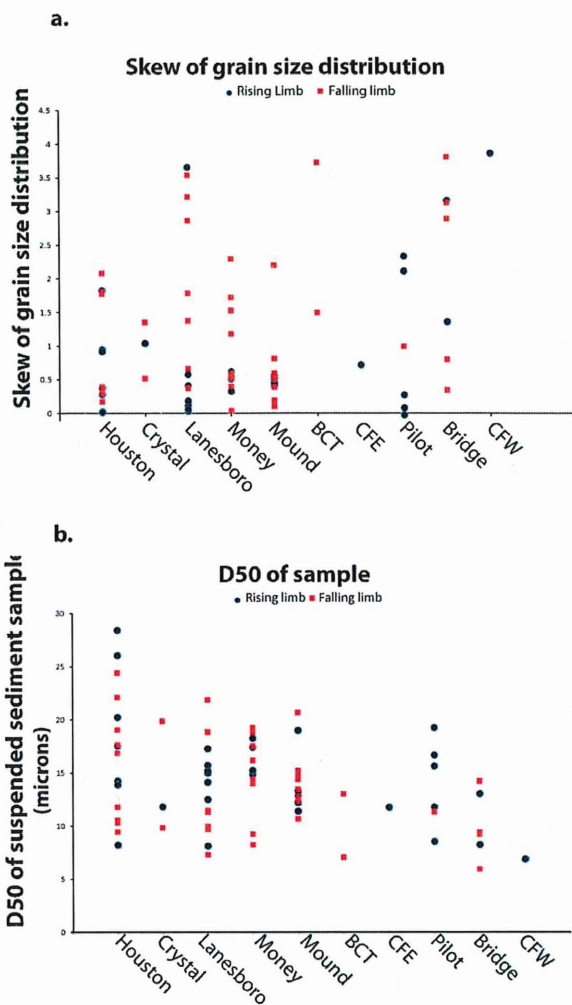


Figure 7.3. Results of suspended sediment samples that were analyzed for grain size distribution. Samples were split into rising limb and falling limb of the hydrograph and plotted for each location, but do not show any apparent difference between the rising and falling limbs of the hydrograph. From Stout, 2012.

8. Terrain analysis

The goal of the terrain analysis was to use high-resolution Digital Elevation Models to predict source areas of erosion based on the Stream Power Index (SPI). For the purposes of terrain analysis, three general geomorphic regions were considered, including driftless bluffland (blue in Figure 3.1), driftless Karst (brown in Figure 3.1) and upper Plains (yellow in Figure 3.1).

Digital terrain analysis leverages high-resolution digital elevation models (DEMs) to predict critical sources areas of erosion based on topographic terrain attributes (Passalacqua et al., 2015). SPI, which is a secondary terrain attribute, incorporates two primary terrain attributes: flow accumulation and slope (Florinsky, 2012; Moore et al., 1991; Wilson and Gallant, 2000). Simply put, SPI is the natural log of the product of flow accumulation and slope. Intuitively, areas with both steep slopes and a high potential for flow accumulation (i.e., overland flow) will generally yield greater amounts of sediment.

Obviously, the SPI analysis does not include other important factors such as soil type, land use, bedrock geology, climate, meteorology, vegetative cover, or landforms. These landscape characteristics are, however, integrated into topography. Previous studies have demonstrated that SPI can predict critical

source areas of erosion at the field scale within watersheds (Bi et al., 2006; Galzki et al., 2011; Jacoby et al., 2011). A preliminary study in three small sub-watersheds of the Root River basin has also demonstrated the efficacy of using SPI to predict erosion in southeastern Minnesota (Dogwiler and Hooks, 2012). Whereas many previous studies have incorporated only limited (or no) field-based validation of terrain analysis-based predictions, Dogwiler and Hooks (2012) applied a rigorous field-based validation and statistical analysis into their predictions of critical source areas of sediment.

Figure 8.1 summarizes the general steps used to calculate and validate the SPI-based predictions in this study. Red boxes represent the GIS-based derivation of SPI using a 3-meter resolution DEM for the Root River Watershed. A 3-meter resolution was chosen for multiple reasons. Firstly, the computational resources required to process the whole Root River watershed at a higher resolution are beyond what even a high-end GIS workstation can reasonably handle. Secondly, a sensitivity analysis performed by processing the SPI for a small section of the watershed showed that at higher resolution (1-meter) there was minimal-to-no improvement in the results or interpretation. Conversely, at lower resolutions (6-meter to 30-meters) the spatial extent of land surface represented by a DEM cell was much larger than the size of the vast majority of observed erosional features. As a result, many observed erosional features were not resolved within the GIS-based model and the results and efficacy of model predictions diminished rapidly.

The method used to calculate the SPI generally followed those described in Galzki et al. (2008), with a few modifications. The DEMs were derived from airborne lidar surveys commissioned by the Minnesota Department of Natural Resources (MnDNR) in fall 2008 during leaf-off and post-snow melt conditions. The primary DEMs have 1-meter horizontal resolution and stated vertical accuracies in the range of 12-20 cm, with the accuracies generally improving toward the west where there is less tree canopy and topographic relief. The DEMs were aggregated to a 3-meter resolution from their native 1-meter resolution. No further hydrologic conditioning (including pit-filling) of the DEMs was performed. Our preliminary analyses of sub-watersheds within the watershed indicated that hydrologic conditioning of the DEMs, as provided by MnDNR did not improve the results or predictiveness of the SPI. Given our robust field verification procedures and these preliminary analyses, we determined that minimal manipulation of the DEMs was the most prudent approach for the analysis.

In order to analyze and interpret the meaning of the SPI values we developed a robust field verification procedure. Green boxes in Figure 8.1 represent the workflow of the obtaining and making the field-based observations of erosion that were used to validate the SPI-based predictions of erosion. The majority of the field sites were chosen randomly by generating a random point raster in ArcGIS. The initial random point raster for the watershed was then clipped using a 100 m buffer along public roadways. This was necessary because we were constrained to using public right-of-ways to view the landscape since most lands in the watershed are privately held. The number of points in the initial random point raster was chosen iteratively so that the final clipped set of points was between 200 and 250 points, which was deemed a logistically feasible number of points to field verify based on the constraints of time and funding.

Verification sites were visited during the spring after snowmelt but before the vegetation was active or crops were planted (otherwise erosion may be obscured from view). and the condition of the landscape was noted. Particularly, any signs of erosion were noted and the presence of best management practices (BMPs), such as grass waterways, riparian buffers, contour farming, and other erosion mitigation BMPs were noted if they were present at the site. If erosion was observed at the verification point it was assigned a value of 1 if it was subjectively deemed as minor and 2 if it was deemed major erosion. We defined minor erosion as erosion that was likely recent in occurrence (i.e., less than one

year) and unlikely to be observable after a field was plowed or a sequence of normal freeze-thaw cycles over the courses of a typical year. Major erosion was defined as erosion that would likely still be observable after a plowing or a typical year of freeze-thaw cycles. A limited number of additional verification points were subjectively chosen in the field when easily observable erosional features were spotted during the course of the random point field verification. To minimize bias in the data set every subjectively chosen erosion site was also paired with observations at a nearby site lacking evidence of erosion.

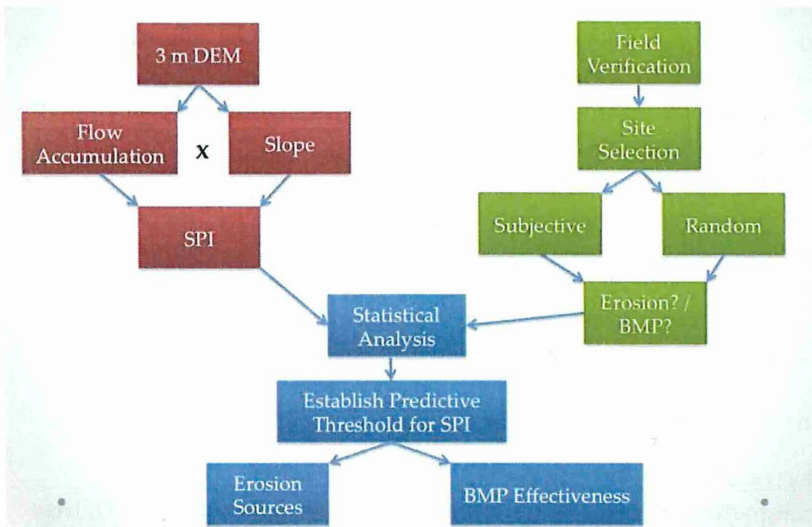


Figure 8.1. Flow chart illustrating the basic steps involved in using the Stream Power Index (SPI) to identify critical source areas of erosion.

SPI calculations and field verification data were analyzed using Pearson’s Correlation and logistic regression and probability modeling techniques. The statistical analysis provides a quantitative description of the predictive threshold for the SPI score. The predictive threshold is defined as the SPI value above which erosion is more probable than not. In other words, the statistical analysis segregates the SPI values into two groups based on their correlation with the observations of erosion at the field verification sites. The threshold is the minimum SPI value where erosion is statistically probable on the associate area of the landscape. Any portion of the landscape with an SPI value above the threshold is likely to experience erosion. Conversely, areas with SPI values lower than the threshold will likely not experience erosion. An additional statistical analysis evaluated the effect of BMPs on the predictive SPI threshold.

Terrain Analysis Results

SPI values calculated for the Root River Watershed ranged from -13.82 to 10.72, with a median value (50th percentile) of -1.13. Two field verification data sets were used for the statistical analysis. One was collected by Dogwiler and Hooks (2012) in spring 2012 in their study of three small sub-watersheds of the Root River (Figure 3). The three sub-watersheds were chosen for the Dogwiler and Hooks (2012) study because they represent the three geomorphic regions of the Root River Watershed (Figure 3.1). The second verification data set was collected in spring 2013 from throughout the Root River Watershed. Spring 2013 was an extremely wet spring in the watershed during which 30 – 35 inches (762 – 889 mm) of precipitation occurred from mid-March through June. As a result, erosion was widespread and frequently encountered. Spring 2012, in comparison, was a drier than normal spring in terms of precipitation.

For the spring 2012 field verification dataset, the logistic regression and probability modeling analysis indicated a correlation between higher SPI values and observed erosion. The spring 2013 field verification dataset did not show a strong correlation between SPI value and observed erosion. However, the ubiquity of erosion caused by the extreme frequency and magnitude of precipitation may not be the ideal conditions for collecting a verification data set. Areas of observed erosion in spring 2013 were re-analyzed based on notes and photographs and assigned an erosion magnitude value of 0, 1, or 2 according to the following criteria:

- 0 (zero): sites with no observed erosion
- 1: sites with minor erosion, which was defined as erosion causing gullies and rills estimated as unlikely to survive an annual freeze-thaw cycle or plowing
- 2: sites with major erosion, which was estimated as likely to survive the effects of an annual freeze-thaw cycle or plowing.

Reanalysis of the spring 2013 field verification data based on the erosion magnitudes for each site yielded a significant correlation between SPI value and probability of erosion for sites with an erosion magnitude of 2. For both the spring 2012 and 2013 data sets there was a statistically significant reduction in the probability of erosion at sites with BMPs for the same SPI value. Based on the field verification data, the following conclusions may be made (also see Figure 8.2 and 8.3):

After controlling for whether each verification site had a BMP present:

- The odds of erosion **increase by 3.9%** for every one percentile increase in SPI
- The odds of erosion are approximately **43 times higher** when the SPI percentile equals 100, than when the SPI percentile equals 1.09 (the minimum SPI percentile for the field verification sites)
- The odds of erosion at non-BMP sites are about **2.4 times higher** than for BMP sites.

Based on Figure 8.3 the predictive SPI threshold above which erosion is likely to occur is the 72nd percentile (0.29 SPI) for sites with no BMP present. At sites with BMPs, the predictive SPI threshold is the 96th percentile (3.54 SPI). This indicates that about 28% of the Root River watershed has SPI scores above a threshold at which erosion is likely to occur when BMPs are not present. These areas are shown (in red) in Figure 8.4. The eastern blufflands area of the watershed has a higher concentration of high SPI values than the central and western regions. The Bridge Creek sub-watershed, which is in the eastern blufflands area of the watershed has a much lower predictive SPI threshold than the Root River as a whole and areas lacking BMPs are much more likely to erode. The reasons for Bridge Creek's increased tendency for erosion is not clear. In terms of geology, soils, climate, and landuse distributions it is similar to other sub-watersheds such as Crystal Creek, which have erosional potential that closely mimics the overall Root River watershed. This leaves differences in agronomic practices and the topography of the eastern blufflands as possible explanations for the differing response. Identifying additional sub-watersheds with high erosional probabilities similar to Bridge Creek could provide useful insight for targeting BMPs to critical source areas of sediment erosion.

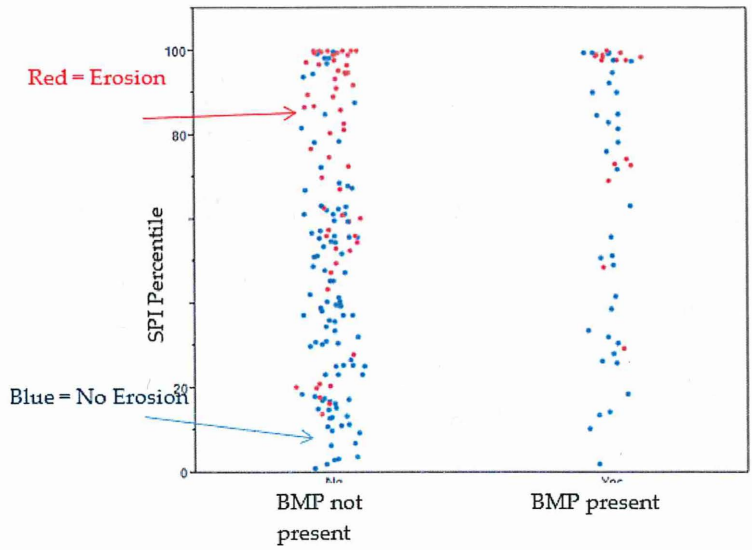


Figure 8.2. Relationship of SPI score (y-axis) to the occurrence of erosion (dot color) and the presence of a BMP (x-axis). Higher SPI scores are statistically correlated with a higher probability of erosion.

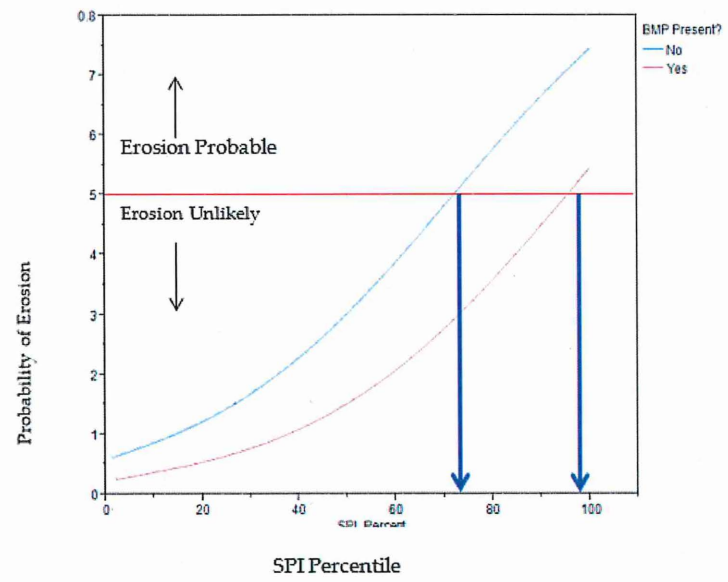


Figure 8.3. Predictive threshold determination for the SPI score. SPI scores (x-axis) that plot with a probability of greater than 0.5 (y-axis) correlate with areas of the watershed likely to erode. Thus, any non-BMP site (blue line) in the watershed with a SPI score greater than the 72nd percentile is likely to erode at some point. BMPs (red line) significantly reduce the probability of erosion.

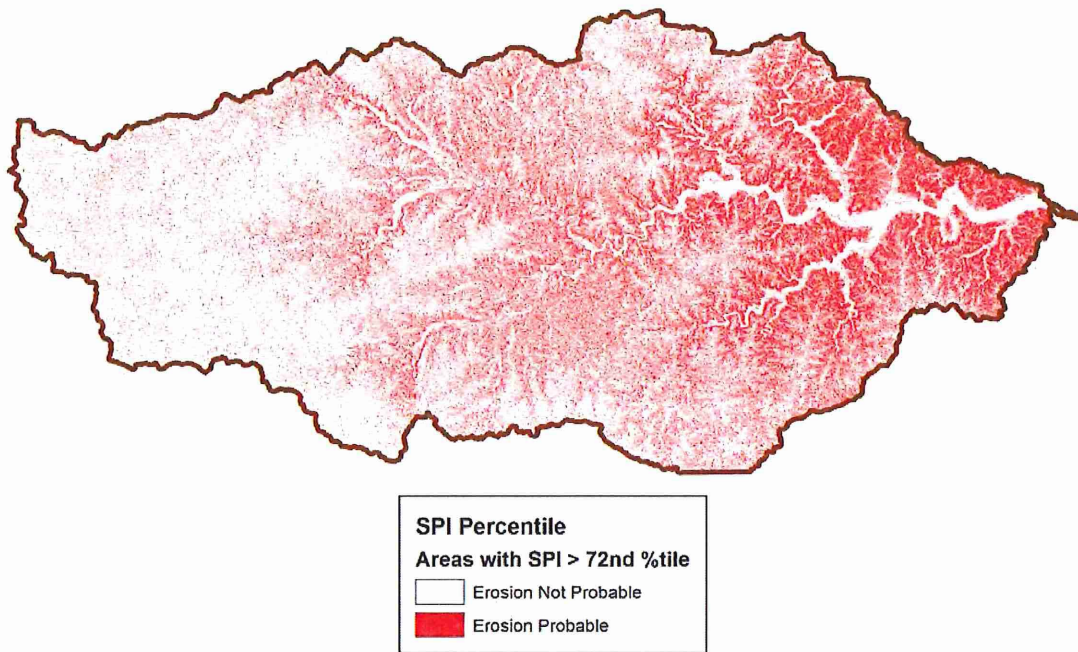


Figure 8.4. Map of the Root River Watershed showing the areas with SPI values greater than the statistically determined predictive threshold (>72nd percentile or >0.29 SPI). Approximately 28% of the watershed is comprised of areas with a probability of erosion. These areas seem to be most concentrated in the bluffland region of the watershed, including the Money Creek and South Fork sub-watersheds. Areas in the Upper Plains Agricultural Region (see Figure 3.1) have a lower concentration of high SPI values.

9. Mapping of existing water detention basins

Water detention basins are potentially important sinks for water and sediment. While it is known that there are many small detention basins distributed throughout the Root River watershed, it was unclear how comprehensively they had been mapped. In an attempt to identify detention basins from aerial lidar data and/or air photos, we implemented four methods found in the literature.

1. Threshold RGB values for water surfaces on orthophotos and use a MatLab pixel finder algorithm to identify detention basins
2. Use a lidar-derived curvature threshold (tails of distribution) to delineate detention basins on the landscape
3. Perform an unsupervised raster classification to classify DEMs or orthophotos into similar pixel groups and then threshold the classification categories/classes
4. Use the methods of Liu and Wang (2008) to locate and derive spatial attributes for detention basins. This approach requires artificially filling depressions in the DEM using an algorithm that performs a minimum elevation/least cost search, subtracting the unfilled DEM from filled DEM to identify filled depressions, then applying an area, perimeter, or asymmetry threshold to depressions to separate detention basins from topographic artifacts.

We found that none of the methods found in the literature were effective in the Root River Basin, in part due to the complexity of the terrain and also due to the moderate quality of the available lidar data. The first three methods failed because it was too difficult to delineate detention basins 1) using pixel color because there was a wide variety of water surface colors that overlapped with canopy and crop cover colors, 2) using a curvature threshold because planform and profile curvatures were too subtle around detention basins to differentiate from the rest of the landscape (i.e. curvature of detention basins did not fall in the tail of the distribution as initially expected) and, 3) using an unsupervised raster classification because elevation and pixel color classifications had too much overlap with one another (i.e. detention basins did not fall into one or two distinct classification groups). We also attempted using the algorithm of Liu and Wang (2008), separating detention basins from artifacts on the filled-unfilled raster. We applied an area threshold to classify depressions, but the approach was only modestly successful when checked against aerial photographs. The primary problem with this approach appeared to be the fact that many detention basins were not identified by the depression filling algorithm because they were full of water when the lidar was flown and therefore did not appear as sufficiently deep depressions. As a result, we decide that the best representation of ponds and detention basins was the coverage available from the Minnesota Department of Natural Resources.

10. Mapping and quantifying sedimentation in cutoff meander bends

Meander cutoffs are potentially important sediment sinks in river systems. We developed a GIS tool to automatically map meander cutoffs throughout the Root River Basin (see Appendix A). Our GIS analysis initially identified a total of 41 potential cutoffs, the majority of which occurred in the transition between the Upper Plains and Transitional Karst zones of the watershed (Figure 10.1). Five of these were later determined not to be actual cutoffs and were eliminated from the analysis. During summer 2014 we visited the 20 largest cutoffs and the majority were found to not contain measureable amounts of stored sediment. In the vast majority of those cases it appeared that there was an insufficient amount of sand being transported in the river to plug the two ends of the cutoff. Therefore, the river would use both channels or switch frequently back and forth between the two channels, purging them of sediment frequently.

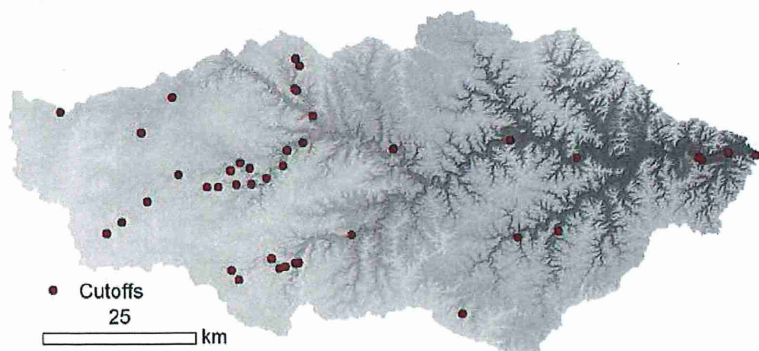


Figure 10.1. Channel cutoffs initially identified throughout the Root River channel network.

We measured sediment deposition in a total of eight cutoffs, measuring the depth of deposition with a soil probe in many locations within the cutoff and collecting representative samples for bulk density and

grain size analysis (Figure 10.2). Red dots in Figure 10.2 indicate cutoffs that are known to have cut off from the main channel within the timeframe of our air photo records. Thus, we have good temporal constraints on the timing of these cutoffs. Cutoffs noted as 'old' in Figure 10.2 became disconnected from the channel prior to our air photo records. While these cutoffs cannot be used quantitatively in the sediment budget because we do not know the time period over which the sediment accumulated, we sampled these cutoffs to determine if/how the sedimentary facies (grain size) in the deposits differ from those of recent cutoffs.

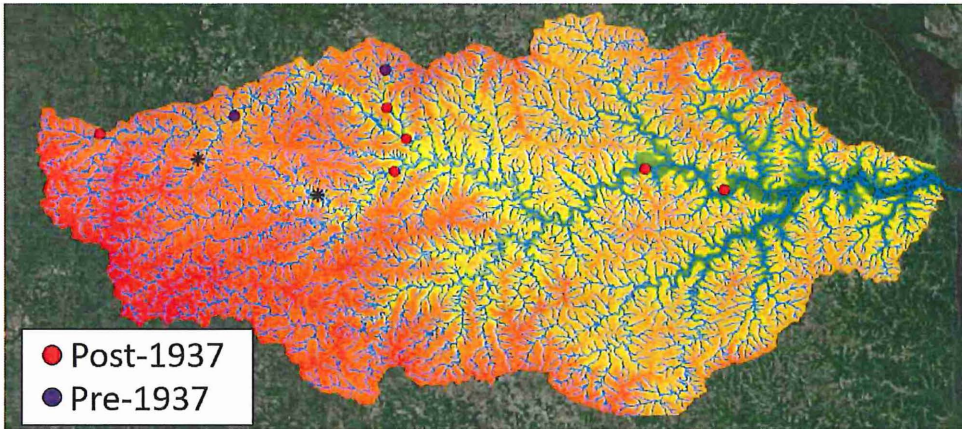


Figure 10.2. Map of cutoffs that were measured for depth of sediment deposition during summer 2014. New cutoffs are those which have formed within the air photo record (since 1937).

Two cutoffs (labeled 1 and 2) were found to contain substantially more sediment than others, both located on the lower mainstem Root River. Figure 10.3 shows the pattern of sediment depths measured in cutoff 1, with mud depths ranging from 0.6 to 1.9 m and a spatially interpolated average of 1.2 m. In cutoff 2, near Rushford, the vast majority of the samples fall within the range of 0.1 to 0.8 m. Grain size distributions were very consistent throughout all of the channel cutoffs, with small plugs of sandy material at the up- and down-stream ends of the cutoff and very fine grained silt and clay filling most of the cutoff meander bend. Accounting for grain size and bulk density, Table 10.1 shows total sediment storage in each of the cutoffs. Cutoffs 1 and 2 contain a total of 86,000 Mg of sediment. Both cutoffs occurred in the interval between the 1991 and 2003, so taking 10 years as the minimum age of each cutoff we estimate a maximum rate of sediment storage of approximately 9000 Mg/yr. The combined rate of sediment storage for all other cutoffs measured falls within the range of uncertainty of this estimate and thus we estimate sediment storage in cutoffs to be no more than 9000 Mg per year, a relatively small number compared with other sediment sources and sinks in the budget.

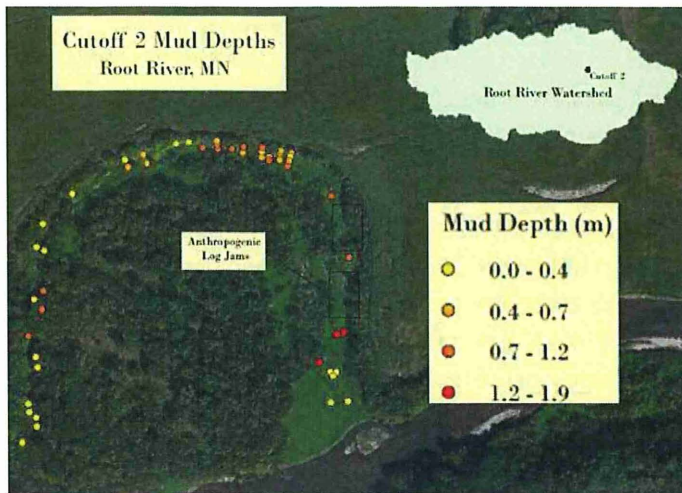


Figure 10.3. Depth of sediment deposition measured in cutoff 2, near Rushford. Color indicates the depth of fine grained sediment (primarily silt and clay). Samples were collected for grain size and bulk density analysis. Sediment depths were interpolated between sample locations to compute sediment storage within each cutoff.

Table 10.1. Summary data for sediment storage in cutoff meander bends

Cutoff	Average Depth (m)	Density (g/cm ³)	Area (m ²)	Volume (m ³)	Mass (Mg)	Timing (years)	Rate (Mg/yr)
1	1.21	1.25	41,220	49,999	62,499	10	6,250
2	0.58	1.25	33,390	19,242	24,052	10	2,405
3	0.03	1.25	3,080	94	118	7	17
33	0.17	1.25	533	88	110	7	16
36	0.36	1.25	2,606	948	1,185	7	169
37	0.71	1.25	1,205	856	1,070	7	153
38	0.87	1.25	610	532	665	38	17
39	0.80	1.25	250	199	249	38	7

11. Sediment fingerprinting

Sediment fingerprinting is a technique that utilizes the geochemical signatures of suspended sediment, compared with sediment collected from potential source areas within the watershed to determine the fraction of sediment derived from each source. The technique has advanced rapidly over the past 20 years and has been used successfully in a wide variety of landscapes (Gellis and Walling, 2011; Koiter et al., 2013; Smith and Blake, 2014; Belmont et al., 2014). We have used a suite of three tracers Lead-210 (²¹⁰Pb), Cesium-137 (¹³⁷Cs) and Beryllium-10 (¹⁰Be) measured in samples collected from 2010 to 2014 to determine the relative importance of different sediment sources in this study. Beryllium-10 and ²¹⁰Pb are naturally-occurring tracers that are delivered to soil surfaces via atmospheric deposition (Oldfield and Appleby, 1984; Willenbring and Von Blanckenburg, 2010; Belmont et al., 2014). Specifically, ¹⁰Be is produced when cosmic rays interact with the nucleus of oxygen in the atmosphere and is subsequently delivered to Earth's surface, where it adsorbs to soil particles within the top meter of the soil profile. Lead-210 is part of the decay chain of naturally-occurring Uranium-238 and is continually delivered to Earth's surface and adsorbs to soil particles within the top few cm of the soil profile. Cesium-137 was produced as a result of nuclear weapons testing in the 1940s-1960s. These specific tracers were selected because they have significantly disparate half lives, 22, 30, and 1.4 million years for ²¹⁰Pb, ¹³⁷Cs, and ¹⁰Be,

respectively. Generally, upland sediment is rich in all three tracers. Sediment that is temporarily deposited in floodplains, which is subsequently re-mobilized by bank erosion, is deficient in ^{210}Pb and ^{137}Cs after 50-60 years because of their short half lives. As shown in section 7 above, grain size distributions of suspended sediment did not demonstrate hysteresis and therefore we used a simple grain size correction factor, as discussed in Stout et al., 2011.

The primary sources of fine sediment are agricultural fields, forested hillslopes (both shown in the top two images of Figure 11.1) and streambanks (many varieties of which exist throughout the Root River watershed, shown in the rest of the images in Figure 11.1). The bottom seven photos in Figure 11.1 illustrate the diversity of streambank heights (~ 1 m to > 5 m), grain size distributions (silt loam with high cohesion to sand with low cohesion), and morphologies (actively slumping to vegetated and relatively stable). Sediment source fingerprints indicate a good amount of separation between the three major sources, agricultural fields, forested hillslopes, and floodplains and alluvial terraces. There was good agreement between samples collected during this project with those collected previously.





Figure 11.1. Representative images illustrating the various sediment sources in the Root River watershed. Forested hillslopes and agricultural fields are depicted in the top two images. The seven images below depict the variety of streambanks that exist throughout the watershed.

Tracer concentrations for each fingerprinting sample were compared using a dissimilarity matrix (Figure 11.2). Each case was fourth root transformed, and a non-metric Multidimensional Scaling Analysis (nMDS) was used to determine the clustering of fingerprints in two dimensions. The stress score of the analysis was 0.019, where a stress value of <0.1 is considered acceptable. The results illustrate that the fields and hillslopes have some amount of overlap in the tracers used to determine source area fingerprints. This is largely attributed to the range of overlap in both the ^{210}Pb and ^{10}Be concentrations. But floodplains are entirely independent, primarily because they lack ^{210}Pb and ^{137}Cs . Using all available source area fingerprinting data we fit probability density functions to the data and calculated averages (see table 11.1). All of the distributions were well represented as Weibull distributions. Figures 11.3 and 11.4 show the distributions of tracer concentrations in Bridge Creek and Crystal Creek, respectively. Overlap of the probability density functions of tracer concentrations demonstrate why it is necessary to use the suite of all three tracers to differentiate sources. Note that the ^{137}Cs and ^{210}Pb amounts measured on suspended sediment are consistent with the lower end of what is measured in agricultural fields. Results are consistent between the two small watersheds in that agricultural fields are identified

as the dominant sediment source at the edge of field and small watershed scale, but in both cases the ^{10}Be concentrations associated with suspended sediment at the small watershed scale are diluted by a ^{10}Be deficient source, presumably sediment derived from deep (>1 m) gullies on the hillslope or agricultural fields and/or sediment derived from within the subsurface Karst system.

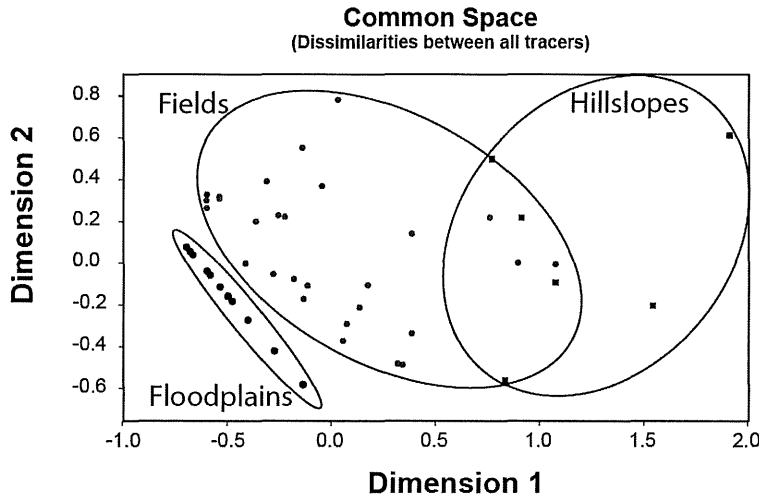


Figure 11.2. Sample concentrations were compared using a dissimilarity matrix. Each was 4th-root transformed, and non-metric Multidimensional Scaling (nMDS) was used to determine the clustering in two dimensions (stress score = 0.019 where <0.1 is acceptable). Results illustrate that fields and hillslopes have slight overlap due to similar ranges in ^{210}Pb and ^{10}Be concentrations

Table 11.1. Average tracer concentrations for sediment source areas, derived from probability density functions

Tracer	Field Average	Hillslope Average	Floodplain Average
Beryllium-10	5.59×10^8 at/g	7.71×10^8 at/g	4.04×10^8 at/g
Lead-210	2.14 pCi/g	4.96 pCi/g	NA
Caesium-137	0.30 pCi/g	1.80 pCi/g	NA

Bridge Creek

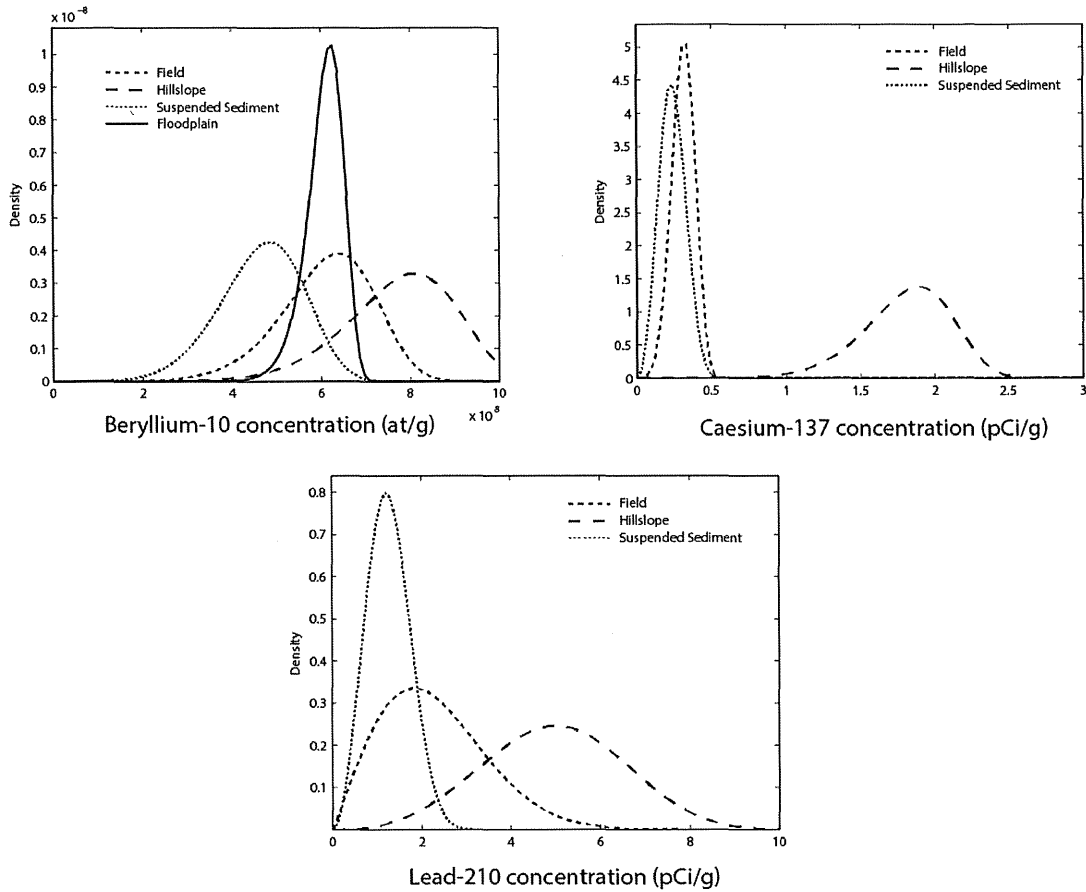


Figure 11.3. Distributions of tracer concentration in source areas in Bridge Creek (field, hillslopes, and floodplains) and the distribution of tracers in suspended sediment samples. ^{210}Pb and ^{137}Cs concentrations in suspended sediment are well constrained. Agricultural fields are the dominant source of sediment at the small watershed scale. However, the ^{10}Be concentrations in the suspended sediment samples is not well constrained by the ^{10}Be fingerprint of the floodplain, suggesting another source area that is contributing depleted ^{10}Be sediment, such as deep (> 1m) gullies.

Crystal Creek

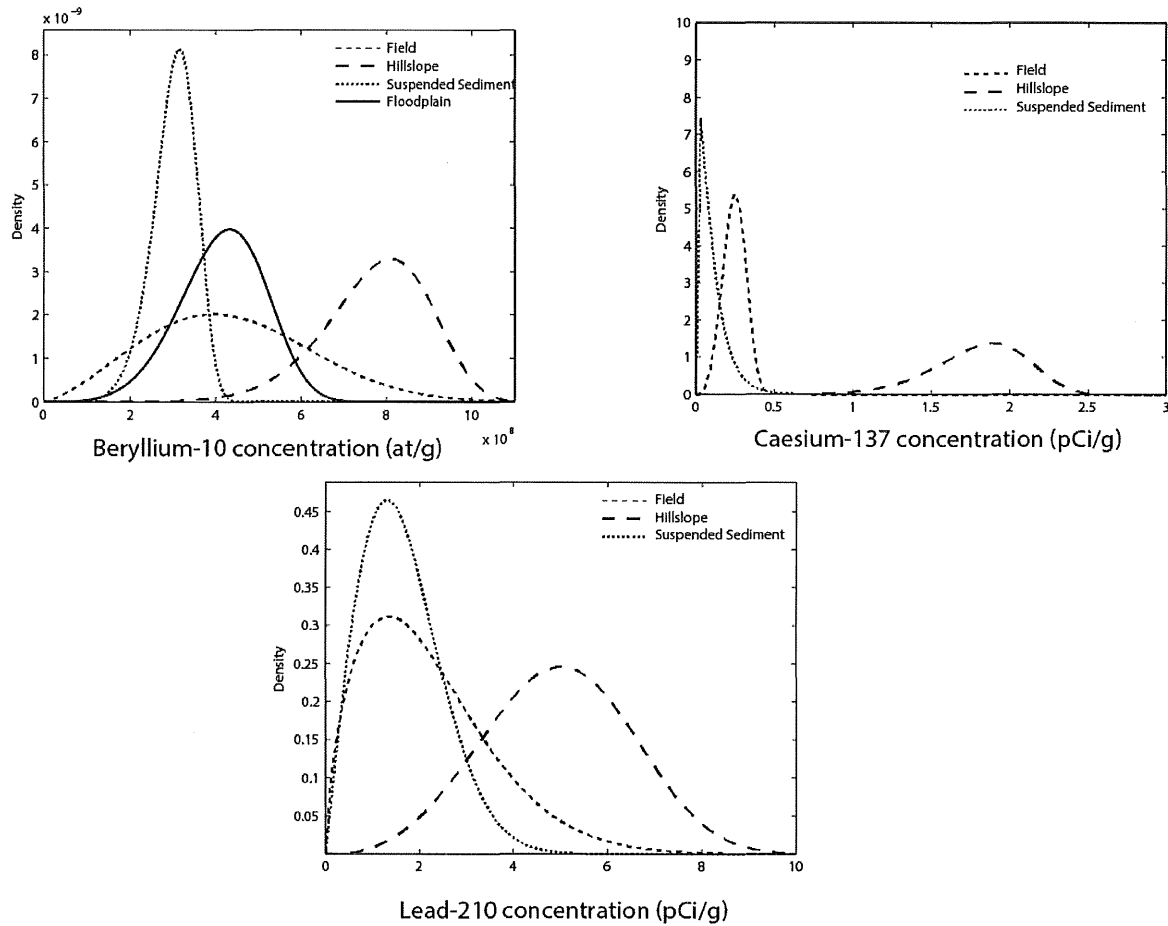


Figure 11.4. Distributions of tracer concentrations in source areas and suspended sediment in Crystal Creek are similar to those observed in Bridge Creek. Specifically, ^{210}Pb and ^{137}Cs concentrations demonstrate that agricultural fields are the dominant sediment source at the field and small watershed scale, but ^{10}Be in suspended sediment sources at the Crystal Creek outlet are somewhat diluted by a depleted ^{10}Be source such as deep gullies.

Because the ^{137}Cs concentrations exhibited such a stark difference between the fields and hillslopes, we used the ratio of $^{137}\text{Cs}:^{10}\text{Be}$ for all of the hillslope source samples. Then the average, maximum and minimum values were used to determine the contributing percentage from hillslopes to the suspended sediment sampled

$$\% \text{ HS contribution} = \left(\frac{^{137}\text{Cs}:^{10}\text{Be} \text{ sus. sediment}}{\text{average } ^{137}\text{Cs}:^{10}\text{Be} \text{ of hillslopes}} \right) * 100$$

We did this for the maximum and minimum values of the ratio – which provides a minimum and maximum estimate of hillslope contribution.

To determine the contribution from agricultural fields, we calculated the average concentration of ^{210}Pb in the field source samples, as well as the maximum and minimum values, and calculated the percentage field by:

$$\%Field = ({}^{210}Pb \text{ susp. sed.} / \text{average } {}^{210}Pb \text{ field}) * 100$$

We did this for each of the maximum and minimum values, again providing a minimum and maximum estimate of field contribution.

Lastly, floodplain contribution was calculated as:

$$\%Floodplain = 100 - (\% Field + \% HS)$$

Figure 11.5 and Table 11.2 show the percentage of sediment derived from agricultural fields for each of the small watersheds and major sub-basins within the Root River watershed. Samples collected from the outlet of Bridge Creek and Crystal Creek indicate that 60-70% of the sediment is derived directly from agricultural fields with relatively little sediment being reworked from storage within the system and a minority, but not negligible, amount of sediment derived from a ${}^{10}Be$ deficient sediment source such as deep gullies or the Karst system. The North Branch, South Fork and Money Creek all fall within 25-30% of sediment at their mouths derived from agricultural fields, with the remainder derived from floodplains, much of which are composed of historical agricultural sediment (Stout et al. 2014). Thus, the bulk of sediment in these sub-watersheds is derived from legacy sediment, which, given the prevalence and size of alluvial terraces distributed throughout the watershed, may take many decades to deplete. The South Branch exhibits a slightly higher fraction of sediment derived from agricultural fields (~50%), which is consistent with it having somewhat steeper topography, and therefore likely a higher sediment delivery ratio, compared with the North Branch.

At Mound Prairie, the most downstream sampling site on the mainstem Root River, sediment fingerprinting indicates that approximately 44% of sediment is derived from agricultural fields, averaged across the entire watershed (Figure 11.5). Considering the fact that this whole-watershed average is somewhat higher than the averages observed in the North Branch, South Fork and Money Creek, it is expected that Rushford Creek and other small, direct tributaries to the mainstem contain relatively high proportions of sediment derived from agricultural fields. This hypothesis is supported by the fact that these areas exhibit some of the highest USLE erosion rates in the watershed (see SWAT model results below) and likely have a relatively high sediment delivery ratio due to their proximity to the outlet and relatively steep terrain.

Uncertainty surrounding the mean concentration of tracers in fingerprinting samples can arise from various sources that are difficult to quantify. Errors arising from laboratory measurements, uncertainties inherent to the un-mixing model, and systematic uncertainties in the collection and measurement of tracer concentrations can all propagate through the fingerprinting analysis and result in some level of uncertainty. The nature of these uncertainties provides insight as to how much variation can be expected from the estimates of source apportionment in the river. Systematic measurement errors can be minimized by using good lab practices and having a good experimental design. One of the most difficult uncertainties to address is our confidence in the representation of all source areas. The difficulty in representing all source areas is largely due to the spatial and temporal variations in erosion and deposition of sediment on upland source areas and within the channel, especially in the complex terrain of the Root River Basin. However, this uncertainty can be quantified by calculating the relative uncertainty of the average concentration in the source areas and propagating the errors through the un-mixing model. In addition, due to the lag times during transport of sediment through the system and the fact that ${}^{210}Pb$ and ${}^{137}Cs$ decay over 50-75 years, agricultural field and hillslope sediments do not immediately lose their terrestrial signature immediately. For example, sediment that was eroded from a field and deposited in a floodplain 22 years ago would appear as 50% field sediment and 50% streambank sediment. Within 66 years that

same sediment would appear to be composed of 12.5% field sediment and 87.5% streambank sediment. For more information, see Belmont et al., 2014.

Due to variable erosion rates on both the hillslopes and fields as well as a difference in tillage practices on the fields, the concentrations of ^{210}Pb , ^{137}Cs and ^{10}Be were highly variable. As a result, these variable source concentrations resulted in a moderate level of uncertainty surrounding the true value that should be used as an average source concentration. Uncertainty of the source area concentrations was calculated as the percentage of difference between the average source value and the most disparate value measured. Floodplains and fields had the lowest relative uncertainty (28 and 32%) while hillslopes had a very large uncertainty of 84%. The high uncertainty on the hillslopes is largely due to the spatial differences in erosion on the hillslopes. Agricultural field source areas had less uncertainty surrounding the source concentrations as the majority of samples came from two small watersheds (Bridge Creek and Crystal Creek). Each source area uncertainty value was propagated through the un-mixing model and used to calculate a percentage of uncertainty for each of the sub-watersheds. Bridge Creek had the highest source of uncertainty as one of the field samples had an extremely high ^{210}Pb concentration (4.51 pCi/g) relative to the other samples collected in the watershed. However, keeping this sample in the dataset is reasonable as it is an example of the potential for smaller watersheds to be dominated by field sediments. Even though Bridge Creek had a high uncertainty (38%, meaning that it could be as high as 80% or as low as 40%, see Table 11.2), it was similar to all other watersheds. As a result of propagating the errors through the un-mixing model the percentage of sediments derived from fields can vary as much as 35% for the main stem of the Root River and as little as 21% for the North Branch.

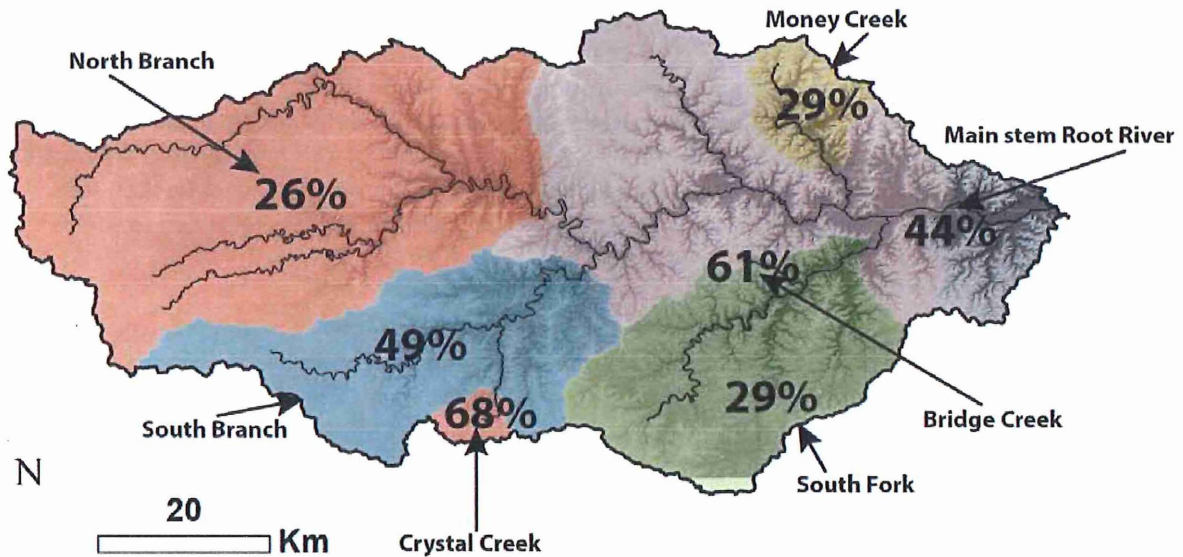


Figure 11.5. Map of the Root River showing the spatial distribution of the percent of suspended sediment sourced from agricultural fields.

Table 11.2. Average contributions from source areas to suspended sediment loads

Sampling Station	Area (km ²)	Field (%)	Hillslope (%)	Floodplain (%)	Uncertainty (%)
Bridge Creek	19	61	18	21	38
Crystal Creek	15	68	15	17	31
North Branch	1382	26	16	58	21
South Branch	743	49	15	36	38
South Fork	747	29	11	60	22
Money Creek	153	29	9	62	23
Main Stem Root River	4120	44	13	43	35

12. Meander migration and channel width analysis

Introduction

River channels typically comprise less than 1% of a watershed in terms of areal extent, but are often among the most dynamic portions of the landscape where the confluence of all flow and sediment transport are densely concentrated. As a result, they are largely unsteady, exhibiting immense variability in time and space, and can serve as large amplifiers or buffers of sediment conveyance, acting as both sediment sources and sinks. The river channel is integrally connected to the floodplain as sediment is exchanged between the two during processes of channel widening/narrowing, meander migration, and overbank deposition. Channels can serve as net sources of sediment during times of channel widening and serve as net sediment sinks during periods of channel narrowing. Similarly, as a channel migrates laterally one bank erodes sediment from the floodplain (a sediment source) while the other bank typically deposits sediment that is ultimately accreted (laterally as a bank or bar deposit or vertically as an overbank deposit) to build the floodplain on the opposite side of the channel (a sediment sink). This exchange of sediment between the channel and floodplain can, but does not necessarily, result in a net addition of sediment to the channel. Lauer and Parker (2008) showed that the difference in elevation between eroding and depositing channel banks, together with extension of the outer bank is equal to the local, net addition of sediment added to the channel. This can be computed from the following equation

$$E_{Local,net} = C * (H_{bf} + \Delta\eta) * \Delta S_o - C * H_{bf} * \Delta S_i$$

where $E_{Local, net}$ is the net volume of sediment added to the channel, C is the migration rate, H_{bf} is the bank full elevation, $\Delta\eta$ is the difference in elevation between the outer and the inner banks, ΔS_o is the length of the outer bank, and ΔS_i is the length of the inner bank. For channels in equilibrium ($\Delta s = 0$), this local, net contribution must be equaled by over bank deposition.

Over annual to decadal timescales, river channel width, depth and slope adjust in response to the magnitude and duration of flows as well as the amount and type of sediment supplied. Belmont et al., (2011) and Gran et al., (2011) showed that channel migration and widening were moderately important sediment sources in the naturally rapid-incising Le Sueur watershed in south-central Minnesota. In a setting more similar to the Root River, Trimble, (1999) demonstrated that Coon Creek, Wisconsin had stored the majority of sediment eroded from hillslopes in the mid to late 19th century and subsequently downcut through those 'legacy' deposits of sediment, causing the floodplain to become a net sediment source throughout the 20th century.

We had several reasons to expect that meander migration and channel widening/narrowing might be important processes in the sediment budget of the Root River. First and foremost, the Root River has a similar landscape setting and has experienced a similar geologic and human history to Coon Creek. In addition, paleo-channel scars are evident in high-resolution topography data throughout the wide alluvial valley along the mainstem Root River. These suggest high levels of historical channel activity along the mainstem Root River. Furthermore, previous terrace mapping identified large and readily erodible alluvial terrace deposits lining the Root River and all major tributaries (Stout and Belmont, 2014). Further analyses involving geochemical sediment fingerprinting indicated that a considerable amount of sediment is derived from channel bank/floodplain sources at the mouth of the watershed and each of the major sub-basins.

Methods

We digitized channel banks from historic air photos for 11 periods (1937, 1947, 1953, 1976, 1991, 2003, 2006, 2008, 2010, 2011, 2013) along 130 km of the mainstem Root River as well as 6 periods along major tributaries (Figure 12.1). We used the Planform Statistics Tool (Lauer and Parker, 2008) to interpolate a channel centerline for each set of bank lines. From the digitized banks, we calculated channel width at 10 m intervals along the centerline. Spatial correlation tests (Geary C) indicate that raw data collection at 10 m, and subsequent decimation to 25, 50, 100 m increments, capture all spatial variability in channel width.

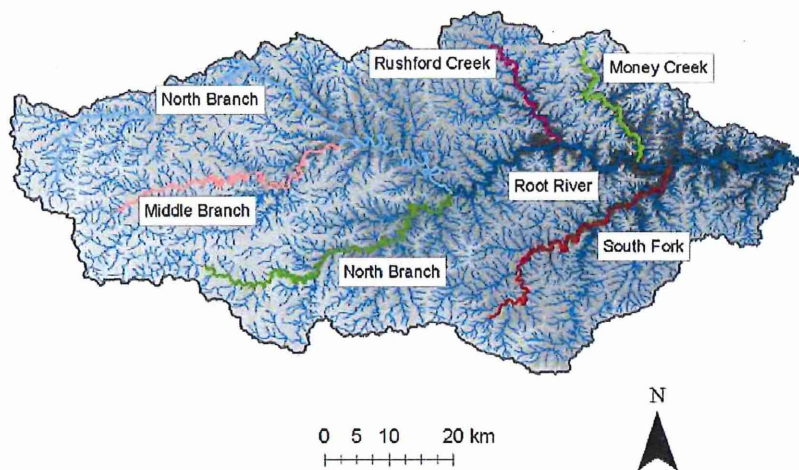


Figure 12.1. Map of all major tributaries throughout the Root River watershed, which have had right and left banks digitized in order to analyze channel widening and meander migration for the 1930s through 2013.

Channel widths were compared at 10 m intervals between each photo date in order to estimate continuous channel width changes along the mainstem Root River and understand river dynamics at small spatial scales over time. The data were plotted to visualize differences in means and extremes of width change over the period of study. While this helped discern local-scale process interactions, a second reach-scale (10 km) analysis provides data that are more directly relevant to the sediment budget. We differentiate 11 reaches along the mainstem Root River, with reach 1 being the most downstream (Figure 12.2). Reaches were aggregated into three larger sections that were identified as geomorphically distinct based on valley confinement, slope and planform geometry (Figures 12.2 and 12.3). Section 1 is the laterally unconfined lower section of the Root River with relatively low sinuosity and occasional levees and dikes that have been constructed to protect local infrastructure. Section 3 is a highly sinuous stretch of the Root River, upstream from the confluence with the South Branch in which

the channel is relatively steep and confined within a meandering bedrock valley. Section 2 is a transition reach between the steep bedrock section and laterally unconfined section. Section 2 contains many active point bars and visually appears to be most dynamic and occurs around the anomalous decrease in slope (which represents a decrease in sediment transport capacity) showing in Figure 3.5 above. Figure 12.4 illustrates peak flows measured at Houston, near the mouth of the Root River throughout the period of record with blue bars indicating the years with digitized aerial photographs.

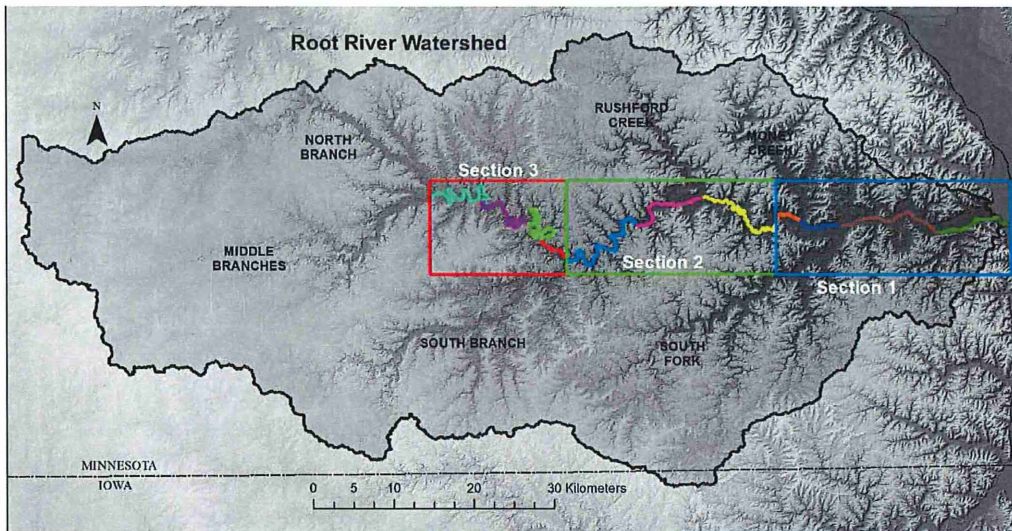


Figure 12.2. Three geomorphically distinct sections of the mainstem Root River.

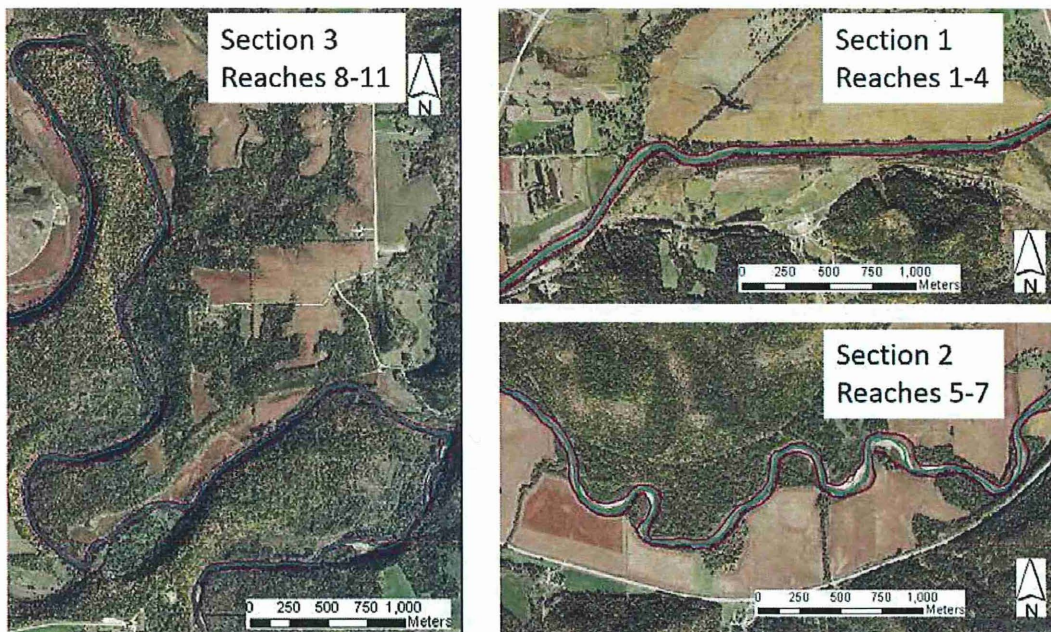


Figure 12.3. Visual representation of the planform geometries and features of the three geomorphically distinct reaches of the Root River mainstem.

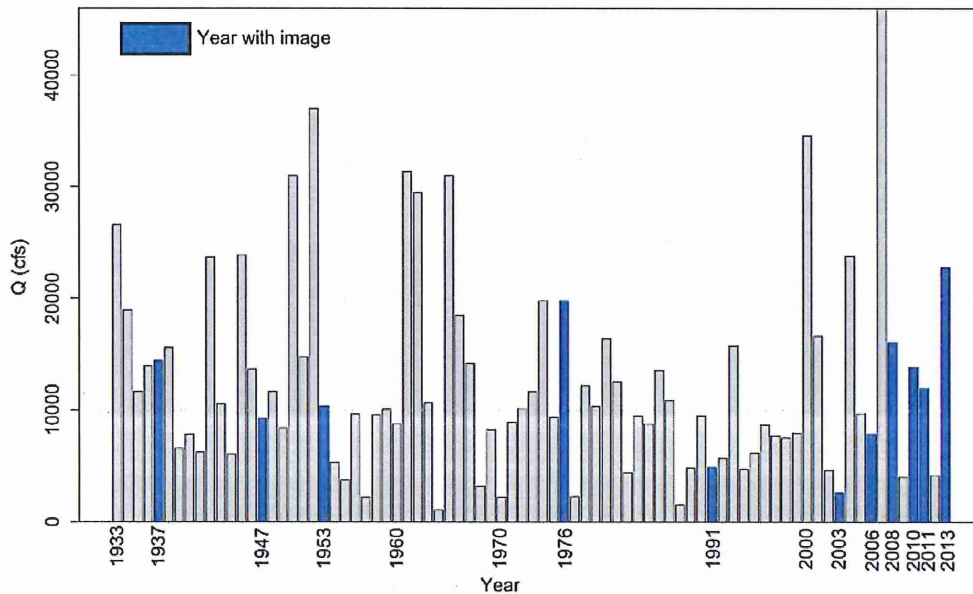


Figure 12.4. Bar plot indicating the magnitude of annual peak flows recorded at the mainstem Root River gage near Houston. Blue bars indicate years for which historical air photos were analyzed.

We field-validated channel widths at 19 locations. For field validation, we delineated a reach that was ten times the average bankfull width at each site, collected GPS points at the start and end of each reach, and measured channel width using a laser range finder at 10 to 12 locations within each site (Figure 12.5). Field-measured widths were higher than the calculated widths in all cases but one, but the offset is relatively small (RMSE = 2.9m) and was relatively consistent. Much of this offset is presumably accounted for by actual widening that occurred in the 3 years between the 2011 aerial photo used for analysis and 2014, when field validation was completed, as this period includes two high flow years (2013 = 22,800 cfs, 2014 = 8,070 cfs at the Houston gage).

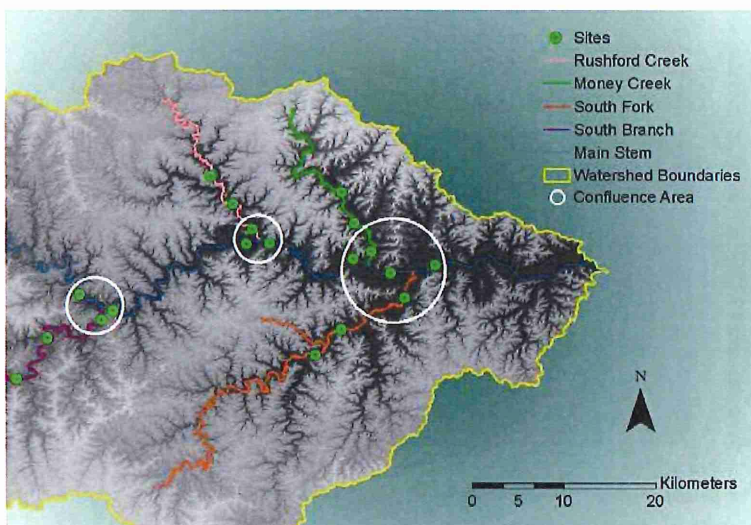


Figure 12.5. Channel width validation sites.

Bank elevations were extracted from the 2008 lidar DEM along the digitized banklines. Buffers of different areas were created to extract elevation using the Planform Statistics Toolbox developed by Wes Lauer (<http://www.nced.umn.edu/content/stream-restoration-toolbox>). After testing several different buffer sizes (1, 2, 3, 5, 6, 10 m), an area of 2 m landward times 25m in the downstream direction was chosen to be the most representative of actual bank heights (Souffront, 2014). Results indicated that larger bounding boxes introduce more error because they often included parts of hillslopes or off-channel terraces at higher elevations, while the 1 m bounding box was too small because in some cases it did not extend beyond the channel and up onto the actual floodplain or terrace.

Bank digitization uncertainty and error estimates

In order to estimate the minimum level of detection (LOD) for width changes resulting from erroneous bank delineations (causing false width changes), streambanks along 3 km river segment were delineated four times (independently) for the 1937 and 2013 air photos by an experienced GIS analyst (Bastiaan Notebaert, KU Leuven). With perfectly consistent bank delineations, the actual channel width would be the same in all cases. However, the results demonstrated slight differences in how the banks were delineated (Figure 12.6). These results demonstrated that poorer image quality (1937 being poorer than 2013) led to greater variation in streambank delineations, and allowed us to estimate 95% confidence intervals on the LOD for width changes.

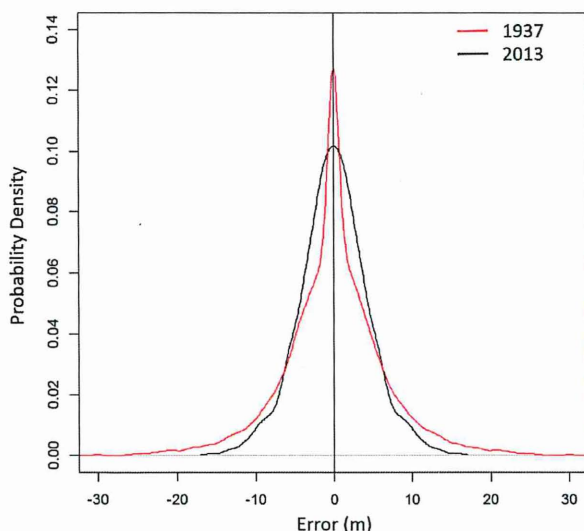


Figure 12.6. Error distributions of false width change measurements resulting from erroneous bank delineations. The quality of the images played a clear role in the maximum degree of delineation error- indicated by the maximum breadth of 1937 (red) versus 2013 (black) lines.

A similar method was used to estimate the LOD for channel migration. From the four bank delineations (described previously), channel centerlines were interpolated and compared to one another to estimate erroneous migration. Again, with perfectly consistent delineations, the centerlines would also align, resulting in no observed migration along the 3 km river segment. As expected, results demonstrated uncertainty arising from digitization, the degree of which was related to the quality of the image (Figure 12.7). Current results indicate the 95th percentiles of erroneous migration are 3.9 m (2013), 5.8 m (1991), and 7.1 m (1937). Dividing the magnitude of error by the timespan between two photos would yield an error estimate as a rate (m/y).

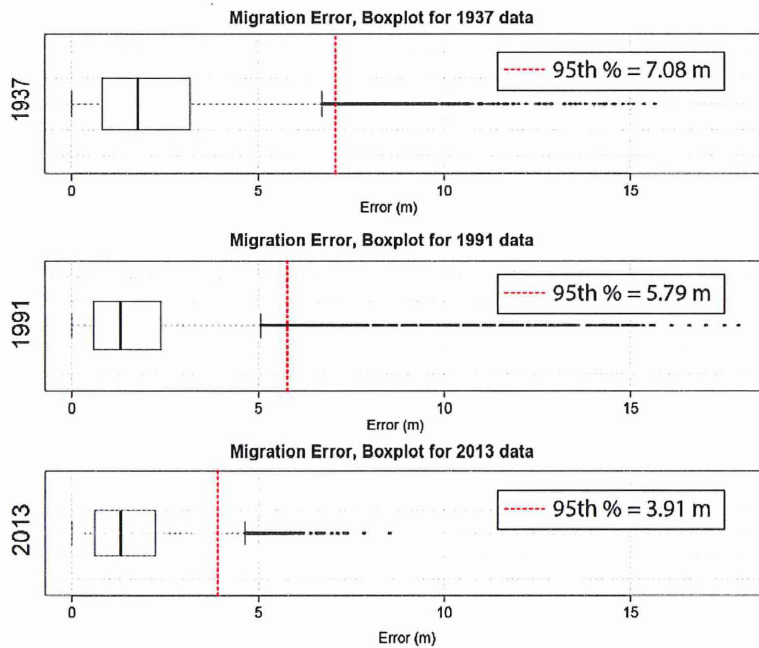


Figure 12.7. Distribution of migration errors estimated from repeat migration measurements along centerlines interpolated from bank delineations on 1937 and 2013 air photos.

Bank elevations

Bank elevations were extracted from lidar data in order to calculate the difference in elevation between the banks ($\Delta\eta$), which is essential for computing the net, local source of sediment derived from channel migration and widening/narrowing. To extract elevations, polygon boxes were generated as a buffer along the manually digitized channel banklines using the Planform Statistics Toolbox developed by J. Wesley Lauer (<http://www.nced.umn.edu/content/stream-restoration-toolbox>). Breaks in elevation were used to identify the edge of bank on the lidar and 2010 aerial photographs were used to verify ambiguous areas where the rise in elevation was too gradual or difficult to identify. A python script was used to calculate $\Delta\eta$ from opposing banks at each 25 m increment. The script extracted the elevations from the lidar data using the Zonal Statistics as Table function from the Arcpy module and then subtracting left and right arrays of data.

Channel cross sections

Multiple locations throughout the watershed were surveyed to estimate average bankfull depth. Cross sections were measured in summer 2012 using a Nikon NPL-332 Total Station at 6 different locations that span the range of channel sizes in our study area. Each survey was between 150 and 200 m long with 15 meter spacing between cross sections. Historical cross sections near Houston obtained from the US Geological Survey Minnesota Water Resources Division were also used. Average bank height was estimated for these sites and extrapolated to reaches with the same stream order and similar channel width throughout the rest of the channel network.

Sediment mass

Contributions of fine sediment to the channel from meander migration and widening were calculated for the most recent decades by multiplying the channel width or migration rate, bulk density and grain size, and difference in elevation between the two banks or total bank height, for channel migration or channel widening, respectively. Sediment contributions were calculated at the scale of each 25 m increment for channel migration and at the scale of ten times the average reach width for channel widening. Sediment mass contributed to the channel was computed using the following formulas:

$$E_M = C \Delta\eta S D_{<67} \rho$$

$$E_W = W \left[2 \left(H_{bf} + \frac{\Delta\eta}{2} \right) \right] S D_{<67} \rho$$

where E_M is the net, local sediment mass contributed to the channel from meander migration, C is the migration rate, $\Delta\eta$ is difference in elevation between the banks, S is the length of the bank ($S = 25$ m for channel migration; $S = 10$ times the average width of the reach), $D_{<67}$ is the percent of sediment smaller than $67 \mu\text{m}$, ρ is the bulk density, E_W is the net, local sediment mass contributed to the channel due to channel widening, W is the channel widening/narrowing rate, and H_{bf} is the average bankfull height of the channel. A python script was used to compute total sediment contributions due to channel migration by multiplication of the variables organized as numpy arrays.

Results

Channel length

As a result of cut offs and meander migration, total channel length of the mainstem study area has been variable over time with no consistent increasing or decreasing trend. Changes in total length since 2003 are minor, with total lengths ranging from 128.7 to 129.2 km (<0.5% difference in total channel length, Table 12.1). Before 2003, changes in total length appear somewhat more variable on a decadal scale, in some cases decreasing more than a kilometer (1947 to 1953) and in other cases increasing by 2.5 km (1975 to 1991).

Table 12.1: Channel length (in kilometers) over time for each reach (columns) at each time step.

Length (km)												Total
Year	11	10	9	8	7	6	5	4	3	2	1	
1937	16.85	11.63	12.93	4.60	19.84	13.77	17.20	3.86	5.44	13.96	10.43	130.5
1947	16.93	11.74	13.03	4.59	20.09	12.77	16.06	3.90	5.47	14.01	10.44	129.0
1953	16.70	11.59	12.85	4.59	19.67	12.59	15.99	3.90	5.49	14.01	10.42	127.8
1975	16.88	11.71	12.82	4.72	19.64	12.22	15.20	3.93	5.50	14.10	10.43	127.2
1991	16.97	11.83	13.00	4.82	19.92	12.73	16.26	4.03	5.51	14.15	10.50	129.7
2003	16.98	11.78	12.94	4.88	19.85	12.25	15.78	4.03	5.51	14.17	10.50	128.7
2006	16.98	11.78	12.93	4.92	19.78	12.33	15.92	4.03	5.50	14.17	10.51	128.9
2008	17.00	11.80	12.87	4.84	19.73	12.31	16.05	4.04	5.51	14.17	10.51	128.8
2010	17.00	11.84	12.89	4.88	19.82	12.40	16.19	4.05	5.51	14.17	10.49	129.2
2011	16.97	11.80	12.84	4.81	19.68	12.29	16.13	4.03	5.51	14.16	10.50	128.7
2013	16.95	11.79	12.81	4.83	19.68	12.35	16.37	4.06	5.51	14.17	10.50	129.0

*color ramp corresponds to magnitude to illustrate trends and is applied to each reach individually

Channel width

Mean channel width for individual reaches and the entire study area have undergone some major changes since 1937. While a considerable amount of variability occurred over the past eight decades, there has been a slight general trend of widening, especially apparent in individual reaches (Table 12.2). Along several reaches, the channel has been wider at some point in the past than in was in 2013 (most commonly 1953, which followed an exceptionally high flow year). When considering the entire study area, important narrowing occurred between 1953 and 1975, and between 2003 and 2006. All except one reach (#1) narrowed between 1953 and 1975. Between 2003 and 2006, narrowing is also observed along 9 reaches, while (significant) widening is evident for the remaining 2 reaches. A consistent pattern of widening occurred between 2006 and 2013. There are also some spatial variations in the widening since 2006: some reaches (#8,7,6) reached their widest state in 2011 and have narrowed slightly since then, while most reaches exhibit narrowing and widening at different times during this seven-year period, even if it resulted in a general widening trend. Changes in channel width for the entire 130 km study reach are shown as box and whisker plots for multiple time periods in Figure 12.8.

Table 12.2. Average width of the channel (in meters) for each reach (columns) at each time step.

Year	Mean Width (m)											
	11	10	9	8	7	6	5	4	3	2	1	Average
1937	32.3	39.9	36.3	41.5	42.4	44.5	50.4	53.6	54.0	53.9	52.2	44.3
1947	36.7	44.3	42.0	55.9	42.1	47.6	52.1	63.5	57.9	61.4	52.0	48.0
1953	39.7	43.7	43.4	61.3	46.5	55.2	53.5	68.2	67.2	67.2	57.3	52.0
1975	36.2	38.9	37.3	47.5	42.6	42.8	46.0	50.2	51.7	63.1	58.1	45.6
1991	36.4	39.0	42.3	43.1	42.5	43.3	49.4	53.4	57.4	68.1	60.0	47.5
2003	35.6	36.1	39.5	41.2	43.5	48.6	49.7	56.1	55.9	66.6	60.7	47.4
2006	34.8	37.7	43.0	37.2	41.1	43.0	47.6	51.3	51.6	63.5	56.6	45.4
2008	34.9	36.5	40.4	47.1	44.0	48.2	50.1	52.2	51.1	62.8	57.9	46.8
2010	36.8	39.8	43.4	48.9	47.6	50.0	51.9	56.2	55.8	67.7	64.9	50.0
2011	38.4	37.9	42.6	55.1	48.1	53.5	56.4	57.5	55.3	67.5	63.3	51.1
2013	39.4	42.0	44.7	52.8	47.8	52.8	57.7	60.8	59.7	69.0	63.7	52.3

*color ramp corresponds to magnitude to illustrate trends and is applied to the entire table and separately to average column

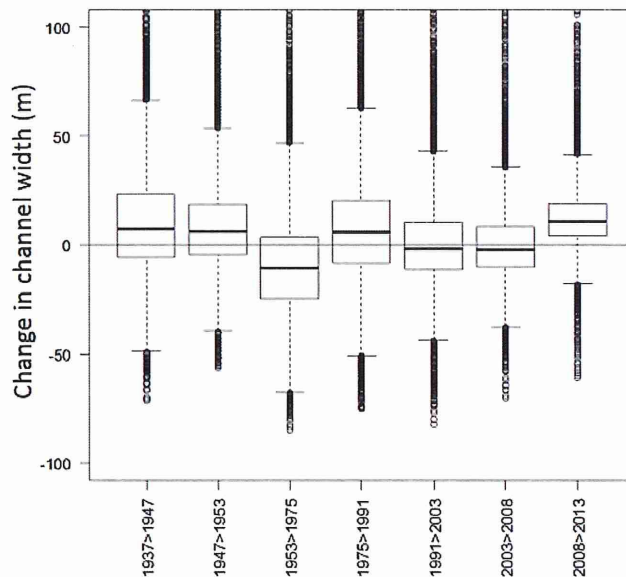


Figure 12.8. Box and whisker plots indicating the distribution of changes in channel width measured for the entire 130 km reach of the mainstem Root River.

Channel Area

The changes in channel length and width are combined to quantify total changes in channel surface area. Although channel width is more interesting from a hydrological point of view, channel surface area is more useful for the sediment budget, as it is directly related to the mass balance of sediment exchange between the channel and floodplain. For example, if channel widening was compensated by shortening, surface area could remain constant, resulting in zero net influence on the budget. The overall pattern indicates that the channel surface area is at its largest in 2013. This pattern is comparable with the pattern in channel width, with major decreases in channel area between 1953 and 1975, and between 2003 and 2006. Similar to analyses of channel length and width, the patterns for the individual reaches are slightly different, and some reaches have their maximum surface area in 1953, 2010 or 2011 (Table 12.3).

Table 12.3. Total surface area (km²) of the channel for each reach (columns) at each time step.

Year	Area km ²											Total
	11	10	9	8	7	6	5	4	3	2	1	
1937	0.544	0.464	0.470	0.191	0.841	0.613	0.866	0.207	0.294	0.752	0.544	5.785
1947	0.621	0.521	0.547	0.257	0.847	0.608	0.837	0.248	0.316	0.860	0.543	6.204
1953	0.663	0.507	0.558	0.282	0.915	0.695	0.856	0.266	0.369	0.942	0.597	6.650
1975	0.612	0.455	0.478	0.224	0.836	0.522	0.700	0.197	0.285	0.890	0.606	5.805
1991	0.618	0.462	0.550	0.208	0.847	0.551	0.803	0.215	0.316	0.964	0.630	6.163
2003	0.604	0.425	0.511	0.201	0.863	0.596	0.785	0.226	0.308	0.943	0.637	6.099
2006	0.592	0.444	0.556	0.183	0.812	0.530	0.758	0.207	0.284	0.900	0.595	5.860
2008	0.594	0.431	0.520	0.228	0.869	0.593	0.804	0.211	0.282	0.890	0.609	6.031
2010	0.625	0.471	0.560	0.238	0.944	0.620	0.840	0.228	0.308	0.960	0.681	6.474
2011	0.652	0.447	0.547	0.265	0.946	0.657	0.910	0.232	0.305	0.956	0.664	6.582
2013	0.668	0.496	0.573	0.255	0.941	0.652	0.945	0.247	0.329	0.978	0.668	6.752

*color ramp corresponds to magnitude to illustrate trends and is applied to each reach individually

Channel Migration

Despite increases in high- and low-flows (60% and 80% increases, respectively since 1990), there have been no significant increases in channel migration for any reach over the past eight decades. This is an interesting result for the geomorphic community, as it contradicts contemporary theory that migration is directly related to in-channel flows. At the same time, this interesting observation has important implications for future sediment reduction strategies, as discussed below in the SWAT modeling section. While the results do not indicate any significant temporal shifts, they revealed consistently high migration rates along reaches 5, 6, and 8 (Table 12.4). This indicates that reach-scale factors are driving elevated erosion, supported by Souffront (2014), indicating that areas of extreme channel migration had higher occurrence in cultivated areas. These highly active reaches may be large components of the floodplain sediment exchange that was found to exert a large control on sediment flux along the Root River (Stout et al., 2012). It is tempting to conclude that bank stabilization efforts targeting these highly active reaches may be an important component of a sediment reduction strategy. However, localized bank stabilization projects are expensive and may be more likely to exacerbate bank erosion immediately up or downstream, as has been observed at the Old Barn Resort, near Preston. Such projects may be useful in cases where infrastructure is directly at risk or where significant benefits to

habitat can be expected, but such bank stabilization projects are very unlikely to be a key component of any sediment reduction strategy at the scale of the entire Root River Basin.

Table 12.4. Average channel migration (m/y) of the channel for each reach (columns) at each time step.

Average meander migration rate (m/yr)												
	11	10	9	8	7	6	5	4	3	2	1	Average
1937_1947	1.18	1.04	2.44	1.68	1.44	1.42	2.16	0.86	0.77	0.92	0.83	1.34
1947_1953	2.58	2.97	2.88	2.80	2.41	1.94	3.26	1.97	1.92	0.97	2.20	2.35
1953_1976	0.85	0.69	1.20	1.03	0.59	1.11	1.27	0.69	0.69	0.63	0.67	0.85
1976_1991	0.82	0.81	1.13	0.81	0.80	1.52	1.61	0.71	0.35	0.54	0.49	0.87
1991_2003	0.30	0.23	0.51	0.84	0.65	0.86	0.87	0.46	0.32	0.20	0.26	0.50
2003_2006	1.19	0.87	1.06	1.79	1.72	1.98	1.73	1.17	1.07	0.93	1.07	1.33
2006_2008	1.48	1.59	2.00	2.61	2.21	2.26	2.68	2.00	1.52	1.53	1.69	1.96
2008_2010	1.08	1.29	1.44	1.46	1.31	1.74	2.01	1.64	1.20	1.15	1.13	1.40
2010_2011	3.00	3.65	3.12	4.28	3.16	4.32	3.60	2.84	2.05	2.22	1.94	3.11
2011_2013	0.84	1.04	1.33	2.03	1.33	1.81	1.90	1.29	0.77	0.82	0.84	1.27

Zooming in beyond the reach scale, Souffront (2014) demonstrated that local-scale (101 – 102 m) avulsions changed notably post-1970s (Figure 12.9). The longitudinal trend analysis clearly demonstrates a decrease in the frequency of channel avulsions along specific portions of the Root River, especially since the 1990s. This further supports our results indicating that changes in water supply (discharge) have not caused proportionate changes in channel morphology, whereas increased riparian vegetation along specific parts of the channel may be armoring banks against erosion. The floodplain and terrace maps from Stout et al. (2014) indicate that near-channel terraces increase downstream from knickzones, potentially increasing near-channel sediment sources. Additional, in-depth analyses of local-scale factors driving erosion and storage are currently under investigation by PhD student Mitchell Donovan at USU.

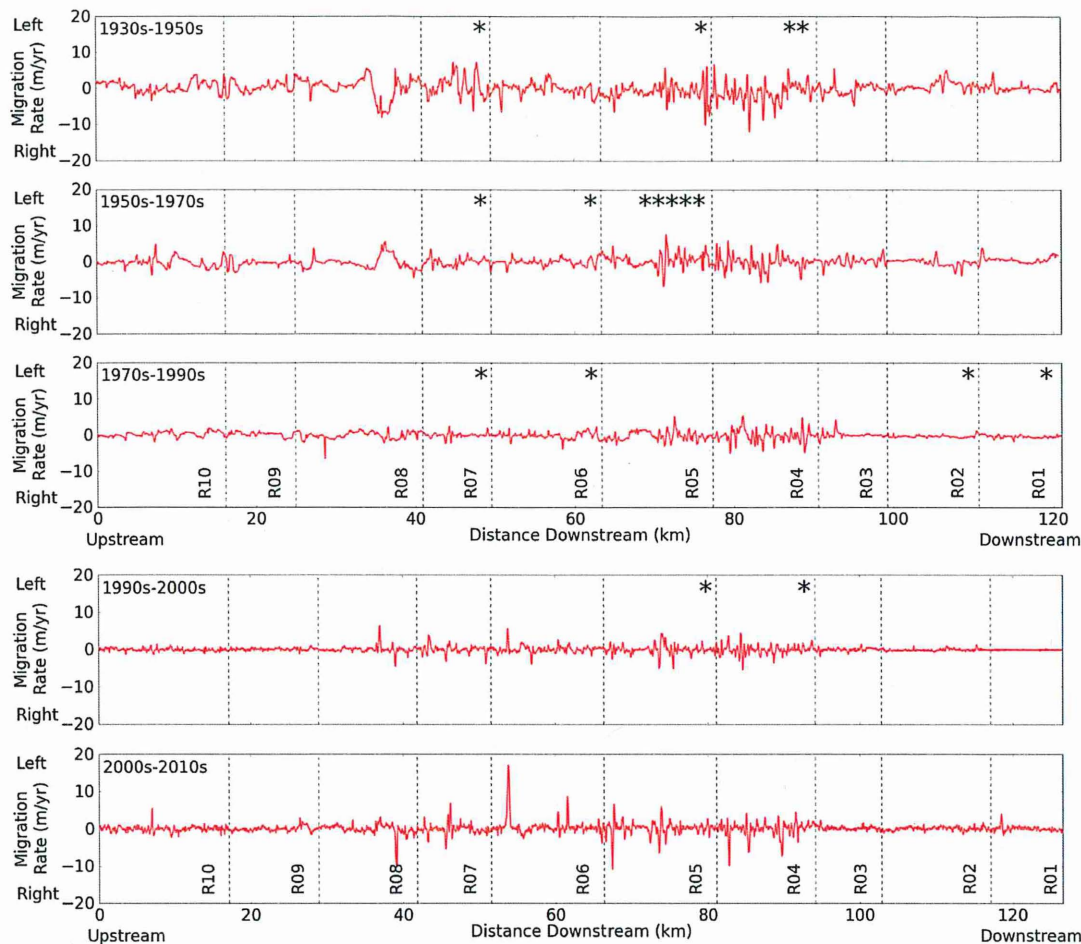


Figure 12.9. Migration rates for the main stem of the Root River from upstream to downstream. Migration to the left bank is positive; migration to the right bank is negative. Dashed lines are reach divisions. Stars on top of each reach area represent avulsions and abrupt changes in channel width. Figure from Souffront, (2014), using reach delineation thereof.

Migration rates followed a similar pattern in the tributaries. Table 12.5 shows the average migration rates for the tributaries of the Root River. Channel widening results for the tributaries of the Root River for the last two decades still follow the widening-narrowing pattern. Table 12.6 shows average widths for the major tributaries for the past two decades. This analysis shows that tributaries stored sediment in their floodplain by narrowing during 1990s-2000s and have since been eroding this sediment as part of the widening -narrowing adjustment pattern.

Table 12.5. Tributary migration rates for major tributaries of the Root River for recent decades

Tributary	Average Migration rates (m/yr)	
	1990s-2000s	2000s-2010s
South Fork	0.29	0.53
Rushford Creek	0.30	0.59
South Branch	0.41	0.49

North Branch	0.45	0.52
Money Creek	0.23	0.33
Middle Branch	0.50	0.46

Table 12.6. Tributary average width measured on a reach-by-reach basis for recent decades

South Fork

Reach	Length (m)	Average Width (m)			Percent Change (%)		Delta width (m)	
		1991	2003	2010	1990s-2000s	2000s-2010s	1990s-2000s	2000s-2010s
reach5	15600	10.19	8.67	8.45	-0.15	-0.03	-1.52	-0.22
reach4	16250	14.25	13.99	14.03	-0.02	0.00	-0.26	0.04
reach3	16620	15.43	12.88	13.79	-0.17	0.07	-2.55	0.91
reach2	16800	16.26	14.23	14.65	-0.12	0.03	-2.03	0.42
reach1	9910	19.43	17.72	17.45	-0.09	-0.02	-1.71	-0.27
Total					-0.11	0.01	-1.61	0.18

Rushford Creek

Reach	Length (m)	Average Width (m)			Percent Change (%)		Delta width (m)	
		1991	2003	2010	1990s-2000s	2000s-2010s	1990s-2000s	2000s-2010s
reach3	14420	9.97	6.48	9.27	-0.35	0.43	-3.49	2.79
reach2	15340	12.36	8.61	10.59	-0.30	0.23	-3.75	1.98
reach1	3410	16.52	13.87	15.94	-0.16	0.15	-2.65	2.07
Total					-0.27	0.27	-3.30	2.28

South Branch

Reach	Length (m)	Average Width (m)			Percent Change (%)		Delta width (m)	
		1991	2003	2010	1990s-2000s	2000s-2010s	1990s-2000s	2000s-2010s
reach6	14700	14.9	10.82	11.38	-0.27	0.05	-4.08	0.56
reach5	14510	13.51	9.4	8.7	-0.30	-0.07	-4.11	-0.70
reach4	16240	14.56	10.28	10.89	-0.29	0.06	-4.28	0.61
reach3	16380	16.36	12.46	12.55	-0.24	0.01	-3.90	0.09
reach2	16080	18.86	14.48	17.94	-0.23	0.24	-4.38	3.46
reach1	8900	20.33	15.34	17.23	-0.25	0.12	-4.99	1.89
Total					-0.26	0.07	-4.29	0.99

North Branch

Reach	Length (m)	Average Width (m)			Percent Change (%)		Delta width (m)	
		1991	2003	2010	1990s-2000s	2000s-2010s	1990s-2000s	2000s-2010s
reach6	13520	16.74	14.56	17.97	-0.13	0.23	-2.18	3.41
reach5	11840	42.05	16.03	21.23	-0.62	0.32	-26.02	5.20
reach4	13170	26.74	19.96	24.47	-0.25	0.23	-6.78	4.51
reach3	12470	24.31	19.16	23.39	-0.21	0.22	-5.15	4.23

reach2	12970	24.65	19.98	24.83	-0.19	0.24	-4.67	4.85
reach1	16290	26.49	20.73	25.37	-0.22	0.22	-5.76	4.64
Total					-0.27	0.25	-8.43	4.47

Money Creek

Reach	Length (m)	Average Width (m)			Percent Change (%)		Delta width (m)	
		1991	2003	2010	1990s-2000s	2000s-2010s	1990s-2000s	2000s-2010s
reach2	10460	8.69	7.47	9.62	-0.14	0.29	-1.22	2.15
reach1	10120	10.21	8.21	11.14	-0.20	0.36	-2.00	2.93
Total					-0.17	0.32	-1.61	2.54

Middle Branch

Reach	Length (m)	Average Width (m)			Percent Change (%)		Delta width (m)	
		1991	2003	2010	1990s-2000s	2000s-2010s	1990s-2000s	2000s-2010s
reach6	9830	9.61	7.32	9.88	-0.24	0.35	-2.29	2.56
reach5	12680	13.84	9.5	12.87	-0.31	0.35	-4.34	3.37
reach4	11820	16.4	13.12	17.49	-0.20	0.33	-3.28	4.37
reach3	12130	15.13	13.67	17.37	-0.10	0.27	-1.46	3.70
reach2	12340	20.08	17.25	20.7	-0.14	0.20	-2.83	3.45
reach1	14200	24.47	19.95	24.84	-0.18	0.25	-4.52	4.89
Total					-0.20	0.29	-3.12	3.72

Bank heights extracted from throughout the channel network were used to calculate the difference in elevation between opposing banks ($\Delta\eta$). Figure 12.10 shows the absolute elevation of right and left banks as well as delta eta for a representative reach (1). Average $\Delta\eta$ values ranged from 0.13 m to 0.78 m along the mainstem Root River. Results for all other reaches are documented in Souffront (2014). Reach 2 had the smallest difference in bank heights with an average of 0.13 m. Reach 11, furthest upstream, had the greatest difference in bank heights with an average of 0.78 m. Average $\Delta\eta$ values for the tributaries were 1.43, 0.89, 0.92, 1.58, 1.38, and 1.44 meters for South Fork, Rushford Creek, South Branch, North Branch, Money Creek, and Middle Branch, respectively.

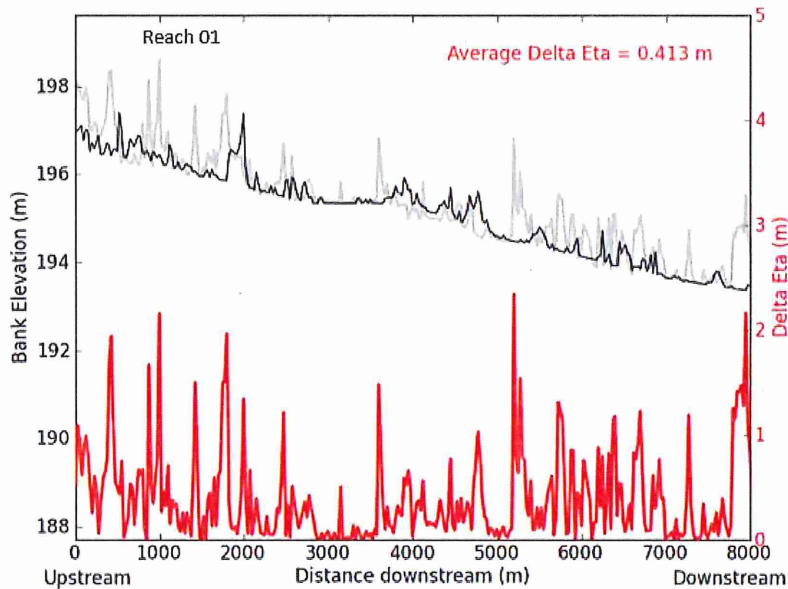


Figure 12.10. Right bank (black), left bank (gray) elevations extracted, and delta eta (red) values computed for Reach 1 (furthest downstream) for the main stem Root River.

Sediment mass results are presented in Table 12.7. The largest fraction of sediment is contributed from the main stem Root River, due to the fact that this portion of the channel network contains the largest cross sectional area and exhibits generally higher migration rates. However, tributaries contribute non-negligible amounts of sediment, comprising nearly half of the total sediment mass calculated. The total amount of fine sediment ($<67 \mu\text{m}$) contributed to the Root River due to lateral channel adjustment for the last decade was estimated to be $3.0 \times 10^5 \text{ Mg/yr}$. The main stem contributes a total of $1.3 \times 10^5 \text{ Mg/yr}$, followed by the North Branch ($4.9 \times 10^4 \text{ Mg/yr}$), Middle Branch ($5.1 \times 10^4 \text{ Mg/yr}$), South Branch ($2.2 \times 10^4 \text{ Mg/yr}$), South Fork ($2.6 \times 10^4 \text{ Mg/yr}$), Rushford Creek ($9.8 \times 10^3 \text{ Mg/yr}$), and Money Creek ($9.8 \times 10^3 \text{ Mg/yr}$). It is noteworthy that the sediment fingerprinting results, discussed above, indicate a relatively low proportion of sediment derived from agricultural fields (and therefore relatively high proportion of sediment derived from bank erosion). These are entirely independent measurements that point toward a similar phenomenon, thus strengthening our confidence that bank erosion is indeed an important sediment source in the North Branch of the Root River. Total uncertainty in these calculations, after propagating error associated with georeferencing historic air photos, digitizing banks, extracting bank elevations, measuring and extrapolating grain size and bulk density and extrapolating cross sections was estimated to be 60%, as discussed in detail by Souffront (2014). Excluding migration or widening rates and lidar elevations that fall below their respective uncertainty values reduces estimates by 25%.

Table 12.7. Total sediment volume and sediment mass contributed to the channel from channel migration and widening for the main stem and major tributaries

Root River Main streams	Widening			Migration			Total		
	Volume (m ³ /yr)	Volume <67 μm (m ³ /yr)	Mass (Mg/yr)	Volume (m ³ /yr)	Volume <67 μm (m ³ /yr)	Mass (Mg/yr)	Volume (m ³ /yr)	Volume <67 μm (m ³ /yr)	Mass* (Mg/yr)
Main Stem	150389	109784	142719	23715	17312	22506	174104	127096	1.3 x 10 ⁵
South Fork	2791	2037	2649	33917	24759	32187	36708	26797	2.6 x 10 ⁴
Rushford Creek	9839	5510	7163	7712	4319	5614	17551	9829	9.8 x 10 ³
South Branch	12490	9118	11853	18407	13437	17468	30897	22555	2.2 x 10 ⁴
North Branch	68353	38278	49761	20856	11679	15183	89209	49957	4.9 x 10 ⁴
Money Creek	8221	6002	7802	5357	3910	5083	13578	9912	9.8 x 10 ³
Middle Branch	51200	37376	48589	20060	14644	19037	71260	52020	5.1 x 10 ⁴
							433307	298165	3.0 x 10 ⁵

13. SWAT model of the Root River Basin

Motivation for development of a SWAT model

The Soil and Water Assessment Tool (SWAT) is a watershed scale model that simulates hydrology, erosion and nutrient fluxes in an effort to predict the impacts of land management practices on water, sediment and chemical fluxes over annual to decadal timescales. The model is well established in the water quality community, has been set up to ingest large amounts of available spatially explicit data (e.g., soils, land use/land cover, precipitation, streamflow) and benefits from a broad and diverse set of independent developers from around the world consistently working to improve representation of key processes and dynamics. In addition, SWAT was selected for this study because it has been extensively applied to agricultural landscapes including karst (*Baffaut and Benson, 2009*) and was previously applied to the South Branch of the RRB by (*Folle et al., 2007*).

SWAT uses a large number of adjustable parameters to allow the modeler to adjust the rates and magnitudes of a wide variety of processes to obtain the best possible calibration. While this may be seen as a strength of SWAT insofar as it allows flexibility to modify the model to essentially any watershed setting, it leaves the model susceptible to problems of equifinality, in which multiple parameter combinations may result in the same output and the modeler is often left with inadequate information regarding which parameter combination most accurately represents the system. Equifinality is particularly problematic if those disparate parameter combinations have substantially different implications for future management decisions. Thus, we have limited our use of SWAT to questions that we feel can be reasonably informed by the model despite potential problems associated with equifinality.

Current sediment reduction strategies commonly consider local reduction of erosion from agricultural fields, riparian corridor and stream banks (MPCA, 2015). Recognizing that near-channel sediment sources dominate sediment loads in the Le Sueur watershed, Belmont et al., 2011 suggested that improved management of water runoff at the watershed scale may significantly reduce loading from near-channel sources downstream. Recent work (Cho et al., in prep) has confirmed that water detention basins distributed throughout the watershed can indeed reduce erosion of near channel sediment sources downstream in the Le Sueur watershed. And such structures have been successfully implemented elsewhere (Kannan et al., 2014). While the Root River is in a substantially different landscape setting and has been subjected to a slightly different land use history, it is useful to explore the local and downstream effects that water and sediment detention structures distributed throughout the basin might have on water quality.

This modeling effort had two key objectives. The first is to simply provide Universal Soil Loss Equation (USLE) soil loss estimates for the entire watershed. USLE estimates soil loss at the plot (sub-acre) scale according to a rainfall erosivity factor, soil erodibility factor, topographic factors and cropping management factors (Wischmeier and Smith, 1978). SWAT-derived sediment loading predictions at the mouth of large watersheds should be used with caution due to inadequacies in sediment routing due to poor spatial resolution and constraints on the physical processes governing erosion, transport and deposition of sediment at the landscape scale. However, USLE estimates of local soil loss provide valuable insight regarding the vulnerability of different portions of the landscape to soil erosion processes, the long-term (annual to decadal) effects of which are reasonably well represented in the equation. The second objective of this modeling effort was to evaluate the effect of introducing surface water impoundment structures in the Root River Basin in an effort to attenuate peak streamflows and reduce the hydrologic flashiness of the system. A few such structures have been utilized within the Root River Basin historically, but the structures are not currently meeting their design objectives due to sedimentation over the past 50-70 years. Could renewal of such structures or new construction of similar structures provide an effective means to reduce sediment loads in the Root River Basin? As discussed above, the karst setting of the Root River Basin does not favor for the formation of natural lakes and may also present challenges for the implementation and maintenance of large detention basins. However, based on conversations with MDA staff, we wanted to verify if such an approach is feasible within certain areas of the RRB.

The evaluation of surface water detentions structures should be considered a preliminary feasibility study. SWAT does not identify the exact location of an impoundment structures beyond the spatial resolution of a subbasin. In conducting this research we found that detention basins are generally not recommended by the MPCA for Karst areas. However, they can be considered as a BMP alternative, if the bottom of the impoundment structure has at least a three feet separation between the seasonally high water table according to MPCA guidelines (MPCA, 2008).

Model Description

The Soil and Water Assessment Tool (SWAT) is a continuous time, semi-distributed hydrologic model (Bekele and Nicklow, 2007) that operates on a daily time step and is capable of predicting the effects of changes in water management in ungaged watersheds (Gassman et al., 2007). This study uses the SWAT2012.exe Revision 622 packaged with ArcSWAT 2012.10_1.15 to build and conduct scenario-based simulations to detain water within specific sub-basins of the RRB SWAT model. Subbasin delineation in

SWAT is accomplished using topography data, by choosing a threshold-based stream channel definition and by specifying locations where a model output is required to facilitate comparison with measured streamflow. The threshold-based stream channel definition option allows us to control the size of the subbasins, which is crucial for capturing variability in precipitation and also to simulate flows at any desired location where flow outputs are needed. A Hydrologic Response Unit (HRU) is defined as the area that consists of a unique combination of land use, soils and topography (Neitsch et al., 2011). A high resolution SWAT model was built by capturing all soils and slope categories based on a 20% land use threshold criteria using the multiple HRUs definition option, resulting in 17,174 HRU's.

Model Assumptions

The following assumptions were considered for setting up the model.

1. Model was initialized with land use data from 2006 (first year when the USDA Cropland Data Layer (CDL) was available). Other than corn-soybean rotation, all other land uses were held constant over the simulation period.
2. Nutrient application was accomplished through commercial N and P fertilizers although other practices are present such as manure application. As specific fields where such practices are used are not known, the dominant practice (using commercial N and P fertilizer, see details about the actual fertilizer applied in, see Appendix B) was assumed for the entire basin where corn-soybean rotation was considered.
3. Crop water needs are satisfied through precipitation and no additional irrigation water was provided to grow crops.
4. Farming practices such as tillage (conventional tillage, see details in Appendix B) were assumed uniform over all fields where corn-soybean rotation were implemented.
5. Hydrologic effects of the karst system (i.e., stream flow loss or gain) were accomplished by altering tributary and main channel transmission losses.
6. Rapid and slow responses of groundwater contribution to streamflow that result from preferential pathways were accomplished by altering groundwater delay times and rate and quantity of groundwater that is fed to streamflow.

Input Data

Topography data

The watershed and stream network were delineated using a 10 m DEM (*U.S. Geological Survey, 2013a; b*). A total of 89 subbasins were delineated by specifying a 3000 ha threshold in addition to six outlet locations where streamflow data were available and therefore where calibration and validation of the model were performed. NHD Flowlines from the National Hydrography Dataset (NHD) were used to burn the stream network into the DEM (*USDA-NRCS et al., 2015*). Outlet locations for streamflow were obtained from MN DNR (*MN DNR and MPCA, 2009*).

Land Cover and Land Use and soils data

Cropland Data Layer (CDL) from year 2006 was used to specify land use-land cover data for the model. Based on 2006 CDL data, the predominant land use for RRB are deciduous forest: 26.1%, corn: 23.3%, grass/pasture: 20.1%, soybeans: 17.8% and alfalfa: 4.5%, which sums to over 90% of the basin. The remaining 10% of the basin area includes land uses such as urban or suburban development, woody wetlands and other crops, including peas and barley among others. SSURGO soils data were used to

characterize soils (IA191, MN039, MN045, MN055, MN099, MN109, and MN169 (*USDA NRCS, 2013; 2014a; b; c; 2015a; b; c*)).

Weather data

Temperature, solar radiation, wind speed, and relative humidity data were obtained from SWAT Global weather database from the year 1998 to 2013. Precipitation data were specified by processing PRISM rasters obtained at a daily time resolution (*PRISM Climate Group*).

Management data

The management scenario implemented for the watershed attempts to capture the general nature of the practices that occur in the basin and does not necessarily reflect a specific practice that would occur at a particular field. Management operations include tillage, planting, fertilizer application, and harvest. A corn-soybean management scenario was implemented for the watershed to capture the general practices that occur in the basin and not necessarily what would occur at each individual field. The FANMAP survey conducted in 2003 documents that over 80% of the South Branch of the Root River implements this management scenario (MDA, 2005).

While the questions we are attempting to answer are not directly related to fertilizer and nutrient management, hydrology and erosion susceptibility are both indirectly controlled by crop growth and therefore care was needed to ensure nutrients were reasonably treated within the model. Fall N fertilizer application is discouraged in southeastern Minnesota based on a study conducted in Olmstead County and recommendations are extended to the Southeastern region of the state (*Randall et al., 2008*). These guidelines were implemented when applying N fertilizer within the model. Spring pre-plant applications of N (as urea) is specified in the model at 152 kg N ha⁻¹ (330 kg urea ha⁻¹ assuming 46% N) for corn cultivation (20% top 10 cm and rest below to avoid volatilization). Although other forms of N are applied (such as anhydrous ammonia, DAP, manure and liquid solutions) and other times of application occur (such as fall application, at planting application and side-dress), these types were not considered for this study as they did not appear common according to (MDA, 2005). The FANMAP 2003 survey also documents that over 90% of farms received commercial N fertilizer. Actual scheduling information is shown in Appendix B. Planting and harvesting dates for corn and soybean were specified as the median value of the range listed in the field crops – usual planting and harvesting dates (*USDA, 2010*). Emergence and growth of other vegetation types were scheduled based on heat units.

Karst data

SWAT does not explicitly model karst features such as sink holes. In this study, karst features were modeled by adjusting the effective hydraulic conductivity of the tributary and main channels during calibration. This is a reasonable approach, as the objective of this study was to capture the lumped effect of karst features and not the specific pathways through which water moves in the Karst system. Minnesota DNR distributes spatial data that locates and differentiates the different karst features (such as sink holes and springs, see Figure 3.4). These data were used to inform the calibration process in a qualitative sense (to initialize the hydraulic conductivity values (Figure 13.1). However, the final ranges did not fully reflect that initial characterization as the complex nature of the karst is fully not captured by the number of karst features alone.

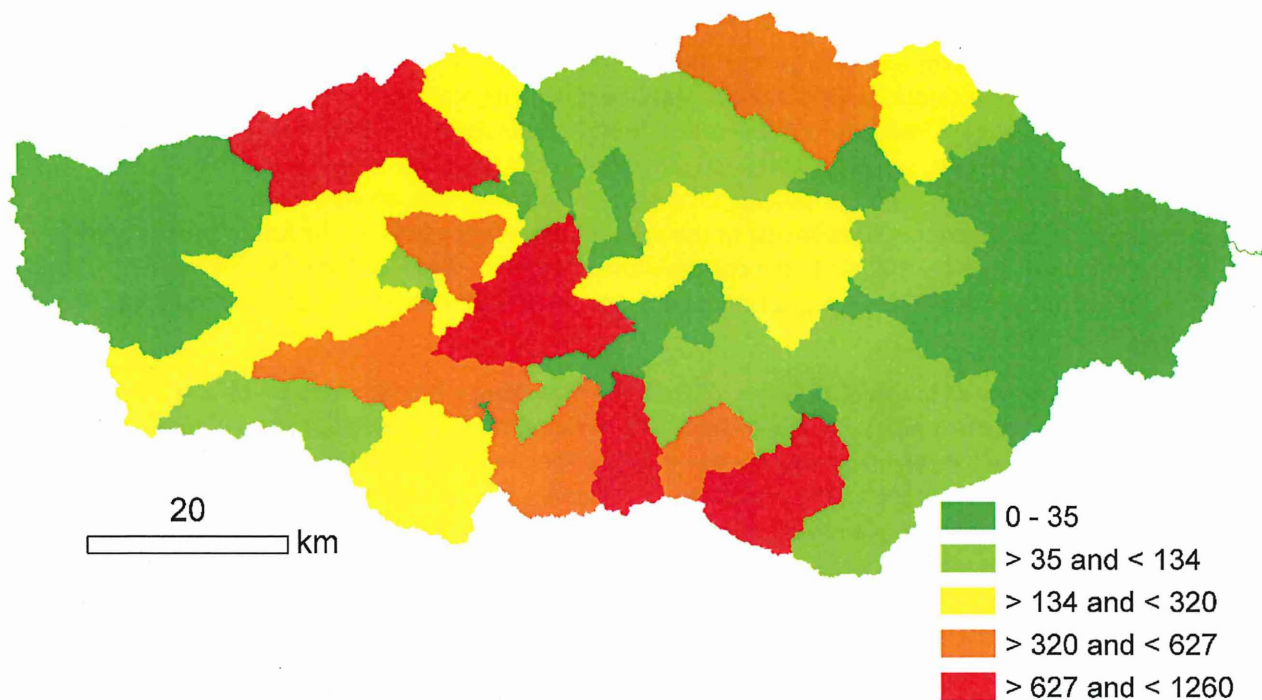


Figure 13.1. Subbasin characterization using number of karst features (from MN DNR data) within each subbasin.

River network and streamflow gages

The river network was delineated by burning the National Hydrography Dataset (NHDplus) stream data into the 10m DEM. The resulting stream network and the five stream gages considered for this modeling effort are shown in Figure 13.2.

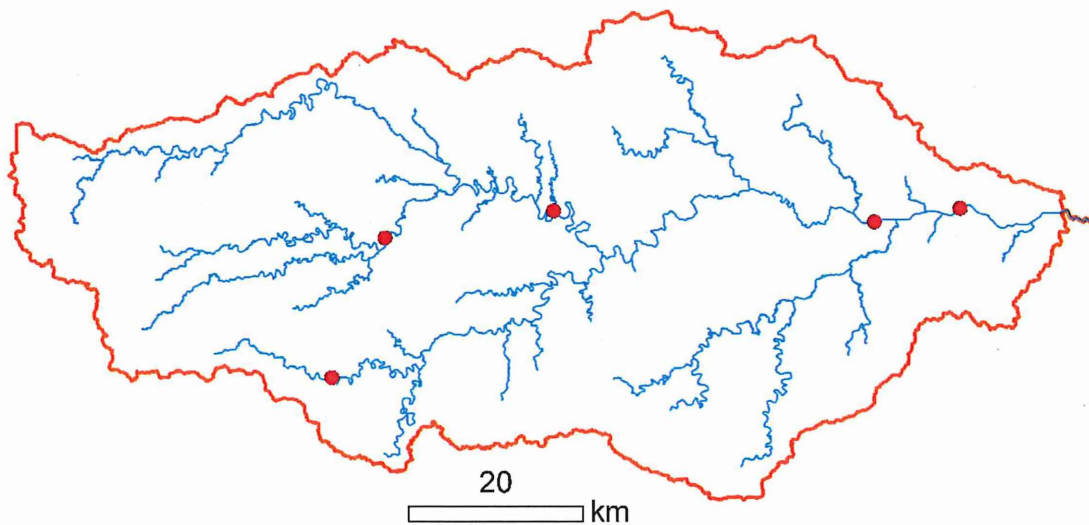


Figure 13.2. Subbasins and river network along with selected gages used in Soil and Water Assessment Tool for model simulation, calibration and validation.

Methods for implementing water impoundment structures

Impoundment structures are used to alter the hydrologic response of a watershed to precipitation events, often in an attempt to reduce the magnitude of high or peak flows. Peak discharge magnitudes, flow volumes and their frequency can be altered with impoundment structures such as detention basins or other flood control structures to help mitigate large floods. Detention basins are engineered to temporarily store storm runoff at suitable locations and later be released with a flow control structure that can be regulated. The effectiveness of the detention basin depends on the total volume of the detention basin. Factors that aid in the determination of basin volume include: (1) release rate, (2) local soil, (3) hydrological and climatological characteristics and the time when stored runoff is to be released (Soong *et al.*, 2009).

Ponds as implemented in SWAT 2012 rev. 622 receive flow from a fraction of the subbasin. The volume of water in the pond is updated at a daily time step. Pond volume at the end of a day is computed as the sum of water stored at the beginning of a day plus the volume of water entering the pond on the same day (as precipitation, surface or sub-surface flow) minus the sum of volume of water flowing out, volume of water evaporating and volume of water lost due to seepage (Neitsch *et al.*, 2011). Inflow to the detention basin (pond) is the sum of surface runoff for the subbasin on any given day, groundwater flow generated within the subbasin, and lateral flow generated within the subbasin. Volume lost to evaporation is calculated as a function of surface area, potential evapotranspiration and an evaporation coefficient. Volume lost to seepage is a function of surface area and effective saturated hydraulic conductivity (Neitsch *et al.*, 2011). In SWAT, ponds are implemented as conceptual water bodies with each subbasin containing only one pond, which receives flow from a specified fraction of the subbasin (Almendinger and Murphy, 2007).

Impoundment structures (also referred to as ponds in this report) were applied in all subbasins in the watershed with different percentages of subbasin area contributing to the impoundment structure. The pond-bottom hydraulic conductivity was varied to account for the order of magnitude variability observed within the Root River Basin. A range of scenarios were simulated to elucidate the effects of pond volume and pond bottom hydraulic conductivity. Four different pond area scenarios were considered, where pond area was equivalent to 20%, 10%, 5% and 1% of the subbasin area, respectively and with a pond depth of 1.2 m. While it is likely that impoundments may be constructed with deeper pools, these simulations provide a reasonable range of water storage volumes and provide an upper constraint on losses due to evapotranspiration and groundwater. The two pond bottom hydraulic conductivity cases considered were, (a) the median value from soils data = 32 mm/hr and (b) a lower value of 1 mm/hr, simulating diminished conductivity as a consequence of deposition of clay particles, microbial activity and deposition of salts (Ahmed, 1997). The fraction of a subbasin contributing flow to the pond was kept constant for all scenarios at 50% of the subbasin area (the average for all subbasins is 2420 ha). Ponds as implemented within the SWAT model have two design volumes, one corresponding to the principal spillway and other the emergency spillway. The pond volume at the emergency condition is implemented as 10% higher than the principal spillway volume.

Calibration and Validation

Evaluation Criteria

Model simulated stream flows were evaluated using two performance criteria, Nash-Sutcliffe Efficiency (NSE) and R^2 . Given the primary hydrologic objective of this modeling effort, evaluation criteria that are sensitive to higher magnitude peaks are essential to determine model performance. NSE is the ratio of the mean squared error to the variance of the observed data. Although, NSE is slightly better because it is sensitive to the observed and model simulated means and variances, both NSE and R^2 are sensitive to

higher magnitude flows. An NSE value of 0 means that the average flow was captured, 1.0 being a perfect fit to observed data, and > 0.5 generally considered a satisfactory model in peer reviewed literature (Moriasi *et al.*, 2007).

NSE and R^2 are computed using the following equations:

$$NSE = 1 - \frac{[\sum_{i=1}^n (Q_{m,i} - Q_{s,i})^2]}{[\sum_{i=1}^n (Q_{m,i} - \bar{Q}_m)^2]}$$

$$R^2 = \frac{[\sum_i^n (Q_{m,i} - \bar{Q}_m)(Q_{s,i} - \bar{Q}_s)]^2}{\sum_i^n (Q_{m,i} - \bar{Q}_m)^2 \sum_i^n (Q_{s,i} - \bar{Q}_s)^2}$$

where,

$Q_{m,i}$ is the measured discharge

$Q_{s,i}$ is the simulated discharge

\bar{Q}_m is the mean of measured discharge

\bar{Q}_s is the mean of simulated discharge

Calibration and validation of flow in RRB

Model performance was evaluated using measured stream flow data from 2000 to 2013 at five streamflow gages. Data were partitioned into calibration and validation datasets with equal data points in each category (with earlier years in the calibration set and later years in the validation set).

Parameters that were varied to achieve calibration are listed in Table 13.1. After populating the model with the best available data, a set of parameters are varied whose values (called calibrated) were reached by varying them using the Sequential Uncertainty Fitting (SUF12) algorithm available through SWAT-CUP.

Model run times (using Intel Xeon CPU 2620 @ 2GHz, 16 GB RAM, 64 bit OS) for the entire RRB were roughly 45 minutes for a 17-year simulation as we have tried to represent the system using the best available data. To reduce run times during model calibration, multiple smaller SWAT models were developed for each of the upstream gages. An upstream to downstream calibration approach was used in an effort to first resolve the flows contributing to the downstream basins, thereby reducing potential for misrepresentation of the system. Once an upstream gage was satisfactorily calibrated and validated, the calibrated model parameters were specified for the appropriate region in the larger model. This approach was applied until all five gages were calibrated. In this process, a common pattern emerged with regards to the basin-wide parameters specified in the *.bsn input file.

Parameter ranges were varied during calibration with consideration of a physically defensible parameter range. Table 13.2 lists the performance metrics for the five gages within RRB where calibration was performed. In reality, any one of the simulations bracketed by the 95% uncertainty band can be considered as a representative simulation. However, for the purpose of a deterministic evaluation criteria, the best simulation was used when reporting the evaluation criteria metrics. Additionally, the parameter combination that provided the best metrics was used for assessing impoundment structure

scenarios. As each gage had different years of stream flow record, the available stream flow data at each stream flow gage was split between calibration and validation sets with the first half included in the calibration set and the second half in the validation set. The period of simulation is from 2000 to 2014 with 1998 and 1999 as warm-up years that were not considered in the analysis. The model performed satisfactorily for both these periods as shown in Table 13.2.

Table 13.1. Critical SWAT model calibration parameters for the Root River Basin

Parameter	Description	SWAT Default value	Calibrated value	Calibrated Range (if applicable)
<u>.bsn file - General watershed description file</u>				
SFTMP	Snowfall temperature (°C)	1	2.35	NA
SMTMP	Snow melt base temperature (°C)	0.5	0.14	NA
SMFMX	Melt factor for snow on June 21 (mm H ₂ O/°C-day)	4.5	3.41	NA
SMFMN	Melt factor for snow on December 21 (mm H ₂ O/°C-day)	4.5	2.54	NA
TIMP	Snow pack temperature lag factor	1	0.53	NA
SNOCOVMX	Minimum snow water content that corresponds to 100% snow over (mm H ₂ O)	1	4.35	NA
SNO50COV	Fraction of snow volume represented by SNOCOVMC that corresponds to 50% snow cover	0.5	0.27	NA
IPET	Potential evapotranspiration (PET) method	Penman/Monteith	Hargreaves	NA
ESCO	Soil evaporation compensation factor	0.95	0.81	NA
EPCO	Plant uptake compensation factor	1	0.19	NA
ICN	Daily curve number calculation method	Soil Moisture Method	Plant ET Method	NA
CNCOEF	Plant ET curve number coefficient	1	0.61	NA
CN_FROZ	Frozen soil adjustment on infiltration/runoff	0.000862	0.00167	NA
<u>.gw file - Groundwater input file</u>				
GW_DELAY	Groundwater delay time (days)	31	NA	1.2 - 456.7
ALPHA_BF	Baseflow alpha factor (1/days)	0.048	NA	0.58 - 1.0
GWQMN	Threshold depth of water in the shallow aquifer required for return flow to occur (mm H ₂ O)	1000	NA	1.6 - 1214.6
<u>.sub file - Subbasin general input file</u>				
CH_N1	Manning's "n" value for tributary channel	0.014	NA	0.03 – 0.09
CH_K1	Effective hydraulic conductivity for tributary channel	0	NA	7.8 – 143.8

.rte file – Main channel input file

CH_K2	Effective hydraulic conductivity for main channel	0	NA	0.86 – 93.02
CH_N2	Manning’s “n” value for main channel	0.014	NA	0.034 – 0.047
NA – Not Applicable				

Table 13.2. SWAT model evaluation metrics for the Root River Basin

Stream gage	Calibration years		Validation years	
	NSE	R ²	NSE	R ²
South Branch near Ostrander	0.50	0.67	0.56	0.63
Middle Branch near Fillmore	0.60	0.70	0.56	0.73
Root River near Houston	0.54	0.57	0.59	0.61
Root River near Mound Prairie	0.68	0.72	0.52	0.61
Root River near Pilot Mound	0.69	0.70	0.64	0.67

A global sensitivity analysis was performed using SWAT-CUP (Abbaspour, 2012) and it was found that the parameters shown in Table 13.3 and Figure 13.3 are most sensitive. Multiple regression is performed by regressing the Latin hypercube generated parameters against the NSE values to determine sensitivity. Consequently, a t-test is used to identify the relative significance of a parameter. Higher absolute value of the t-statistic indicates higher sensitivity of the parameter and closer to zero p-value (< 0.05, a 95% chance that the parameters are sensitive) indicates higher significance. Here all seven parameters are sensitive parameters with the GW_DELAY being the most sensitive parameter.

Table 13.3. Sensitive SWAT parameters for the Root River Basin

Parameter	Description ((Arnold et al., 2012; Neitsch et al., 2011)
GWQMN	Threshold depth of water in the shallow aquifer required for return flow to occur (mm H ₂ O)
ALPHA_BF	Baseflow alpha factor (1/days)
GW_DELAY	Groundwater delay time (days)
CH_K2	Effective hydraulic conductivity in main channel alluvium (mm/hr)
CH_N2	Manning’s n value for the main channel (unitless)
CH_K1	Effective hydraulic conductivity in tributary channel alluvium (mm/hr)

CH_N1 Manning's n value for the tributary channel (unitless)

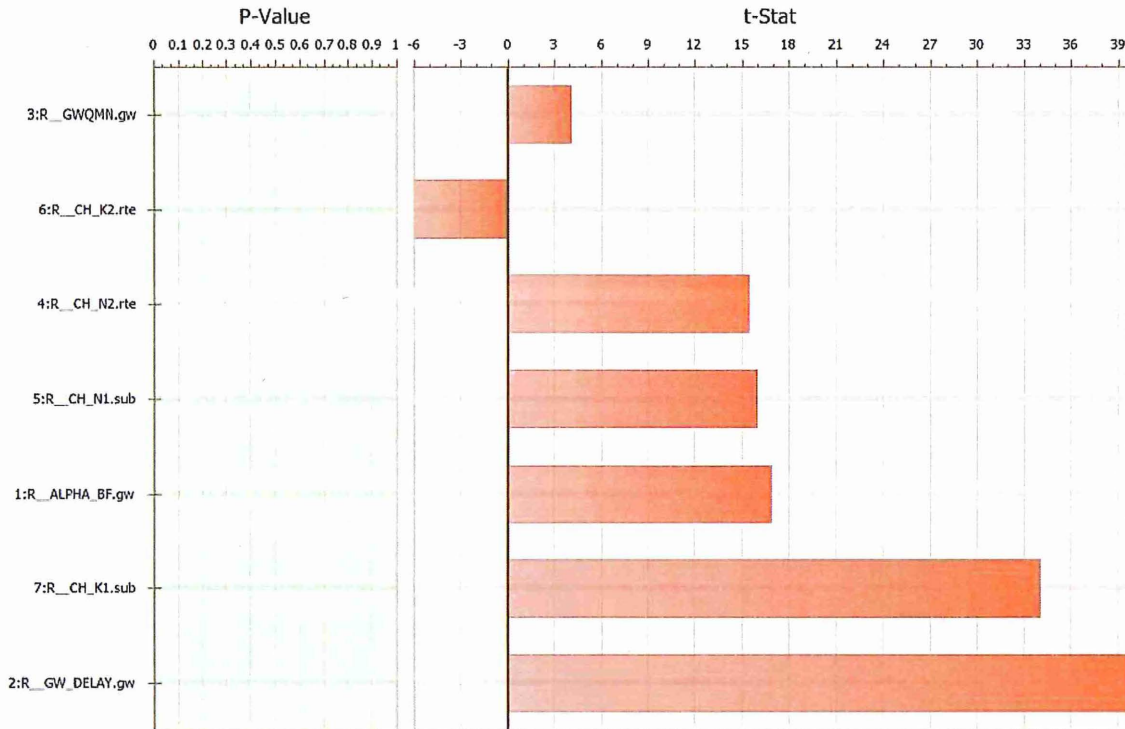


Figure 23.3. Global sensitivity of groundwater, tributary and main channel parameters. Higher absolute value of the t-statistic indicates higher sensitivity of the parameter and closer to zero p-value indicates higher significance. Here all seven parameters are sensitive parameters.

SWAT model hydrologic simulation results

Stream flow simulation at daily time step

The model was able to capture base flows for the gages located in the main stem of the Root River at all three gages (streamflow gages at Pilot Mound, Houston, and Mound Prairie) satisfactorily. However, despite satisfactory NSE and R^2 values, peak flows were less well captured. Measured and predicted peak flow occurrence times were generally well in agreement for all gages. The model performance in the upstream basins (e.g., Middle Branch near Fillmore at and South Branch at Ostrander) where Karst influence is either limited or not well documented also exhibited a similar behavior of under prediction of higher magnitude peak flows.

The greatest challenge in modeling hydrology of the Root River Basin is related to the effects of Karst geology, which impacts the lower two-thirds of the basin. Karst is difficult to represent adequately in SWAT because subsurface flow routes are generally unknown (Ghanbarpour et al., 2010; Kraller et al., 2014). Some streams are known to respond rapidly (within hours) to precipitation, whereas other are slower (response takes weeks). Water can also move between aquifers, further introducing challenges in

modeling such systems. To simulate the hydrologic effects of Karst at the scale of the sub-watersheds, we adjusted channel transmission losses to simulate the presence of losing channels. Inability of the model to capture all peak flows is believed to be the outcome of Karst geology and preferential flow pathways. Overall NSE and R^2 values are well within the acceptable ranges and while predicted peak flows were consistently lower than observed peaks, this systematic offset does not diminish the value of comparing peak flows among different model scenarios with and without impoundment structures.

Annual average water balance

Annual water yield was more sensitive to the pond bottom hydraulic conductivity than it was to the storage volume (Figure 13.4). Although an increase in pond volume resulted in a decrease in the water yield as expected, hydraulic conductivity had a much more pronounced effect on water yield (Figure 13.4). A 10 to 20% increase in pond volume only resulted in a 1% decrease in water yield. However, there was an 8% drop when the pond bottom hydraulic conductivity was increased from 1 to 32 mm/hr (range obtained from SSURGO soil data). There was very little variability regarding the fraction of water following the main hydrologic pathways for all the cases evaluated (Figure 13.5). The major component of the water balance for the entire basin is ET, which accounts for 62% of the precipitation, and did not vary for the scenarios considered. Total aquifer recharge accounts for 25% (computed as annual average) of the precipitation. On average, approximately 1% of the precipitation percolated down to the deep aquifer, which does not reappear as streamflow in SWAT. Except for July, the ET requirements are satisfied by the incoming precipitation. Average annual surface runoff generated is highest for the month of June. High average annual lateral flow in the watershed occurs during the months of April, May and June.

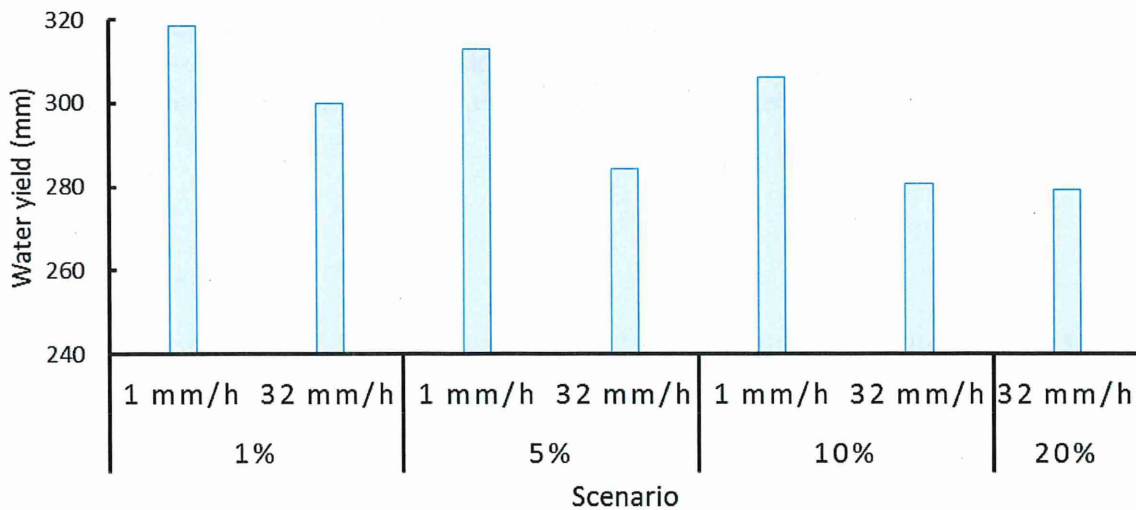


Figure 3. Annual average total water yield in mm from 15 years of model simulation from the year 2000 to 2014. The bottom number in each scenario represents the percent of subbasin area allocated for the impoundment structure and two numbers immediately above represent the pond bottom hydraulic conductivity in mm/hr.

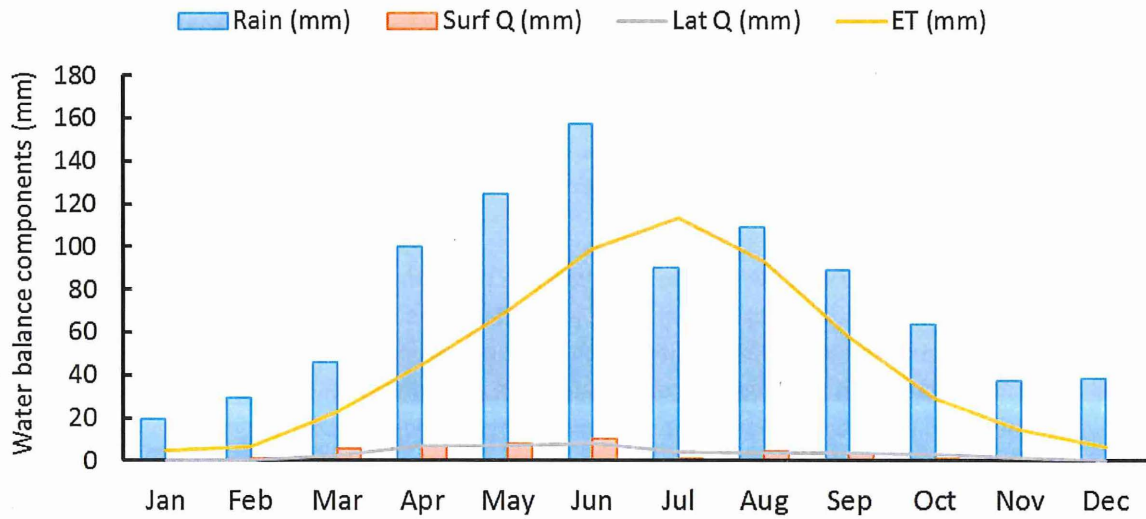


Figure 4. Annually averaged monthly water balance components corresponding to 20% of the subbasin area in ponds and with a pond bottom hydraulic conductivity of 32 mm/hr.

Effect of impoundment structures on streamflow

Streamflow estimates representing current conditions were compared with seven different impoundment scenarios (combination of pond volume and pond bottom hydraulic conductivity). Climate was not altered among scenarios. The two hydraulic conductivity cases are compared at 5 gage locations to capture both spatial and temporal variability. Daily timescale hydrographs covering the entire 15 year simulation period demonstrate the reductions predicted from the 5% and 20% scenarios (Figures 13.6 to 13.10).

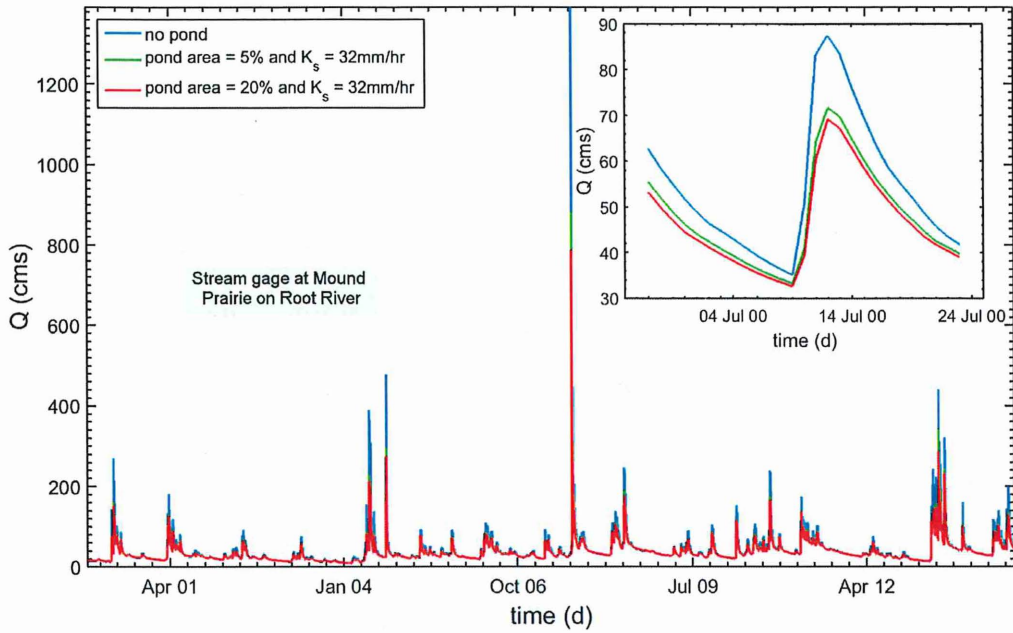


Figure 53.6. Daily streamflow from the year 2000 to 2014 to illustrate the effect of ponds at Mound Prairie stream gage on the main stem of the Root River.

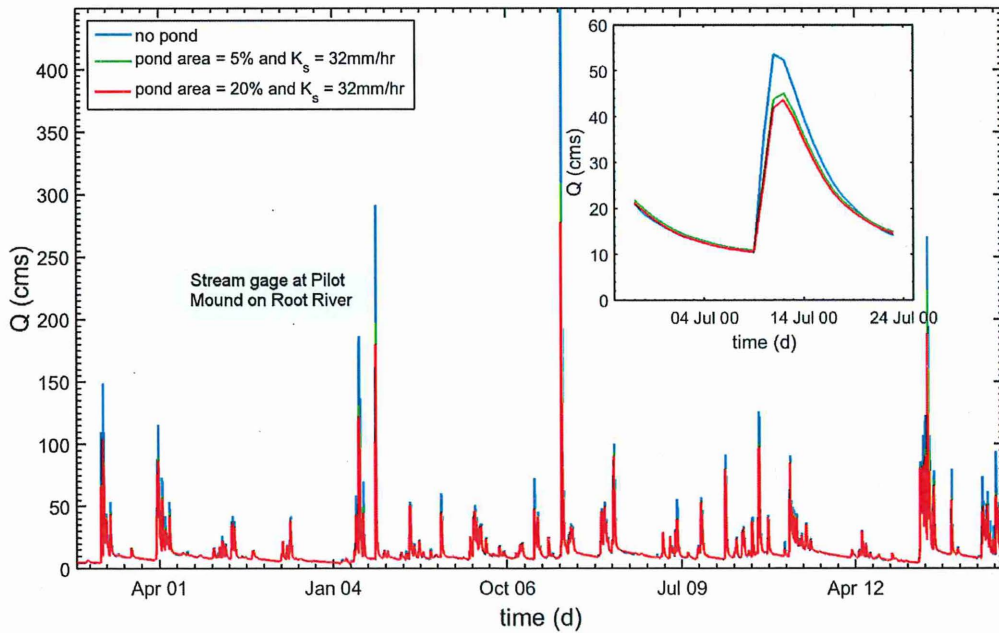


Figure 13.7. Daily streamflow from the year 2000 to 2014 to illustrate the effect of ponds at Pilot Mound stream gage on the main stem of the Root River.

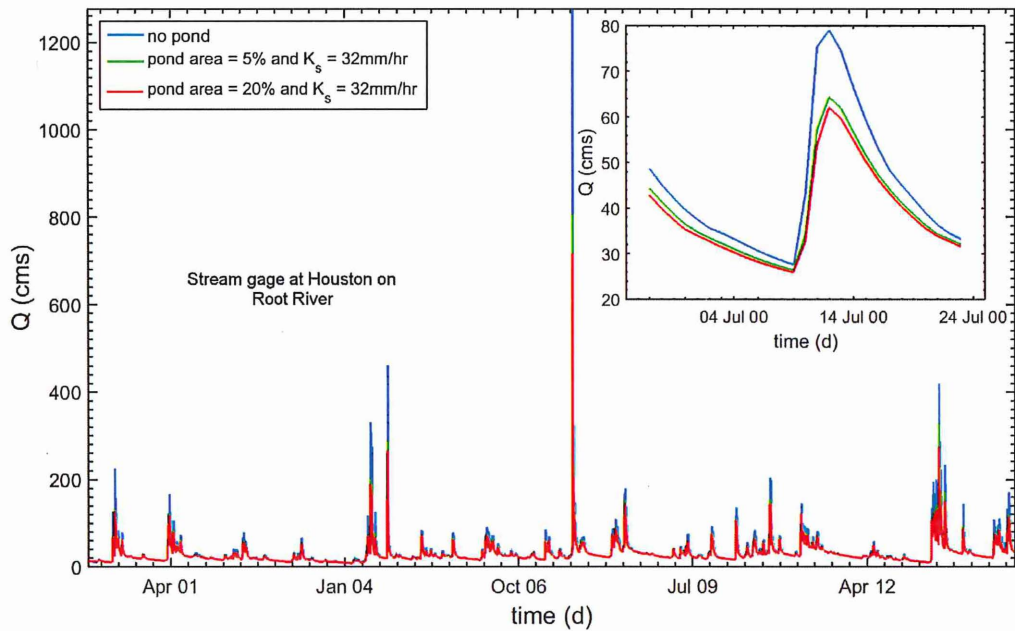


Figure 13.8. Daily streamflow from the year 2000 to 2014 to illustrate the effect of ponds Houston stream gage on the main stem of the Root River.

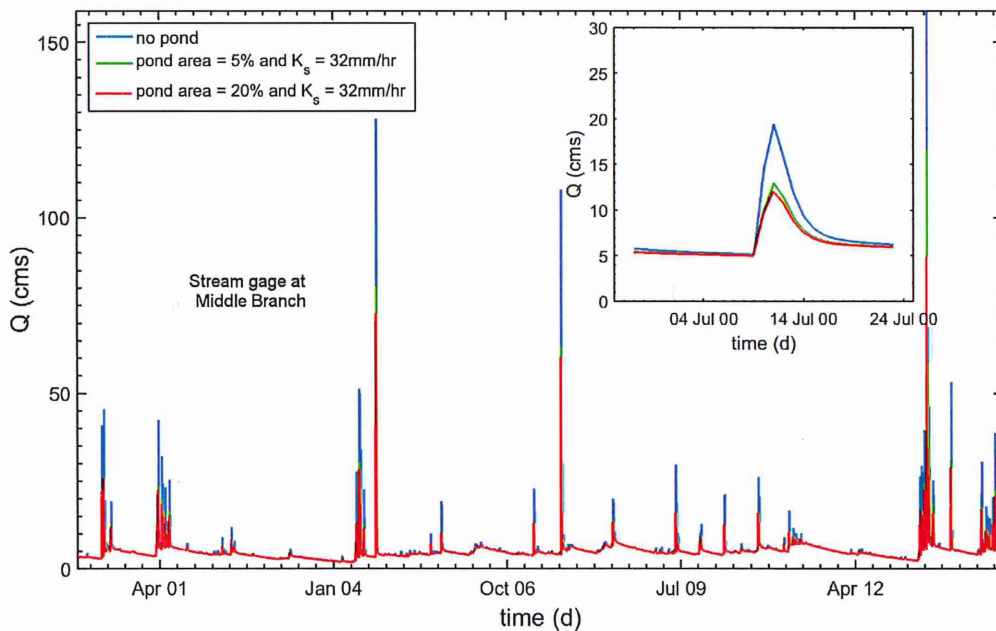


Figure 13.9. Daily streamflow from the year 2000 to 2014 to illustrate the effect of ponds at the Middle Branch near Fillmore stream gage.

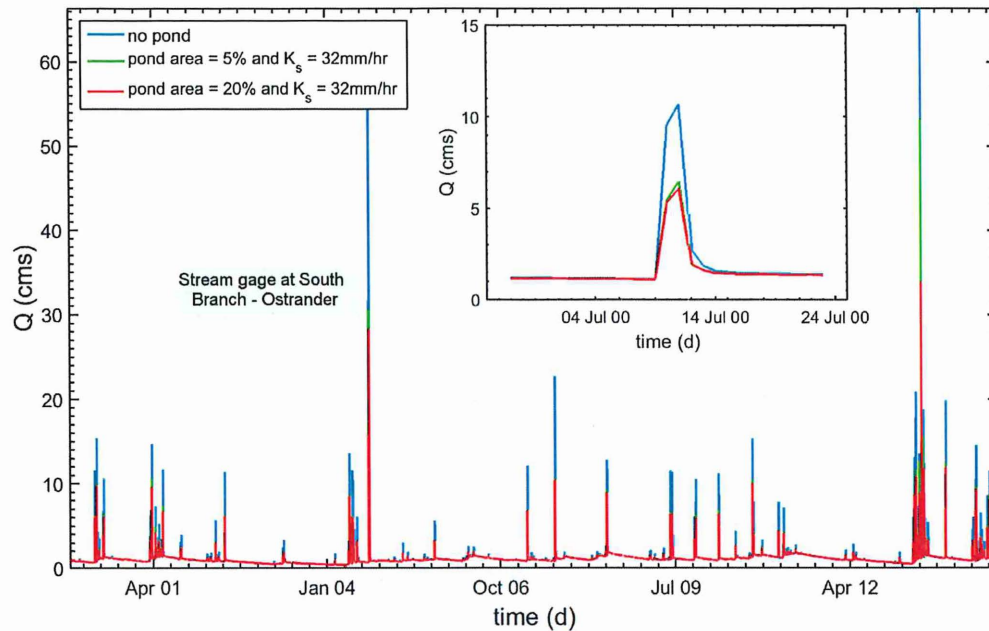


Figure 13.10. Daily streamflow from the year 2000 to 2014 to illustrate the effect of ponds at the South Branch stream gage near Ostrander.

Period of record flow duration curves (FDC) can be used to represent the relationship between the daily average flow and the percentage of time a particular streamflow equals or exceeds for the period of analysis. The entire 15 years of daily averaged streamflow was used to construct the FDC (Figures 13.11 to 13.15). Three cases were compared (no pond, with 5% and $K_s = 32$ mm/hr, and with 20% and $K_s = 32$ mm/hr) at all 5 gages and flows corresponding to 1% or lower exceedance probability were lower with the introduction of impoundment structures.

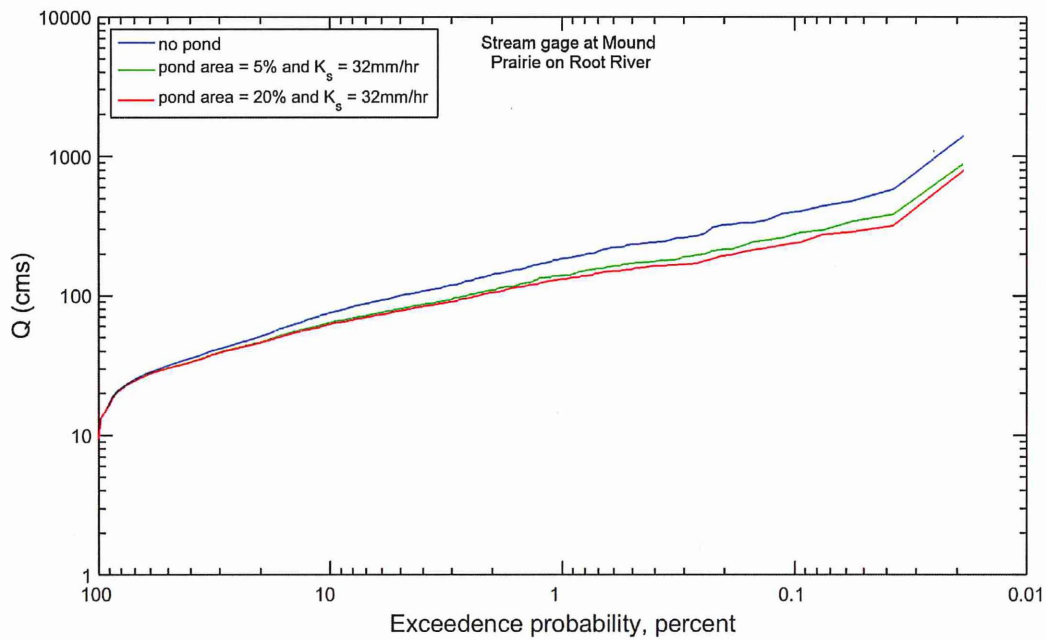


Figure 13.11. Comparison of flow duration curves between the no-pond scenario and two with-pond scenarios at the Mound Prairie stream gage on the main stem of the Root River.

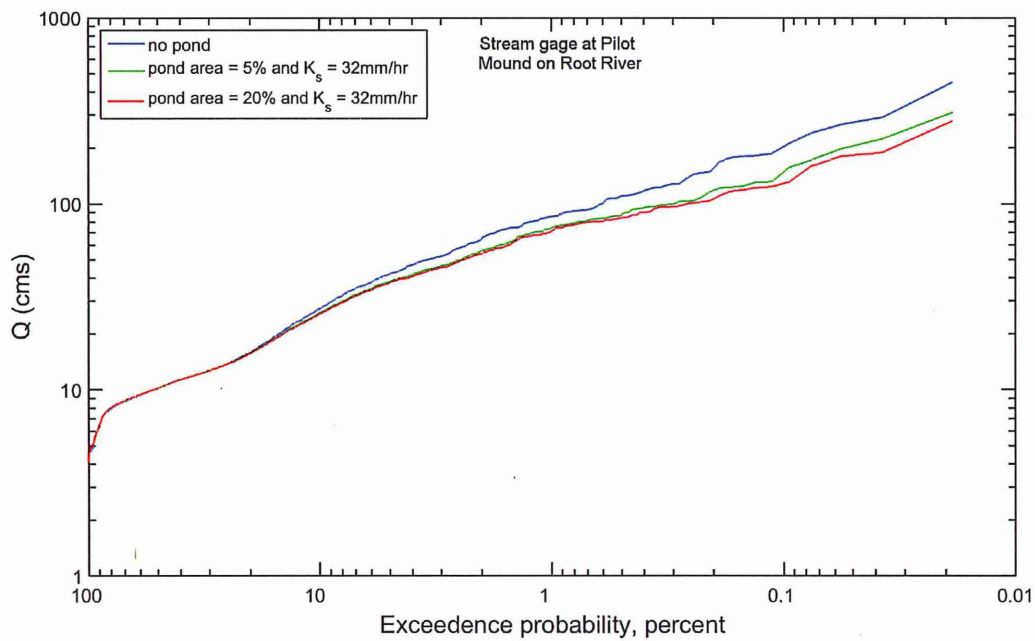


Figure 13.12. Comparison of flow duration curves between the no-pond scenario and two with-pond scenarios at the Pilot Mound stream gage on the main stem of the Root River.

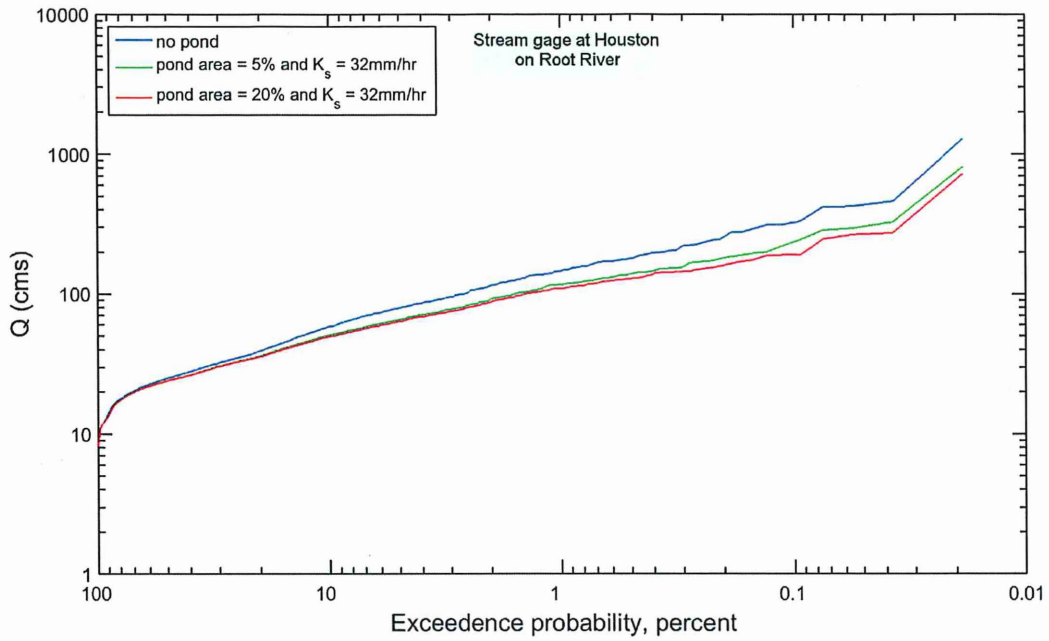


Figure 13.13. Comparison of flow duration curves between the no-pond scenario and two with-pond scenarios at the Houston stream gage on the main stem of the Root River.

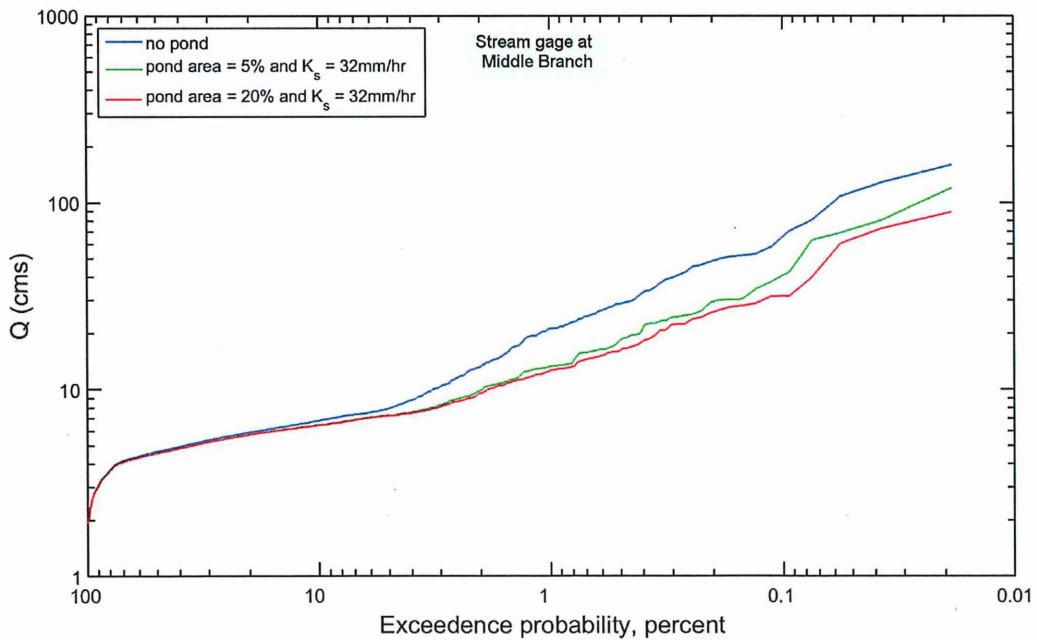


Figure 13.14. Comparison of flow duration curves between the no-pond scenario and two with-pond scenarios at the Middle Branch stream gage.

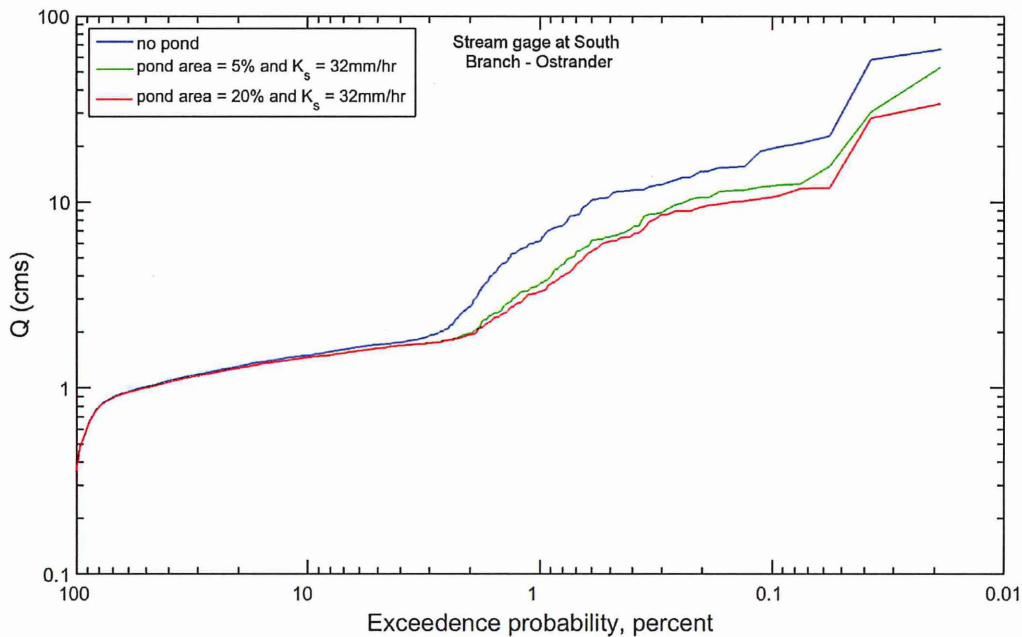


Figure 13.15. Comparison of flow duration curves between the no-pond scenario and two with-pond scenarios at the South Branch stream gage near Ostrander.

Variability of daily streamflow data aggregated monthly for the 15 year simulation period for the impoundment (pond volume represented by 10% subbasin area and $K_s = 32$) versus no-impoundment scenarios are shown using boxplots. Differences between the two cases arise exclusively due to the introduction of ponds as all other variabilities (climate, land use, soil moisture and other factors) were held constant between the two scenarios. Lines horizontally splitting the boxes (at the notch) indicates the median of the distribution of flows for each simulation. Median flows are generally similar for simulations with and without the impoundment structures, but slightly lower for some of the scenarios with ponds (Figure 13.16 to 13.20). Variability of flow (represented by the box height, which shows the 25 to 75 percentile flows, also called the interquartile range (IQR)) are mostly similar between the two scenarios at all five locations, with only slight decreases in the scenario with impoundments. Skewness of the flow distributions (represented by the length of boxes and whiskers on either side of the median) is also similar between the two scenarios. The presence or absence of “extreme” values (or outliers) are generally similar between scenarios, if slightly compressed for the scenario with impoundments. Minimum (represented by the lower whisker) daily-averaged monthly-aggregated flows generally increased with the introduction of ponds for all gages (except gage on the main stem Root River at Pilot Mound) and for all months (except June). The gage at Mound Prairie on the main stem of the Root River also showed an exception to this behavior where a decrease in the minimum flows for March and April can be seen for the with ponds scenario.

The highest magnitude peak flows were consistently reduced, for all months and at all gages in the scenario with ponds. Flows corresponding to the lower quartile (25th percentile) generally decreased for the with pond scenario and for all months and for all gages (except gage on the main stem Root River at

Pilot Mound). Upper quartile (75th percentile) flows increased or decreased depending on the month and the gage of interest.

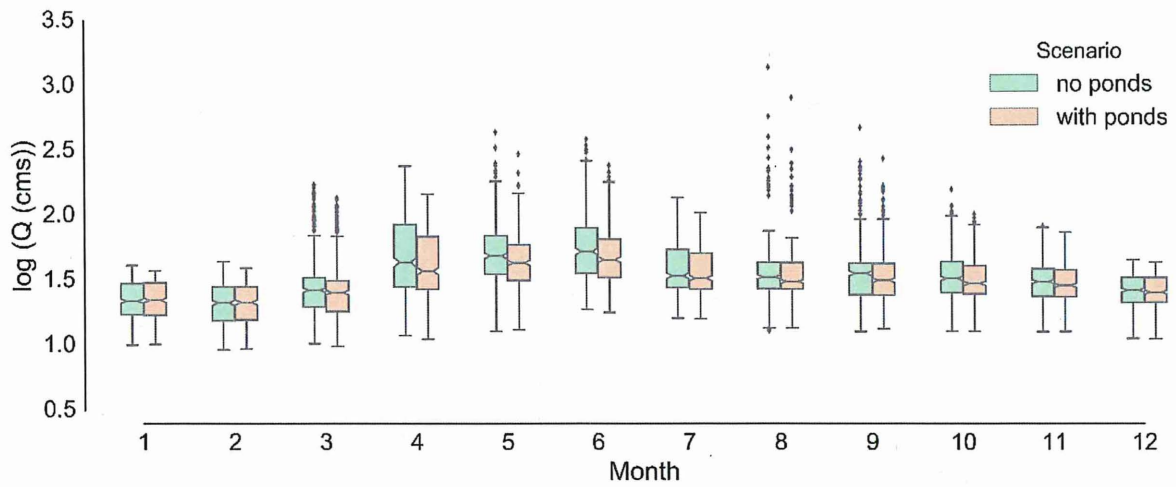


Figure 13.16. Daily streamflow aggregated monthly from the year 2000 to 2014 to illustrate the effect of ponds at the Mound Prairie stream gage on the main stem of the Root River. Streamflow values were log transformed prior to plotting them in the box plot.

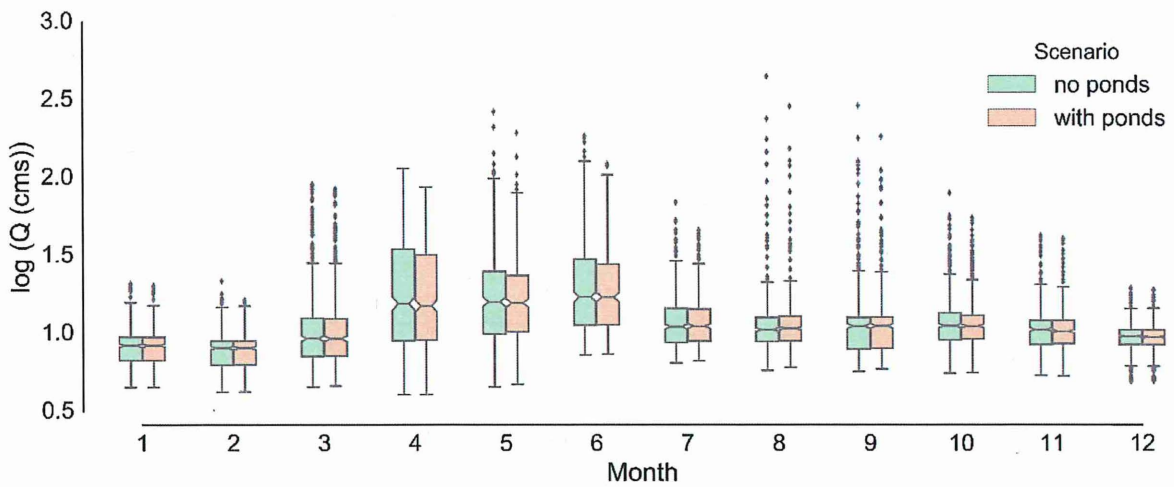


Figure 13.17. Daily streamflow aggregated monthly from the year 2000 to 2014 to illustrate the effect of ponds at the Pilot Mound stream gage on the main stem of the Root River. Streamflow values were log transformed prior to plotting them in the box plot.

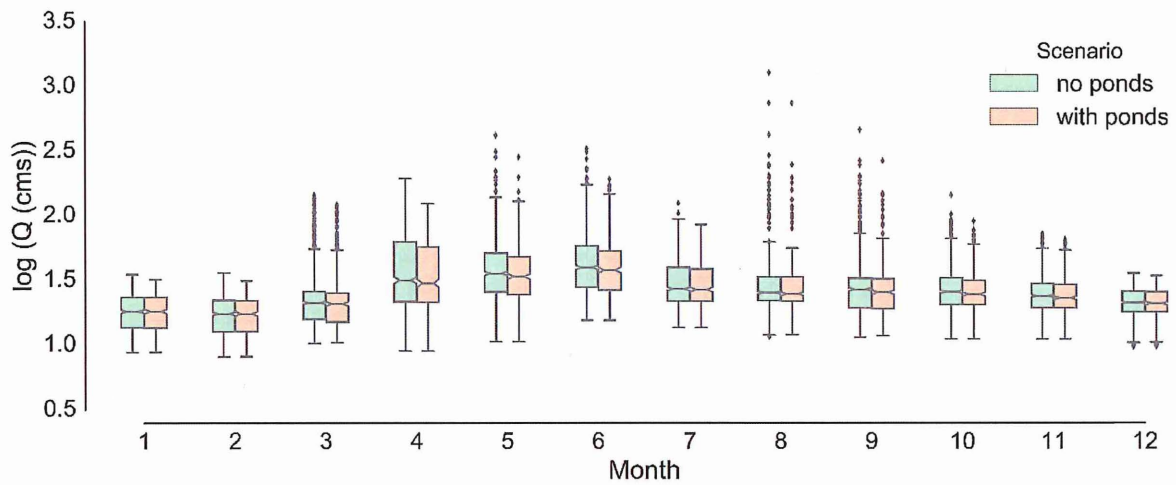


Figure 13.18. Daily streamflow aggregated monthly from the year 2000 to 2014 to illustrate the effect of ponds at the Houston stream gage on the main stem of the Root River. Streamflow values were log transformed prior to plotting them in the box plot.

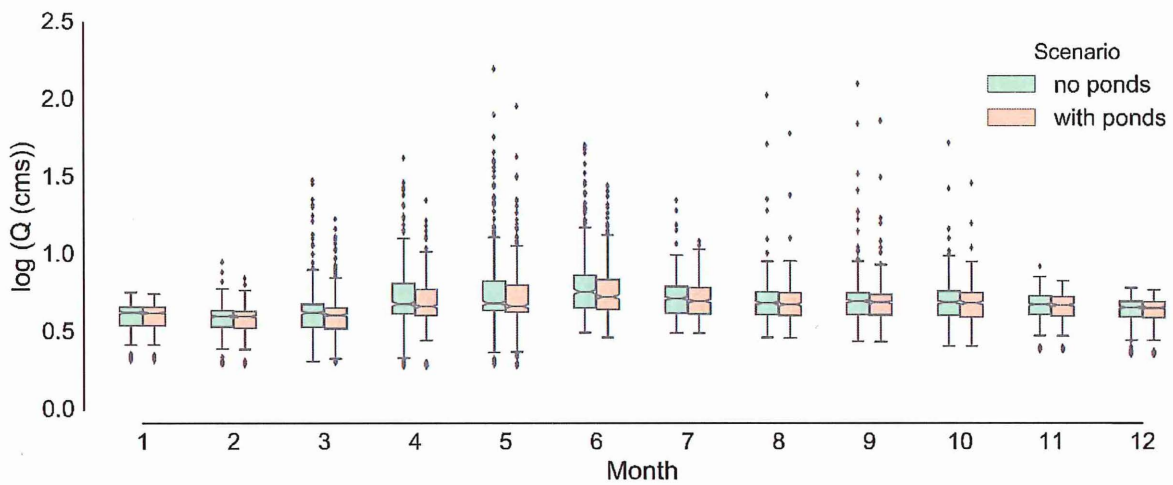


Figure 13.19. Daily streamflow aggregated monthly from the year 2000 to 2014 to illustrate the effect of ponds at the Middle Branch stream gage. Streamflow values were log transformed prior to plotting them in the box plot.

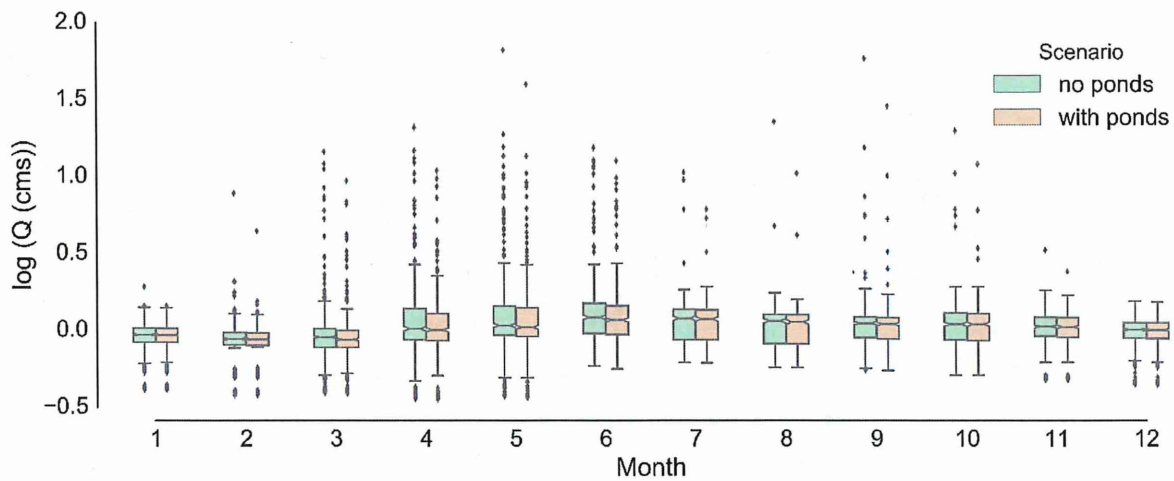


Figure 13.20. Daily streamflow aggregated monthly from the year 2000 to 2014 to illustrate the effect of ponds at the South Branch stream gage. Streamflow values were log transformed prior to plotting them in the box plot.

SWAT model USLE estimates

Soil erosion from the landscape can be determined using the Universal Soil Loss Equation (USLE). Soil loss estimates are computed on a daily time-step in SWAT and is a function of crop growth, rainfall, soil properties, tillage practices and land use among others (Neitsch et al., 2011). The equation used to compute soil loss estimates using USLE in SWAT is shown below. Figure 13.21 shows the USLE soil loss estimates from the SWAT model as the annual average of daily USLE estimates from a 15 year simulation. The spatial distribution of the erosion also accounts for tillage practices (see Appendix B for type of tillage practices used) and are reported from model predictions from the model calibrated for hydrology.

$$sed = 1.292 \times EI_{USLE} \times K_{USLE} \times C_{USLE} \times P_{USLE} \times LS_{USLE} \times CFRG$$

where,

sed = sediment yield (metric tons/ha)

EI_{USLE} = rainfall erosion index

K_{USLE} = USLE erodability factor

C_{USLE} = USLE cover and management factor

P_{USLE} = USLE support practice factor

$CFRG$ = coarse fragment factor

USLE estimates predict high soil erosion rates in parts of the Rushford and Money Creek watersheds, as well as the South Fork Root River and a small strip of the North Branch Root River, near the transition from the Upper Plains to Transitional Karst region.

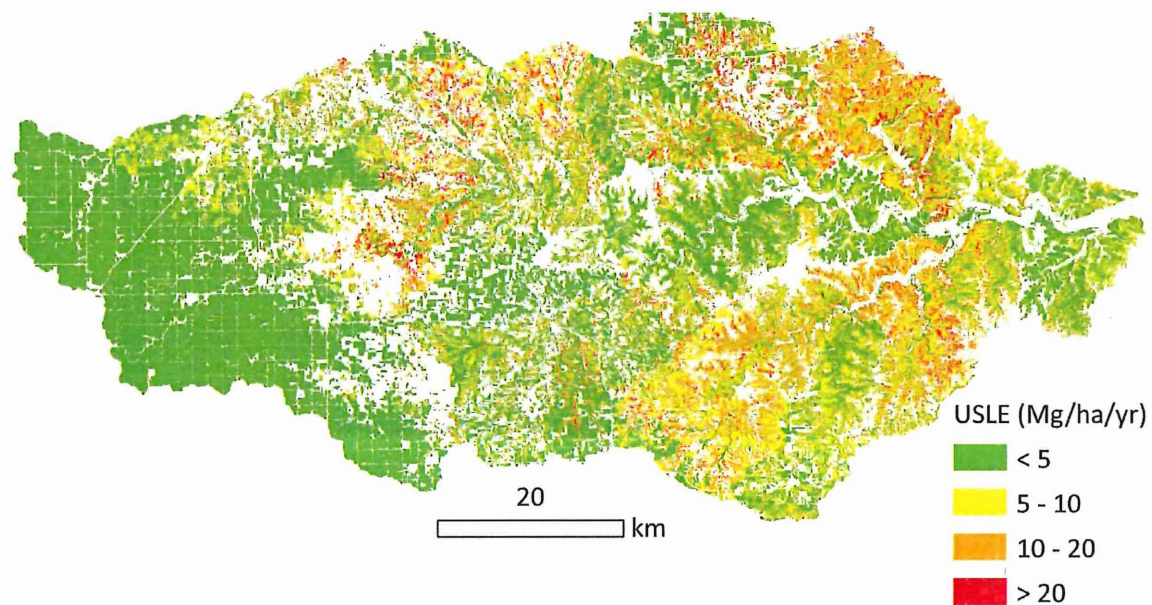


Figure 13.21. Annual average daily soil loss estimates using the USLE method from a 15-year simulation for the RRW using the SWAT model calibrated for hydrology.

14. Integrated sediment budget

A sediment budget is a useful accounting tool that allows comparison of all the major sediment sources and sinks within a watershed within the fundamental constraint of conservation of mass. Many previous studies have used sediment budgets to identify and quantify sediment sources and sinks (e.g., Trimble, 1999; Walling and Collins, 2008; Notebaert et al., 2009; Belmont et al., 2011). Developing a sediment budget that accounts for all sources and sinks provides more reliable and useful information at the watershed scale than any model or measurement of any single source or sink could provide alone. For example, watershed scale hydro-erosion models are subject to equifinality problems, as discussed above, and typically very little information is available to constrain changes in sediment delivery from different sources over a wide range of spatial scales. Similarly, measurements of individual sources or sinks are typically conducted on small scales and therefore suffer from the same uncertainties regarding sediment delivery and extrapolation over large spatial scales. In the rare case that measurements of erosion or deposition can be made over large spatial scales (Schaffrath et al., 2015), very small systematic offsets or uncertainties over large areas can introduce large errors in mass balance calculations.

We have generated and utilized a wide variety of data to constrain our sediment budget for the Root River watershed. Water and sediment fluxes measured at gaging stations provide a firm constraint on total sediment efflux from the watershed, acknowledging that the annual loads are themselves subject to some uncertainty. To constrain sources and sinks, we have used remotely sensed data (historic and modern air photos, digital elevation models, land use and soil maps, etc.), and an extensive array of field measurements (grain size and bulk density surveys, channel cross section surveys, sheet and rill erosion surveys, direct measurements of deposition in channel cutoffs, etc.) and other methods (e.g., geochemical fingerprinting). Some of these measurements provide information that can be used

quantitatively in the sediment budget, while others provide information that can only be used in a qualitative manner to confirm or refute the general understanding provided by the sediment budget. Each of the independent measurements or constraints are also subject to a variety of uncertainties, which have been discussed in the relevant sections above. The most parsimonious way to close a sediment budget and account for uncertainties is to reduce or increase estimates by a uniform percentage across all sources and sinks. A simple conservation of mass equation can be used to define a sediment budget at the river reach or channel network scales, as shown in the equation below:

$$I-O=\Delta S$$

where I represents sediment inputs, O represents the output or efflux from the watershed, and ΔS represents the change in sediment storage.

As discussed in section 6 of this report, the average annual TSS load of the Root River at the Mound Prairie gage is approximately 253,000 Mg/yr. Adding the 9,000 Mg/yr that is estimated as stored in meander cutoffs brings the total amount of sediment to be accounted for to 263,000 Mg/yr. Sediment fingerprinting results suggest that 44% (+/- 17%) of that sediment is derived from agricultural soil erosion within the past 20-50 years, with 43% (+/- 17%) derived from streambank/floodplain erosion and the remainder (~13%) derived from soil erosion on mostly forested hillslopes and other sources. Combining these fingerprinting results with the average sediment load estimated at Mound Prairie yields approximately 115,000 Mg/yr (+/- 20,000 Mg/yr) of sediment derived from upland agricultural fields and 112,000 Mg/yr (+/- 19,000 Mg/yr) derived from erosion of streambanks/floodplains and approximately 34,000 Mg/yr (+/- 6000 Mg/yr) derived from hillslopes. It is possible that the uncertainty associated with hillslopes may be underestimated (and therefore the source over-estimated) due to geochemical overlap between hillslopes and other sources and the relatively small number of sediment source samples analyzed.

Taking the recent channel migration and widening rates measured from air photos, we estimate a total of 300,000 Mg/yr derived from widening and meander migration (Table 12.7, Figure 14.1), subject to a propagated uncertainty of 60%. Thus, the sediment fingerprinting and air photo estimates for the percentage of sediment derived from bank erosion overlap at their upper and lower bounds, respectively. It is to be expected that the air photo analysis would result in an overestimate because the analysis does not account for sediment deposited in the floodplain or channel downstream. Also, any digitization error in locations that have not experienced any actual change still results in a perceived migration rate. It is noteworthy that the fingerprinting and air photo analyses are in good agreement regarding the relatively high percentage of sediment derived from streambanks in the North Brach sub-watershed. In addition to the net contribution of sediment derived from channel widening and migration, we estimate an additional 450,000 Mg/yr is exchanged within the channel-floodplain system.

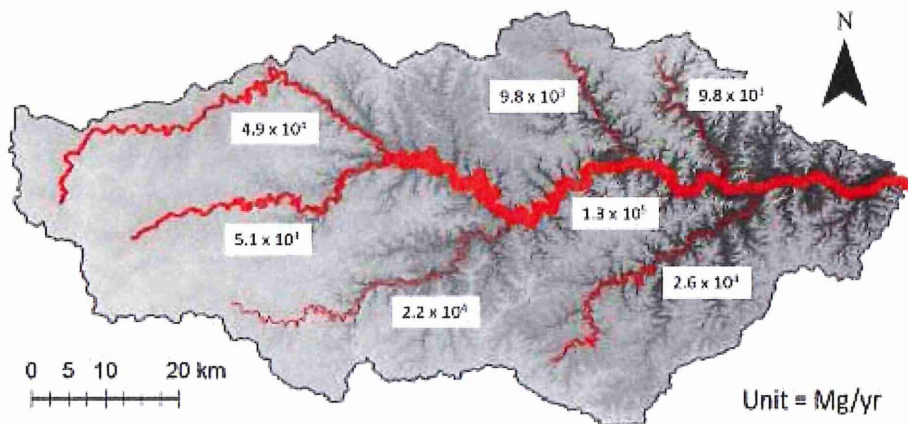


Figure 14.1. Net, local annual sediment loads contributed from channel widening and meander migration for the mainstem Root River and major tributaries.

Estimates of upland erosion contain similar scaling issues that can only be resolved within the context of the sediment budget. For example, the USLE estimates result in an average soil loss rate of 10.9 Mg/ha/yr, equivalent to 4.5 million Mg of sediment eroded and transported at local scales throughout the watershed. Combining this estimate with the fingerprinting constraint and measured sediment loads (which indicate that only 115,000 Mg/yr of this sediment is transported all the way to Mound Prairie gage) suggests a watershed-average sediment delivery ratio of 2-3%, a reasonable number given the size and physiographic setting of the Root River watershed. Sediment gaging data collected by Minnesota Department of Agriculture, Fillmore County and others empirically demonstrate this sediment delivery scaling effect is most pronounced between the smallest two scales monitored (edge of field and small watershed, see Figure 6.2). The fact that similar reductions in sediment loads are not observed at progressively larger scales is because the decrease in sediment delivery from upland sources is offset by increased sediment contributions from streambank sources.

While it was initially thought that channel cutoffs might constitute significant sediment sinks, our extensive mapping and monitoring campaign have concluded otherwise. We conclude that these features likely do not collectively store more than 9000 Mg/yr, a number that is sufficiently large and robust to include explicitly in the sediment budget, but in the end represents a very small (but quantifiable) fraction of total storage in the watershed as inferred from the low sediment delivery ratios observed for agricultural field sediment and streambank erosion, discussed above. Further, while we recognize that karst pathways may result in sediment laden springs at some times and in some locations, our results suggest that sediment loading from springs is a sufficiently small number that it is not useful to represent in the watershed sediment budget.

In conclusion, Figure 14.2 depicts our best understanding of the sediment budget of the Root River watershed. The budget is primarily constrained by measured sediment loads, field surveys, grain size and bulk density measurements and sediment fingerprinting data, and is further supported by analysis of lidar topography data, historical air photos and other analyses conducted as part of this project and related studies. Despite the various amounts and types of uncertainties associated with the myriad measurements that have contributed to this study, this general depiction of the sediment budget is unlikely to change significantly with additional data collected over the next few years.

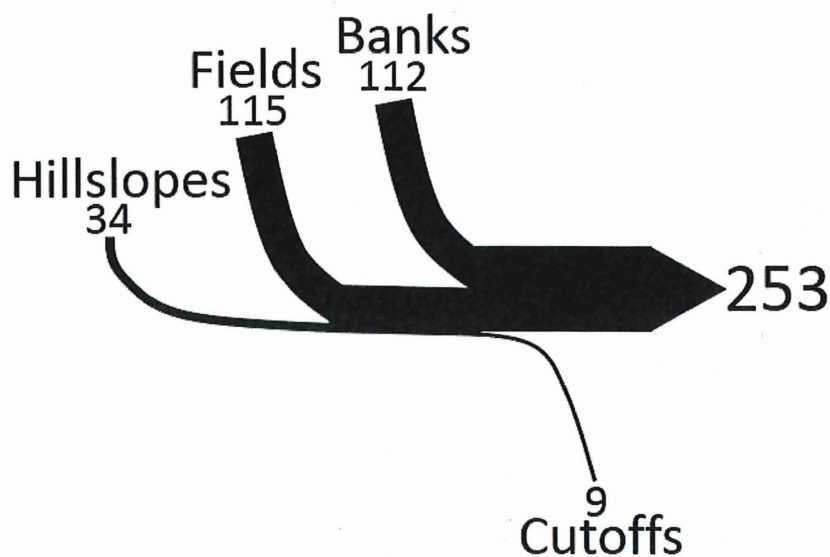


Figure 14.2. Sediment budget for the Root River watershed, 2009-2014. Loads are reported in Mg/yr.

References cited

- Abbaspour, K. C. (2012), SWAT-CUP 2012. Calibration and uncertainty programs.
- Ahmed, N. (1997), *Ground water: Protection alternatives and strategies in the USA*, ASCE Publications.
- Almendinger, J. E., and M. S. Murphy (2007), Problems and Solutions in Applying SWAT in the Upper Midwest USA, in *4th International SWAT Conference*, edited, Delft, The Netherlands.
- Amatya, D. M., M. Jha, A. E. Edwards, T. M. Williams, and D. R. Hitchcock (2011), SWAT-based streamflow and embayment modeling of karst-affected Chapel branch watershed, South Carolina, *Transactions of the ASABE*, 54(4), 1311-1323.
- Archer, C. L., and Caldeira, K. (2008). Historical trends in the jet streams. *Geophysical Research Letters*, 35(8).
- Arnold, J. G., J. R. Kiniry, R. Srinivasan, J. R. Williams, E. B. Hansey, and S. L. Neitsch (2012), Soil and Water Assessment Tool. Input/ Output documentation. Version 2012.
- Baffaut, C., and V. Benson (2009), Modeling flow and pollutant transport in a karst watershed with SWAT, *Transactions of the ASABE*, 52(2), 469-479.
- Bekele, E. G. and J. W. Nicklow (2007). Multi-objective automatic calibration of SWAT using NSGA-II. *Journal of Hydrology* 341(3-4): 165-176.
- Beach, T. (1994). The fate of eroded soil: Sediment sinks and sediment budgets of agrarian landscapes in southern Minnesota, 1851-1988. *Annals of the Association of American Geographers*, 84(1), 5-28.
- Belmont, P. (2011). Floodplain width adjustments in response to rapid base level fall and knickpoint migration. *Geomorphology*, 128(1), 92-102.

- Belmont, P., Gran, K.B., Schottler, S.P., Wilcock, P.R., Day, S.S., Jennings, C., Lauer, J.W., Viparelli, E., Willenbring, J.K., Engstrom, D.R., Parker, G. (2011) Large shift in source of fine sediment in the Upper Mississippi River. *Environmental Science and Technology*. 45, 8804–8810.
- Belmont, P., Stevens, J.R., Czuba, J.A., Kumarasamy, K., Kelly, S.A. (in press) Comment on “Climate and agricultural land use change impacts on streamflow in the upper midwestern United States” by Satish C. Gupta et al. *Water Resources Research*.
- Belmont, P., Willenbring, J.K., Schottler, S.P., Marquard, J., Kumarasamy, K., and Hemmis, J.M. (2014). Toward generalizable sediment fingerprinting with tracers that are conservative and nonconservative over sediment routing timescales. *Journal of Soils and Sediments*, 1-14.
- Bi, H., Li, X., Guo, M., Liu, X., and Li, J., 2006, Digital Terrain Analysis Based on DEM: *Frontiers of Forestry in China*, v. 1, no. 1, p. 54-58.
- Brierley, G. J., and Fryirs, K. A. (2005). *Geomorphology and river management. Application of the river styles framework*. Malden, MA. Blackwell Publishing.
- Carter, J., Owens, P. N., Walling, D. E., and Leeks, G. J. (2003). Fingerprinting suspended sediment sources in a large urban river system. *Science of the total environment*, 314, 513-534.
- Chapman, D. V. (Ed.). (1996). *Water quality assessments: a guide to the use of biota, sediments and water in environmental monitoring* (p. 626). London: E & Fn Spon.
- Collins, A. L., and Walling, D. E. (2004). Documenting catchment suspended sediment sources: problems, approaches and prospects. *Progress in Physical Geography*, 28(2), 159-196.
- Dalzell, B. J., and D. J. Mulla (2007), *Sediment, nutrients and pesticides modeling in the South Branch of the Root River, MinnesotaRep.*, MDA.
- De Vente, J., Poesen, J., Arabkhedri, M., and Verstraeten, G. (2007). The sediment delivery problem revisited. *Progress in Physical Geography*, 31(2), 155-178.
- Dogwiler, T., and Hooks, T. L., 2012, *Digital Terrain Analysis of Crystal Creek, Bridge Creek, and South Branch of the Root River Headwaters Reach: Root River Field to Stream Partnership Project: WRC Report 2012-02: Southeastern Minnesota Water Resources Center, Winona State University, Winona, MN, 64p.*
- Florinsky, I., 2012, *Digital Terrain Analysis in Soil Science and Geology*, Amsterdam, Elsevier, 379 p.:
- Foufoula-Georgiou, E., Belmont, P., Wilcock, P.R., Gran, K.B., Finlay, J., Kumar, P., Czuba, J.A., Schwenk, J., and Takbiri, Z. (in press) Comment on “Climate and agricultural land use change impacts on streamflow in the upper midwestern United States” by Satish C. Gupta et al. *Water Resources Research*.
- Foufoula-Georgiou, E., Takbiri, Z., Czuba, J. A., and Schwenk, J. (2015). The change of nature and the nature of change in agricultural landscapes: Hydrologic regime shifts modulate ecological transitions. *Water Resources Research*, 51(8), 6649-6671.
- Galzki, J. C., Birr, A. S., and Mulla, D. J., 2011, Identifying critical agricultural areas with three-meter LiDAR elevation data for precision conservation: *Journal of Soil and Water Conservation*, v. 66, no. 6, p. 423-430.
- Gassman, P. W., M. R. Reyes, C. H. Green and J. G. Arnold (2007). The soil and water assessment tool: historical development, applications, and future research directions. *Transactions of the ASABE* 50(4): 1211-1250.

- Gellis, A. C., and Walling, D. E. (2011). Sediment source fingerprinting (tracing) and sediment budgets as tools in targeting river and watershed restoration programs. *Geophysical Monograph Series*, 194, 263-291.
- Ghanbarpour, M. R., K. C. Abbaspour, G. Jalalvand, and G. A. Moghaddam (2010), Stochastic modeling of surface stream flow at different time scales: Sangsoorakh karst basin, Iran, *Journal of Cave and Karst Studies*, 72(1), 1-10.
- Gran, K.B., Belmont, P., Day, S.S., Finnegan, N., Jennings, C., Lauer, J.W., Wilcock, P.R. (2011) Landscape evolution in south-central Minnesota and the role of geomorphic history on modern erosional processes. *GSA Today*. 21 (9): 7-9
- Green, J. A., Barry, J. D., and Alexander Jr, E. C., 2014, Springshed Assessment Methods for Paleozoic Bedrock Springs of Southeastern Minnesota: Minnesota Department of Natural Resources, 48p.
- Groisman, P., Knight, R., and Karl, T. (2001). Heavy Precipitation and High Streamflow in the Contiguous United States: Trends in the Twentieth Century. *Bulletin of the American Meteorological Society*, 219-246.
- Held, I., and Soden, B. (2006). Robust Responses of the Hydrological Cycle to Global Warming. *Journal of Climate*, 19, 5686-5699.
- Jacoby, B. S., Peterson, E. W., and Dogwiler, T., 2011, Identifying the Stream Erosion Potential of Cave Levels in Carter Cave State Resort Park, Kentucky, USA: *Journal of Geographic Information System*, v. 3, no. 4, p. 323-333.
- Kannan, N., J. Jeong, J. Arnold, R. Glick, L. Gosselink, and R. Srinivasan (2014), Hydrologic modeling of detention pond, *International Journal*, 3(2), 657-552.
- Karl, T., and Knight, R. (1998). Secular Trends of Precipitation Amount, Frequency, and Intensity in the United States. *Bulletin of the American Meteorological Society*, 79(2), 231-241.
- Knox, J. C. (1987). Historical valley floor sedimentation in the Upper Mississippi Valley. *Annals of the Association of American Geographers*, 77(2), 224-244.
- Knox, J. C. (2006). Floodplain sedimentation in the Upper Mississippi Valley: Natural versus human accelerated. *Geomorphology*, 79(3), 286-310.
- Kraller, G., M. Warscher, U. Strasser, H. Kunstmann, and H. Franz (2014), Distributed Hydrological Modeling and Model Adaption in High Alpine Karst at Regional Scale (Berchtesgaden Alps, Germany), in *H2Karst Research in Limestone Hydrogeology*, edited, pp. 115-126, Springer.
- Kunkel, K., Andsager, K., and Easterling, D. (1999). Long-Term Trends in Extreme Precipitation Events over the Conterminous United States and Canada. *Journal of Climate*, 12, 2515-2527.
- Liu, H., and Wang, L. (2008). Mapping detention basins and deriving their spatial attributes from airborne LiDAR data for hydrological applications. *Hydrological processes*, 22(13), 2358-2369.
- Minnesota Department of Agriculture (2005). 2003 nutrient management assessment of producers South Branch of the Root River.
- Minnesota Department of Agriculture (2012), Root River field to stream paternship. Innovative research with innovative farmers *Rep.*
- Minnesota Department of Agriculture, (2014). Evaluation of best management practices in impaired watersheds using the SWAT model. Available at:
<http://www.mda.state.mn.us/protecting/cleanwaterfund/research/swatmodel.aspx>Minnesota

Minnesota Pollution Control Agency, (2010). Minnesota's Impaired Waters and TMDLs, 2010 Draft TMDL List. Available at: <http://www.pca.state.mn.us/index.php/water/water-types-andprograms/minnesotas-impaired-waters-and-tmdls/assessment-and-listing/303dlist-of-impaired-waters.html>. Accessed March 2012

Montgomery, D. R. (2007). Soil erosion and agricultural sustainability. *Proceedings of the National Academy of Sciences*, 104(33), 13268-13272.

Moore, I. D., Grayson, R. B., and Ladson, A. R., 1991, Digital terrain modelling: a review of hydrological, geomorphological, and biological applications: *Hydrological Processes*, v. 5, no. 1, p. 3-30.

Moriasi, D. N., J. G. Arnold, M. W. Van Liew, R. L. Bingner, R. D. Harmel, and T. L. Veith (2007), Model evaluation guidelines for systematic quantification of accuracy in watershed simulations, *Transactions of the ASABE*, 50(3), 885-900.

MPCA (2008). The Minnesota stormwater manual. St. Paul, MN.

MPCA (2011), Karst in Minnesota (accessed February 16, 2016) <https://www.pca.state.mn.us/water/karst-minnesota>, edited.

MPCA (2012), Root River Watershed Monitoring and Assessment Report.

MPCA (2015), Root River Watershed Stressor Identification Report. A study of local stressors limiting the biotic communities in the Root River Watershed.

MSUM, and MPCA (2009), State of the Minnesota River. Summary of surface water quality monitoring 2000 - 2008.

Neitsch, S. L., J. G. Arnold, J. R. Kiniry, and J. R. Williams (2011), Soil and water assessment tool theoretical documentation version 2009Rep., Texas Water Resources Institute.

Notebaert, B., Verstraeten, G., Rommens, T., Vanmontfort, B., Govers, G., and Poesen, J. (2009). Establishing a Holocene sediment budget for the river Dijle. *Catena*, 77(2), 150-163.

Passalacqua, P., Belmont, P., Staley, D. M., Simley, J. D., Arrowsmith, J. R., Bode, C. A., Crosby, C., DeLong, S.B., Glenn, N.F., Kelly, S.A., and Lague, D. (2015). Analyzing high resolution topography for advancing the understanding of mass and energy transfer through landscapes: A review. *Earth-Science Reviews*, 148, 174-193.

PRISM Climate Group Oregon State University, <http://prism.oregonstate.edu>, created 4 Feb 2004., edited.

Randall et al. (2008), Best management practices for Nitrogen use in Southeastern MinnesotaRep.

Rasmussen, D. (2005), 2003 nutrient management assessment of producers South Branch of the Root RiverRep.

Rasmussen, N., 2011, Root River Geomorphic Regions (Unpublished Map): Minnesota Pollution Control Agency, Rochester, MN.

Reid, Leslie M., and Thomas Dunne. Rapid Evaluation of Sediment Budgets. Reiskirchen, Germany: Catena, 1996. Print.

Schaffrath, K. R., Belmont, P., and Wheaton, J. M. (2015). Landscape-scale geomorphic change detection: Quantifying spatially variable uncertainty and circumventing legacy data issues. *Geomorphology*, 250, 334-348.

- Schilling, K. E., Jha, M. K., Zhang, Y. K., Gassman, P. W., and Wolter, C. F. (2008). Impact of land use and land cover change on the water balance of a large agricultural watershed: Historical effects and future directions. *Water Resources Research*, 44(7).
- Schottler, S. P., Ulrich, J., Belmont, P., Moore, R., Lauer, J., Engstrom, D. R., and Almendinger, J. E. (2014). Twentieth century agricultural drainage creates more erosive rivers. *Hydrological processes*, 28(4), 1951-1961.
- Smith, S. M., Belmont, P., and Wilcock, P. R. (2011). Closing the gap between watershed modeling, sediment budgeting, and stream restoration. *Geophysical Monograph Series*, 194, 293-317.
- Soong, D. T., E. A. Murphy, and T. D. Straub (2009), Effect of Detention Basin Release Rates on Flood Flows - Application of a Model to the Blackberry Creek Watershed in Kane County, Illinois *Rep.*
- Souffront M.A., (2014) Channel Adjustment and Channel-Floodplain Sediment Exchange in the Root River, Southeastern Minnesota. Graduate Theses and Dissertations. Paper 3334.
- Stout, J. C., and Belmont, P. (2014). TerEx Toolbox for semi-automated selection of fluvial terrace and floodplain features from lidar. *Earth Surface Processes and Landforms*, 39(5), 569-580.
- Stout, J. C., Belmont, P., Schottler, S. P., and Willenbring, J. K. (2014). Identifying Sediment Sources and Sinks in the Root River, Southeastern Minnesota. *Annals of the Association of American Geographers*, 104(1), 20-39.
- Sutherland, A. B., and Meyer, J. L. (2007). Effects of increased suspended sediment on growth rate and gill condition of two southern Appalachian minnows. *Environmental Biology of Fishes*, 80(4), 389-403.
- Trimble, Stanley W. *Historical Agriculture and Soil Erosion in the Upper Mississippi Valley Hill Country*. Boca Raton, FL: CRC, 2013. Print.
- Trimble, S. W., and Crosson, P. (2000). US Soil Erosion Rates--Myth and Reality. *Science*, 289(5477), 248-250.
- U.S. Geological Survey (2013a), USGS NED n44w093 1/3 arc-second 2013 1 x 1 degree ArcGrid.
- U.S. Geological Survey (2013b), USGS NED n44w092 1/3 arc-second 2013 1 x 1 degree ArcGrid.
- USDA-NRCS (2009), Rapid Watershed Assessment Root River (MN / IA) HUC: 07040008*Rep.*
- USDA-NRCS, USGS, and US EPA (2015), Watershed Boundary Dataset for HUC# 07040008, Minnesota (Online WWW). Available URL: "<http://datagateway.nrcs.usda.gov>" (Accessed 10/02/2015).
- USDA (2010), Field Crops - Usual planting and harvesting dates, edited.
- USDA NRCS (2013), Soil Survey Geographic (SSURGO) database for Winona County, Minnesota. MN169, edited.
- USDA NRCS (2014a), Soil Survey Geographic (SSURGO) database for Houston County, Minnesota. MN055, edited.
- USDA NRCS (2014b), Soil Survey Geographic (SSURGO) database for Fillmore County, Minnesota. MN045, edited.
- USDA NRCS (2014c), Soil Survey Geographic (SSURGO) database for Dodge County, Minnesota. MN039, edited.
- USDA NRCS (2015a), Soil Survey Geographic (SSURGO) database for Winneshiek County, Iowa. IA191, edited.

USDA NRCS (2015b), Soil Survey Geographic (SSURGO) database for Olmsted County, Minnesota. MN109, edited.

USDA NRCS (2015c), Soil Survey Geographic (SSURGO) database for Mower County, Minnesota. MN099, edited.

Villarini, Gabriele, James A. Smith, Mary Lynn Baeck, Renato Vitolo, David B. Stephenson, and Witold F. Krajewski (2011). On the Frequency of Heavy Rainfall for the Midwest of the United States, *Journal of Hydrology*, 103-20.

Voss, R., May, W., and Roeckner, E. (2002). Enhanced resolution modelling study on anthropogenic climate change: Changes in extremes of the hydrological cycle. *International Journal of Climatology*, 22, 755-777.

Walling, D. E. (1983). The sediment delivery problem. *Journal of hydrology*, 65(1), 209-237.

Wilcock, P. (2009). Identifying sediment sources in the Minnesota River Basin. Synthesis Report for Minnesota Pollution Control Agency. Available at: <http://www.pca.state.mn.us/index.php/view-document.html?gid=8099>

Wilson, J. P., and Gallant, J. C., 2000, *Terrain Analysis: Principles and Applications*: New York, NY, John C. Wiley and Sons, Inc., p. 479.

Wischmeier, W.H. and D.D. Smith. 1978. "Predicting Rainfall Erosion Losses: A Guide to Conservation Planning." *Agriculture Handbook No. 537*. USDA/Science and Education Administration, US. Govt. Printing Office, Washington, DC. 58pp.

Wisconsin Initiative on Climate Change Impacts (WICCI), 2011, *Wisconsin's Changing Climate: Impacts and Adaptation*: Nelson Institute for Environmental Studies, University of Wisconsin-Madison and the Wisconsin Department of Natural Resources, 217p.

Wobus, C., Whipple, K.X., Kirby, E., Snyder, N., Johnson, J., Spyropolou, K., Crosby, B. and Sheehan, D., 2006. Tectonics from topography: Procedures, promise, and pitfalls. *Geological Society of America Special Papers*, 398, pp.55-74.

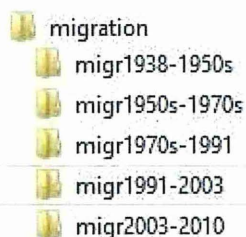
Woollings, T., and Blackburn, M. (2012). The North Atlantic jet stream under climate change and its relation to the NAO and EA patterns. *Journal of Climate*, 25(3), 886-902.

Appendix A

Python script developed to generate channel migration figures

Description: This script creates plots showing migration values in the Y axis and channel downstream distance in the x axis. Migration values are extracted from shapefiles create previously using the Planform Statistics Tool (<http://www.nced.umn.edu/content/stream-restoration-toolbox>).

Framework: The migration shapefiles created need to be organized in the following way:



Where “migration” is the parent folder or workspace and each subfolder represents a migration period where the shapefiles are stored.

The script is written to show 3 migration periods, but this can be modify in the script following instructions in the comments (marked by a #). It is recommended that parameter names are updated to names specific to the current analysis.

```
# 1- imports modules import arcpy import numpy as np
import os import
matplotlib.pyplot as plt
import matplotlib.pyplot as py
```

```
# 2- defines parameters
arcpy.env.overwriteOutput = True
workspace = r'C:\Users\Schumm\Documents\Belmont Lab\GIS_root\migration'
arcpy.env.workspace = workspace decade_3050 =
r'C:\Users\Schumm\Documents\Belmont Lab\GIS_root\migration\migr1938-1950s'
decade_5070 = r'C:\Users\Schumm\Documents\Belmont
Lab\GIS_root\migration\migr1950s-1970s' decade_7090 =
r'C:\Users\Schumm\Documents\Belmont Lab\GIS_root\migration\migr1970s-1991'
```

```
# gets migration 1930s-1950s from shapefiles (migration period 1)
# appends migration values to Y list
arcpy.env.workspace = decade_3050 y = () for reaches
in arcpy.ListFeatureClasses('migration*', 'Polygon'):
with arcpy.da.SearchCursor(reaches, 'Mig_myf') as rows:
for row in rows:
    y.append(-row(0))
```

```
# creates x list depending on Y length every 25
m x_np = np.arange(0, len(y)*0.025, 0.025)
x = x_np.tolist()
```

```

# sets the separation between the ticks and the axes in
the plot py.rcParams('xtick.major.pad')='10'
py.rcParams('ytick.major.pad')='10'

# creates figure, sets size (Change size depending on number of plots within
figure.) fig = plt.figure(1,figsize=(32,18)) # size set for 3 plots

# sets space at the bottom of the figure for xlabel
fig.subplots_adjust(bottom=0.2)

# creates the first subfigure 1 of 3 top plot
ax1 = fig.add_subplot(311) # 311 stands for row,column, plot number

# plots migration vs distance downstream
ax1.plot(x,y,'r-',lw=2)

# plots reach dashed lines.
ax1.plot((16.150,16.150),(-20,20),'k--')
ax1.plot((24.950,24.950),(-20,20),'k--')
ax1.plot((40.850,40.850),(-20,20),'k--')
ax1.plot((49.530,49.530),(-20,20),'k--')
ax1.plot((63.410,63.410),(-20,20),'k--')
ax1.plot((77.290,77.290),(-20,20),'k--')
ax1.plot((90.560,90.560),(-20,20),'k--')
ax1.plot((99.260,99.260),(-20,20),'k--')
ax1.plot((110.610,110.610),(-20,20),'k--')

# sets ylabel to specified string
ax1.set_ylabel('Migration\nRate (m/yr)\n\n',horizontalalignment='center')

# makes xticks invisible
plt.setp(ax1.get_xticklabels(), visible=False)

# sets x and y limits
ax1.set_xlim(0,121) ax1.set_ylim(-
20,20)

# specifies what ticks to show in the y-axis
ax1.set_yticks((-20,-10,0,10,20))

# adds text to the plots at specified locations. ax1.annotate('Right', xy=(0,-19),
xycoords='data',xytext=(-150,0), textcoords='offset points',size=30) ax1.annotate('Left',
xy=(0,16), xycoords='data',xytext=(-150,0), textcoords='offset points',size=30)
ax1.annotate('1930s-1950s', xy=(0,15), xycoords='data',xytext=(10,-1), textcoords='offset
points',size=30) ax1.annotate('*', xy=(49.530,13), xycoords='data',xytext=(-30,1),
textcoords='offset points',size=50) ax1.annotate('*', xy=(77.290,13), xycoords='data',xytext=(-
30,1), textcoords='offset points',size=50) ax1.annotate('***', xy=(90.560,13),
xycoords='data',xytext=(-60,1), textcoords='offset points',size=50)

```

```

# sets the fontsize of the subplot to specified size for item in ((ax1.xaxis.label,
ax1.yaxis.label) + ax1.get_xticklabels() + ax1.get_yticklabels()):
    item.set_fontsize(30)

# gets migration 1950s-1970s from shapefiles
arcpy.env.workspace = decade_5070 y = () for reaches
in arcpy.ListFeatureClasses('migration*', 'Polygon'):
with arcpy.da.SearchCursor(reaches, 'Mig_myr') as rows:
for row in rows:
    y.append(-row(0))

#x = range(0, len(y)*25, 25) **note: use this instead of the next two lines for x-axis to be in
meters** x_np = np.arange(0, len(y)*0.025, 0.025)
x = x_np.tolist()

# creates the second subfigure 2 of 3 **middle
plot** ax2 = fig.add_subplot(312)

# plots migration vs distance downstream
ax2.plot(x, y, 'r-', lw=2)

# plots reach dashed lines ax2.plot((16.150, 16.150), (-
20, 20), 'k--') ax2.plot((24.950, 24.950), (-20, 20), 'k--')
ax2.plot((40.850, 40.850), (-20, 20), 'k--')
ax2.plot((49.530, 49.530), (-20, 20), 'k--')
ax2.plot((63.410, 63.410), (-20, 20), 'k--')
ax2.plot((77.290, 77.290), (-20, 20), 'k--')
ax2.plot((90.560, 90.560), (-20, 20), 'k--')
ax2.plot((99.260, 99.260), (-20, 20), 'k--')
ax2.plot((110.610, 110.610), (-20, 20), 'k--')

# sets ylabel to specified string
ax2.set_ylabel('Migration\nRate (m/yr)\n\n\n', horizontalalignment='center')

# makes xticks invisible
plt.setp(ax2.get_xticklabels(), visible=False)

#sets x and y limits
ax2.set_xlim(0, 121)
ax2.set_ylim(-20, 20)

# specifies what ticks to show in the y-axis
ax2.set_yticks((-20, -10, 0, 10, 20))

# adds text to the plots at specified locations ax2.annotate('Right', xy=(0, -19),
xycoords='data', xytext=(-150, 0), textcoords='offset points', size=30) ax2.annotate('Left',
xy=(0, 16), xycoords='data', xytext=(-150, 0), textcoords='offset points', size=30)

```

```

ax2.annotate('1950s-1970s', xy=(0,15), xycoords='data',xytext=(10,-1), textcoords='offset
points',size=30) ax2.annotate('*', xy=(49.530,13), xycoords='data',xytext=(-30,1),
textcoords='offset points',size=50) ax2.annotate('*', xy=(63.410,13), xycoords='data',xytext=(-
30,1), textcoords='offset points',size=50) ax2.annotate('*****', xy=(77.290,13),
xycoords='data',xytext=(-135,1), textcoords='offset points',size=50)

```

```

# sets the fontsize of the subplot to specified size for item in ((ax2.xaxis.label,
ax2.yaxis.label) + ax2.get_xticklabels() + ax2.get_yticklabels()):
    item.set_fontsize(30)

```

```

# gets migration 1930s-1950s from shapefiles
arcpy.env.workspace = decade_7090 y = () for reaches
in arcpy.ListFeatureClasses('migration*', 'Polygon'):
with arcpy.da.SearchCursor(reaches, 'Mig_myf') as rows:
for row in rows:
    y.append(-row(0))

```

```

#x = range(0,len(y)*25,25) x_np =
np.arange(0,len(y)*0.025,0.025)
x = x_np.tolist()

```

```

# creates the third subfigure 3 of 3 **bottom
plot** ax = fig.add_subplot(313)

```

```

# plots migration vs distance downstream
ax.plot(x,y,'r-',lw=2)

```

```

# plots reach dashed lines ax.plot((16.150,16.150),(-
20,20),'k--') ax.plot((24.950,24.950),(-20,20),'k--')
ax.plot((40.850,40.850),(-20,20),'k--')
ax.plot((49.530,49.530),(-20,20),'k--')
ax.plot((63.410,63.410),(-20,20),'k--')
ax.plot((77.290,77.290),(-20,20),'k--')
ax.plot((90.560,90.560),(-20,20),'k--')
ax.plot((99.260,99.260),(-20,20),'k--')
ax.plot((110.610,110.610),(-20,20),'k--')

```

```

# sets x and y labels to specified strings
ax.set_ylabel('Migration\nRate (m/yr)\n\n\n',horizontalalignment='center')
ax.set_xlabel('Distance Downstream (km)')

```

```

#sets x and y limits
ax.set_xlim(0,121) ax.set_ylim(-
20,20)

```

```

# specifies what ticks to show in the y-axis
ax.set_yticks((-20,-10,0,10,20))

```

```

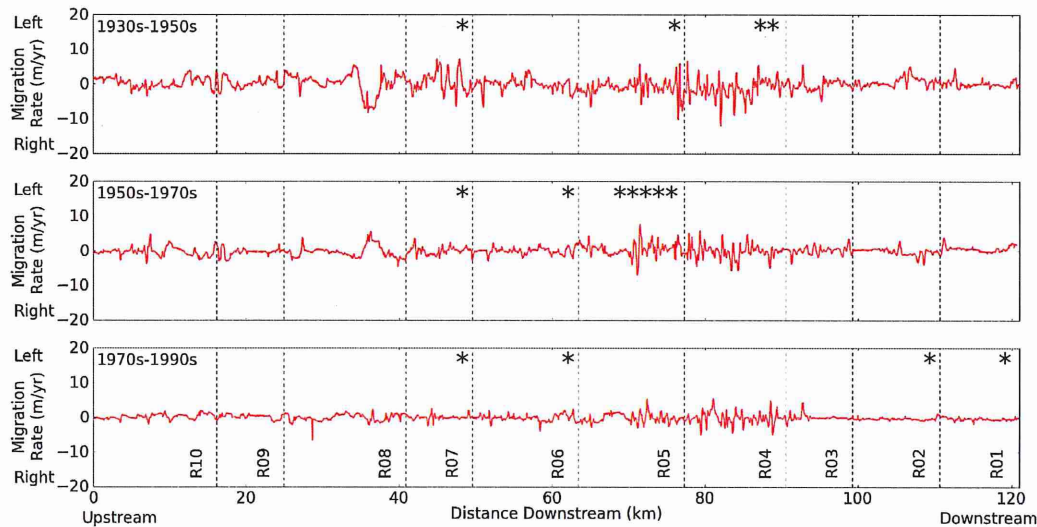
# adds text to the plots at specified locations ax.annotate('Upstream',xy=(0,-20),
xycoords='data',xytext=(-20,-70), textcoords='offset points',size=30) ax.annotate('Downstream',
xy=(121,-20), xycoords='data',xytext=(-150,-70), textcoords='offset points',size=30)
ax.annotate('Right', xy=(0,-19), xycoords='data',xytext=(-150,0), textcoords='offset points',size=30)
ax.annotate('Left', xy=(0,16), xycoords='data',xytext=(-150,0), textcoords='offset points',size=30)
ax.annotate('1970s-1990s', xy=(0,15), xycoords='data',xytext=(10,-1), textcoords='offset
points',size=30) ax.annotate('*', xy=(49.530,13), xycoords='data',xytext=(-30,1), textcoords='offset
points',size=50) ax.annotate('*', xy=(63.410,13), xycoords='data',xytext=(-30,1), textcoords='offset
points',size=50) ax.annotate('*', xy=(110.610,13), xycoords='data',xytext=(-30,1), textcoords='offset
points',size=50) ax.annotate('*', xy=(110.610,13), xycoords='data',xytext=(115,1),
textcoords='offset points',size=50) ax.annotate('R10', xy=(16.150,-20), xycoords='data',xytext=(-
50,50), textcoords='offset
points',size=30).set_rotation('vertical')
ax.annotate('R09', xy=(24.950,-20), xycoords='data',xytext=(-50,50),
textcoords='offset points',size=30).set_rotation('vertical') ax.annotate('R08',
xy=(40.850,-20), xycoords='data',xytext=(-50,50), textcoords='offset
points',size=30).set_rotation('vertical') ax.annotate('R07', xy=(49.530,-20),
xycoords='data',xytext=(-50,50), textcoords='offset
points',size=30).set_rotation('vertical') ax.annotate('R06', xy=(63.410,-20),
xycoords='data',xytext=(-50,50), textcoords='offset
points',size=30).set_rotation('vertical') ax.annotate('R05', xy=(77.290,-20),
xycoords='data',xytext=(-50,50), textcoords='offset
points',size=30).set_rotation('vertical') ax.annotate('R04', xy=(90.560,-20),
xycoords='data',xytext=(-50,50), textcoords='offset
points',size=30).set_rotation('vertical') ax.annotate('R03', xy=(99.260,-20),
xycoords='data',xytext=(-50,50), textcoords='offset
points',size=30).set_rotation('vertical') ax.annotate('R02', xy=(110.610,-20),
xycoords='data',xytext=(-50,50), textcoords='offset
points',size=30).set_rotation('vertical') ax.annotate('R01', xy=(110.610,-20),
xycoords='data',xytext=(100,50), textcoords='offset
points',size=30).set_rotation('vertical')

# sets the fontsize of the subplot to specified size for item in ((ax.xaxis.label,
ax.yaxis.label) + ax.get_xticklabels() + ax.get_yticklabels()):
item.set_fontsize(30)

# saves figure to specified location.
plt.savefig(workspace +
'\figure_name.png',format='png')

# clears figure
plt.clf()

```



Note: Arcgis10.2 and up come with the matplotlib module, for older versions this module has to be downloaded manually before being able to run this script.

Python script developed for automated identification of channel cutoffs

Channel cutoffs are places where the river has (naturally or through human intervention) cut off a meander bend and incised through the floodplain to form a new shorter channel. These cutoffs are potentially an important sediment sink and therefore have been critical in our development of a watershed sediment budget. Previously we have reported our manual mapping of channel cutoffs throughout the Root River watershed. While we believe that the results were as robust as could be done with an exhaustive manual search for these features, an automated tool is preferable to identify the features on such a large scale as the Root River. Further, it is important to automate the process in order to conduct this type of analysis over larger areas in the future.

This script was edited/written for the purpose of identifying possible locations of river meander migration and/or cutoffs. The tool was developed as a Python script and can be run in ArcGIS (with a Graphical User Interface as shown below) or in a Python environment (open source). The user inputs a raster surface, its projection, and the stream network and the tool does the rest. The user also chooses the buffer length as well as the minimum area of the polygons (because the area is dependent on the size of the river). Polygons are created into a shapefile in which the user can add to imagery to locate the areas of interest.

The script described above was edited from an original script developed and written by Sarah Porter, Mark Tomer, David James and Kathy Boomer for use in the ACPF toolbox. The original purpose of the script *Pothole Identification* was to identify potholes with certain parameters to illustrate water sinks within agricultural land for potential management opportunities. In order to use the tool for the reasons described in the description above, the following changes were made:

- Script content pertaining to other ACPF tools
 - To enable the Cutoff Identifier tool to act alone, code within the original script related to other tools (e.g. calling for data created from a previous tool) had to be changed or deleted.
- Script content limiting the Cutoff Identifier to certain areas
 - Codes that limited the tool to particular areas (hydric soils, agricultural land, etc.) were deleted.
- A stream buffer parameter was added to limit the cutoff search to a user-specified buffer.
 - This eliminates polygons outside of where cutoffs may be found.
- A minimum area parameter was added to limit the cutoff search to a user-specified area.
 - With prior knowledge of the stream under investigation, the user can input a minimum area to eliminate polygons that are non-representative of a cutoff.

Description of the Script:

This script was written for the purpose of identifying possible locations of river meander migration and/or cutoffs. The user inputs a raster surface, its projection, and the stream network and the tool does the rest! The user also chooses the buffer length as well as the minimum area of the polygons (because the area is dependent on the size of the river). Polygons are created into a shapefile in which the user can add to imagery to locate the areas of interest.

Import arcpy module

```
import arcpy
from arcpy.sa import *
import sys, string, os, os.path, time
import os
import tempfile
```

Set Temporary Workspace

```
arcpy.env.workspace = tempfile.tempdir
```

Check out any necessary licenses

```
arcpy.CheckOutExtension("spatial")
```

Script arguments (hardcopy to ensure it works).

```
Input_Streamlines = arcpy.GetParameterAsText(0)
```

```
#Input_Streamlines = "streams_types_rr.shp"
```

```
Set_Buffer_Distance = arcpy.GetParameterAsText(1)
```

```
#Set_Buffer_Distance = 10
```

```
Input_surface_raster = arcpy.GetParameterAsText(2)
```

```
#Input_surface_raster = "elev_dem03ra4.asc"
```

```
Min_Area = arcpy.GetParameterAsText(3)
```

```
#Min_Area = 5000
```

```

#Coordinate_System = arcpy.GetParameterAsText(4)

Cutoff_Output = arcpy.GetParameterAsText(4)
#Cutoff_Output = "cutoffs"

# Local variables
Streamline_Buffer = arcpy.CreateUniqueName("temp.shp", tempfile.gettempdir())
Dissolve_Type = "ALL"
Depression_Polygons = arcpy.CreateUniqueName("temp2.shp", tempfile.gettempdir())

# Process: Buffer
arcpy.AddMessage("Creating stream buffer.")
stream_buffer = arcpy.Buffer_analysis(Input_Streamlines, Streamline_Buffer, Set_Buffer_Distance,
"FULL", "ROUND", Dissolve_Type, "")

# Process: Fill
arcpy.AddMessage("Filling DEM.")
Filled_DEM = arcpy.sa.Fill(Input_surface_raster, "")

# Process: Minus
FillReg = arcpy.sa.Minus(Filled_DEM, Input_surface_raster)

# Select Values Greater than Zero
arcpy.AddMessage("Finding depressions.")
AllSinks = Con(FillReg, 1, "", "VALUE > 0")

# Process: Raster to Polygon, Add Area Field, Select Only Areas > 500m
arcpy.AddMessage("Converting rasters to polygons.")
Potholes = arcpy.RasterToPolygon_conversion(AllSinks, Depression_Polygons, "SIMPLIFY", "")
arcpy.AddField_management(Potholes, "Area", "DOUBLE")
arcpy.CalculateField_management(Potholes, "Area", "!shape.area!", "PYTHON_9.3")
arcpy.MakeFeatureLayer_management(Potholes, "Big_Potholes", "'Area' >= {0}'.format(Min_Area))

# Select Polygons that Intersect Buffer
arcpy.AddMessage("Selecting possible cutoff locations.")
arcpy.MakeFeatureLayer_management("Big_Potholes", "cutoffs", "")
arcpy.SelectLayerByLocation_management("cutoffs", "INTERSECT", stream_buffer, \
"", "NEW_SELECTION")
arcpy.CopyFeatures_management("cutoffs", Cutoff_Output)

# Delete Temporary Files
arcpy.Delete_management(Streamline_Buffer)
arcpy.Delete_management(Depression_Polygons)

```

Appendix B

USGS 5384000 Root River near Lanersboro, MN					
Year	Average SSL (tons/day)	Number of Records	Annual Total SSL (tons)	Annual Total SSL (Mg)	
1967	3.3	1	1,205	1,093	
1968	1501	24	549,325	498,339	
1969	6448	28	2,353,546	2,135,101	
1970	3595	15	1,312,078	1,190,297	
1971	6937	14	2,532,060	2,297,046	
USGS 5385000 Root River near Houston, MN					
Year	Average SSL (tons/day)	Number of Records	Annual Total SSL (tons)	Annual Total SSL (Mg)	
1967	45	1	16,425	14,901	
1968	5815	32	2,128,336	1,930,794	
1969	6542	73	2,387,830	2,166,203	
1970	2630	55	960,036	870,930	
1971	4187	54	1,528,377	1,386,520	
1972	1760	1	644,160	584,372	
1973	2636	210	962,307	872,990	
1974	4881	159	1,781,503	1,616,152	
1975	1337	274	487,834	442,556	
1976	797	366	291,631	264,563	
1977	262	365	95,483	86,621	
1978	2755	365	1,005,510	912,184	
1979	2179	365	795,285	721,470	
1980	3468	366	1,269,255	1,151,449	
1981	2413	273	880,841	799,086	
USGS 5385500 South Fork Root River near Houston, MN					
Year	Average SSL (tons/day)	Number of Records	Annual Total SSL (tons)	Annual Total SSL (Mg)	
1975	70.0	163	25,541	23,170	
1976	165	366	60,259	54,666	
1977	79.0	365	28,818	26,143	
1978	417	365	152,057	137,944	
1979	259	365	94,402	85,640	
1980	339	366	124,219	112,689	
1981	917	273	334,564	303,511	

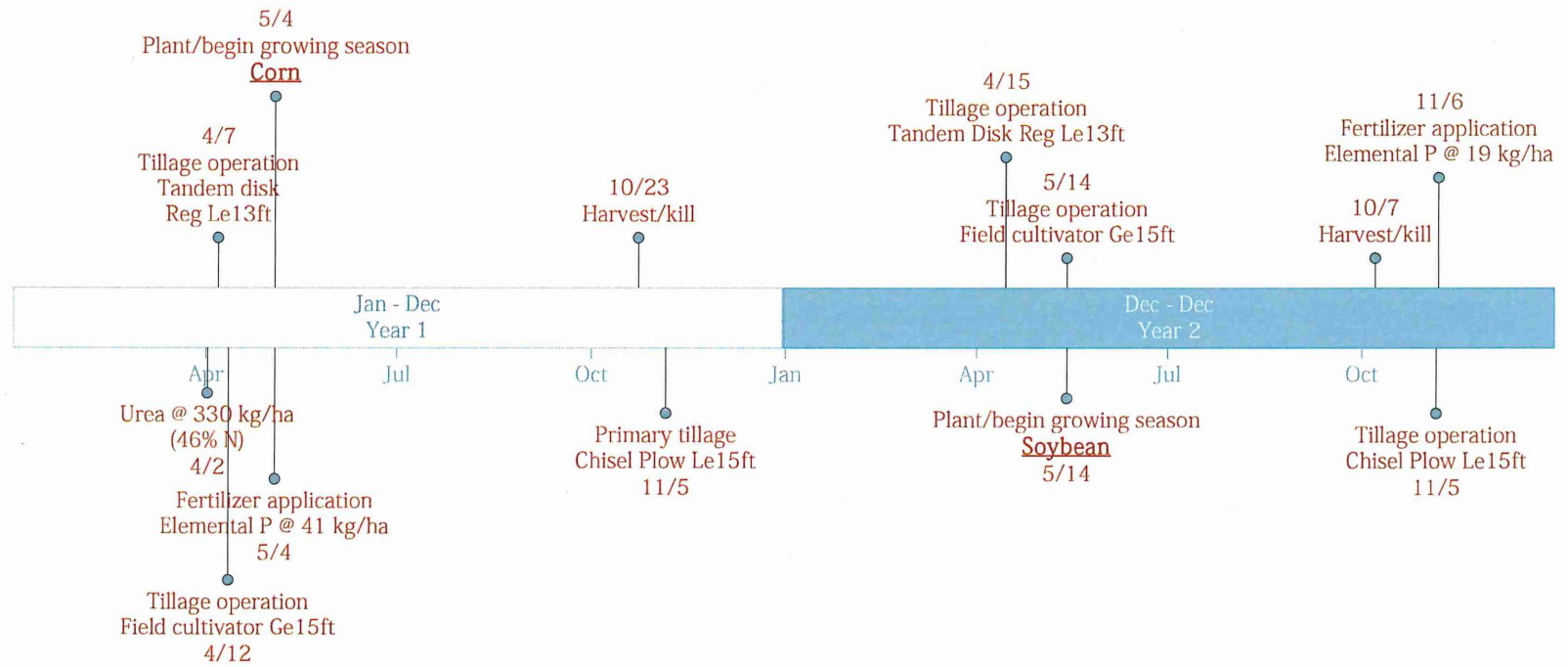


Figure A - 1. Scheduling of management operations under corn-soybean rotation in RRB. Management operations implemented in the model to capture typical practices that occur in the RRB.